

Dissertation
submitted to the
Combined Faculties for the Natural Sciences and for Mathematics
of the Ruperto-Carola University of Heidelberg, Germany
for the degree of
Doctor of Natural Sciences

presented by
MS in Physics: Dmitry Strelnikov
born in Barnaul, Russia
Oral examination: 22.12.2004

Selective Laser-Induced Oxidation of Carbon Chain Molecules in Cryogenic Matrices

Referees: Prof. Dr. Wolfgang Krätschmer
Prof. Dr. Ulrich Platt

Gezielte laserinduzierte Oxydation von Kohlenstoffmolekülen in kryogenen Matrizen.

Eine neue Methode der Laser-induzierten Oxydation wurde entwickelt, die es erlaubt, die IR Absorptionen von solchen Kohlenstoffmolekülen zu ermitteln, von deren man nur die UV/VIS Absorptionen kennt. Dazu haben wir die Moleküle von Kohlenstoff-Dampf in reaktiven Matrizen (O_2 , Ar- O_2) isoliert und durch Erwärmen der Matrix ein Gemisch linearer Spezies bis hinauf zu C_{17} erzeugt. Mit dem Licht eines auf die UV/VIS Absorptions-Wellenlänge der Kohlenstoffketten abgestimmten Excimer-Farbstoff-Laser konnten wir die Kohlenstoffmoleküle gezielt oxidieren, und korrelierte Änderungen in den UV/VIS und IR Spektren beobachten. Nach erfolgreichen methodischen Tests an den Kohlenstoff-Ketten C_9 , C_{11} und C_{13} , bei denen sowohl die UV/VIS als auch die IR Absorptionen bekannt sind, wagten wir uns an das Molekül C_{15} , von dem man nur die UV/VIS Absorption bei 450 nm kennt. Im Verlauf dieser Experimente bemerkten wir, dass ein Absorptionslinienpaar bei 1819 und 1816 cm^{-1} in der Sauerstoffmatrix (1818 cm^{-1} in Argon) der intensivsten IR aktiven Streckschwingung von C_{13} entspricht. Eine Gruppe von Linien bei 1721, 1714, 1707 und 1695 cm^{-1} können "Site-Peak" Absorptionen von C_{15} in einer Matrix aus Sauerstoff (1713, 1700, und 1695 cm^{-1} in einer Ar- O_2 Matrix) zugeordnet werden. Um Daten über die Absorptionen von Oxyden der Kohlenstoff-Ketten vom Typ C_nO oder OC_nO zu gewinnen, haben wir $^{16}O \rightarrow ^{18}O$ isotopisch substituierte Matrizen verwendet. Dabei haben wir entdeckt, dass die zwei Absorptionen bei 1803 und 1844 cm^{-1} in Argon (1800 und 1840 cm^{-1} in Sauerstoff) zu Oxyden und nicht zu reinen Kohlenstoffketten gehören. Weiterhin ist die Absorption bei 2180 cm^{-1} (in einer Sauerstoff Matrix) dem C_6O_2 Molekül zuzuschreiben. Unsere Ergebnisse zeigen, dass in der Literatur einige IR Absorptionen falsch zugeordnet worden sind.

Selective Laser-Induced Oxidation of Carbon Chain Molecules in Cryogenic Matrices.

We have tested and applied a laser-induced oxidation method for identifying IR-absorptions of those carbon molecules which have known UV/VIS absorptions. For this purpose we trapped the molecules of carbon vapor in non-inert matrices (O_2 , Ar- O_2). Upon matrix annealing, molecular growth took place leading to a mixture of linear carbon species up to C_{17} . The output of an excimer-dye laser was employed to photo-bleach selectively the strong UV/VIS absorptions of these trapped carbon molecules. Correlations of the changes in IR and UV/VIS spectra were observed. After successful tests performed on C_9 , C_{11} , C_{13} for which the UV/VIS as well as the IR absorptions are known we applied the method to the C_{15} molecule for which the UV/VIS absorption is at around 450 nm but the IR absorptions are unknown. In the course of this research we found that the 1819, 1816 cm^{-1} pattern of absorptions in an O_2 -matrix (1818 cm^{-1} in an Ar-matrix) can be assigned to the most intense IR-active C_{13} stretching mode. The pattern of absorption lines at 1721, 1714, 1707 cm^{-1} and 1695 cm^{-1} can be assigned as site peaks of C_{15} in an O_2 -matrix (1713, 1700, 1695 cm^{-1} in an Ar- O_2 -matrix). To obtain information about infrared absorptions of carbon chain oxides of the type C_nO and OC_nO , oxygen matrices with replaced $^{16}O \rightarrow ^{18}O$ isotopes were applied. There we found that two absorptions at 1803 and 1844 cm^{-1} in an Ar-matrix (1800 and 1840 cm^{-1} in O_2) belong to oxides of a carbon chain rather than to a pure carbon species. The absorption at 2180 cm^{-1} in an O_2 -matrix was assigned to the C_6O_2 molecule. Our data revise some of the assignments existing in the literature.

Contents

1	Introduction	3
1.1	Experimental methods	4
1.1.1	Production of carbon species	4
1.1.2	Spectroscopic techniques	6
1.1.3	Matrix Isolation	7
1.2	Known experimental data	9
1.2.1	Infrared absorptions of carbon molecules.	9
1.2.2	Electronic absorptions of carbon molecules.	14
1.3	Theoretical studies of small carbon molecules	14
1.4	Computational methods	16
1.4.1	<i>Ab initio</i> method.	17
1.4.2	Configuration Interaction	19
1.4.3	Semiempirical methods.	19
1.4.4	Density Functional Theory approach.	20
1.5	Definition of goals and outline of the work	21
2	Experimental setup and procedure	23
2.1	Carbon source and quadrupole mass spectrometer	24
2.2	Matrix isolation chamber	25
2.3	Infrared spectrometer	26
2.4	UV/VIS spectrometer	26
2.5	Excimer-Dye Laser	27
2.6	Experimental procedure	28

3	Comparison of C_n absorption spectra in solid Oxygen and Argon	29
3.1	Introduction	29
3.2	Experiment details	31
3.3	Results and Discussion	31
4	Selective laser-induced oxidation of carbon molecules	39
4.1	Introduction	39
4.2	Test of the method on known carbon chains	40
4.2.1	Experimental details	41
4.2.2	Results and Discussion	43
4.3	Depletion of C_{15}	55
4.3.1	Experimental details	55
4.3.2	Results and Discussion	56
4.4	Discussion	66
4.4.1	Comparison of experimental and calculated IR-absorption frequencies.	66
4.4.2	Theoretical view on laser-induced reactions.	68
5	Isotopic substitution of oxygen. Implications regarding carbon chain oxides.	70
5.1	Introduction	70
5.2	Experimental details	72
5.3	Results and Discussion	73
6	Conclusions and Outlook	83
	Bibliography	85

1. Introduction

In recent years, many researchers have been paying high attention to carbon molecules. One of the driving forces to study especially small carbon clusters was the hope of many astro-physicists and -chemists to learn more about the absorption lines in the spectrum of the interstellar medium.

A series of diffuse bands of interstellar origin had been discovered on photographic plates early in the 20th century. Nowadays over 200 such bands in the UV, visible (VIS) and near IR regions of the spectrum are reported [1]. Identifying the carriers of these diffuse interstellar bands (DIBs) has become a classic spectroscopic problem which challenges researchers in astronomy, physics and chemistry. Many suggestions of DIB carriers have been put forward. In these attempts an important constrain comes from the known cosmic abundances of elements: Carbon as the most abundant condensable element ought to play a decisive role in forming interstellar grains and molecules. Consequently, some authors suggested that bare carbon chain molecules cause the DIBs [2]. There were also attempts of assigning DIB-carriers to poly-cyclic aromatic hydrocarbons (PAHs), or to cyanopolyen molecules and/or their ions. However, the enigma of diffuse interstellar bands so far remained unsolved.

Absorption and emission lines of carbon molecules were found in comets [3, 4, 5] and other astrophysical objects: interstellar clouds [6, 7] and carbon stars [8].

The discovery of fullerenes [9, 10] and nanotubes [11] strongly enhanced the interest in carbon and its ability to form complex structures was recognized again. The advent of "*Nanotechnology*" became an additional motivation for carbon research. With carbon as building block nanometer sized molecular objects with a certain function could be obtained. So far, however, such objects can be produced without much control. To achieve progress into this direction, the problem of fullerene formation has to be solved. The very probable candidates for fullerene precursors are

carbon chains or rings [12, 13].

Carbon is a quite unique element. Exceptional is the ability to form three types of hybridization (sp^1 , sp^2 , sp^3) and - also extremely important - the ability to polymerize. Carbon in form of graphite (sp^2), diamond (sp^3), fullerenes (sp^{2-3}) and amorphous structures show big differences in properties but are now fairly well understood. In striking contrast, there is not much known about small carbon molecules like $C_2 \dots C_{23}$, which show carbon exclusively in the (sp^1) hybridization. Many of the absorption and emission spectral lines originating from such species are not yet assigned to a definite molecule. Therefore investigation of properties of C_n molecules may be quite rewarding for a better understanding of the nature of carbon. Concerning carbon structures, IR- and UV/VIS-spectroscopy gives us considerable part of such information.

1.1 Experimental methods

Different methods were applied in the research of carbon molecules. The first difficulty of such studies originates from the fact that almost all pure carbon molecules are very reactive. Therefore, one needs techniques to produce and preserve such species from reactions with environment for the time of investigation. There are several methods for production of carbon molecules and clusters.

1.1.1 Production of carbon species

The resistive heating source consists of just two carbon rods to which a voltage is applied. If one brings these rods into contact (and is using an appropriate power supply) a big current heats them up to temperatures greater than 2500 K. The energy of carbon atoms and small molecules becomes sufficient for sublimation, i.e. for their escape from the solid into the gas phase. Resistive heating sources produce mostly atomic carbon and small molecules like C_2 , C_3 . The abundance of the different species can be controlled by current through the rods. High current (high temperature as a consequence) provides more atomic carbon while for low currents also larger molecules like C_5 can be observed. Because of its simplicity and high yield of pure carbon molecules this method is used in our experiments.

The arc discharge source consists of two carbon rods but in the atmosphere of some gas, usually a noble gas. After striking (i.e. igniting) the arc there is no need to keep mechanical contact between rods as in the case of resistive heating source. The arc discharge plucks carbon molecules from the cathode rod, and these molecules can cluster and produce large molecules. Amazingly, such a relatively simple source can produce fullerenes in high yields [10]. Apparently, the presence of the quenching gas leads to much larger molecules than a resistive heating source could provide.

The laser ablation source consists of a vacuum chamber in which a carbon rod or pellet is exposed to a powerful laser. Such source can produce neutrals and molecular ions of various sizes: C^+ , C_2^+ , ..., C_{50}^+ [14] were detected. There are two proposed pathways for production of those carbon molecules: association of small precursors (so-called "bottom up" process) [9] and dissociation of big clusters (so called "top down" process) [15]. The first approach suggest that the carbon molecules in the laser plume can cluster and produce larger ones. The second pathway suggests that the laser beam plucks big clusters from the solid carbon and after that the laser radiation dissociates these big clusters into smaller species. The addition of a quenching gas modifies this method and leads to an enhanced nucleation of large molecules. It is also possible that both, the bottom up and the top down processes take place together at the same time [9]. Very much differently shaped isomers can be produced in this process [12]: chains, monocyclic, bicyclic, tricyclic rings, and fullerenes, especially C_{60} .

The hot-cathode discharge ion source is burning in a suitable hydrocarbon gas and can produce different carbon molecules, mostly hydrocarbons, depending on precursor gases [16]. The species (mostly as anions) can be extracted from the discharge region by electrostatic lenses and then the molecule of interest can be mass selected.

The Cesium-sputter source was used by the group of J.P. Maier [17] to produce various carbon ions and carbon derivatives. Cesium cations bombard a cold graphite cathode and sputter carbon molecules from the rod. Such kind of source also can produce various small molecular ions and allows to eliminate hydrogen containing species.

Electric arc in a hydrocarbon solvent. This method allows to produce carbon chains, terminated by hydrogen atoms, i.e. polyines (H-C-C-...-C-H). The species

remain in the solvent. The electric arc between graphite electrodes in different solvents like acetonitrile, n-hexane, and toluene produces a mixture of polyines. The yield of long polyines increases with increasing of the temperature [18].

1.1.2 Spectroscopic techniques

Many methods were applied in studies of carbon molecules. By means of optical spectroscopy, mass spectroscopy, electron spin resonance, ^{13}C nuclear magnetic resonance, and Coulomb explosion different properties can be investigated. Most important results until 1998 are reviewed in [19, 20].

Mass selection provided considerable part of known information about carbon molecules. The leading group in this direction is the group of J.P. Maier in Basel [16]. After production of molecules from precursor gases in a discharge, the ionized molecules (usually anions) are mass selected by a quadrupole mass filter and co-deposited with noble gas (usually neon) on a cold substrate. There the ions can be neutralized and subjected to normal matrix isolation spectroscopy (which will be discussed in the next section).

Gas-phase laser spectroscopy. Carbon molecules, usually produced by laser ablation of a graphite rod in a helium gas flow, can be studied in gas phase with the help of semiconductor lasers. The width of the laser line is narrow enough to observe rotational transitions of molecules. So, from the spectrum one can deduce the moment of inertia and make some conclusions about the size and structure of molecules. The groups of Saykally in Berkeley and Giesen in Köln have obtained rovibrational spectra for several carbon molecules [21, 22, 23, 24]. The semiconductor lasers can be tuned only over a small range (several wavenumbers) and thus a prior knowledge of the approximate position of the absorption is required. Matrix data have turned out to be helpful in this respect.

Cavity ring-down spectroscopy (CRDS) has two advantages: insensibility to fluctuations in laser output and the great sensitivity due to the enormous pathlengths the beam can travel through the sample. CRDS has thus become the method of choice for ultra-sensitive, quantitative absorption measurements. A tunable laser beam is reflected back and forth from the mirrors at the ends of the laser cavity which contains the sample molecules in the gas phase. The intensity of laser beam

is measured after every pass through. From the decay rate one can deduce the absorption coefficient. The CRDS in carbon research is applied by Ref. [25, 26].

Photoelectron spectroscopy can be applied to a molecular beam of mass selected species (usually anions) by irradiating the beam with a laser. This leads to photoelectron detachment. From the kinetic energies of detached electrons one can obtain information about electron affinities and vibrational levels of the neutral species (including non-active infrared transitions) [27].

Helium nanodroplets. In recent years this new interesting technique for spectroscopic studies was developed [28, 29]. It combines the matrix isolation, laser-, gas-phase, and mass spectroscopy. Furthermore it is very sensitive by the use of mass spectrometry. The helium nanodroplets, containing up to several thousands He atoms, are produced by supersonic expansion of He through a cold nozzle. Then the beam of superfluid He clusters is allowed to pick up the molecules under investigation. One then can excite a molecule by a suitably tuned laser. The absorbed energy dissipates to the He atoms of the droplet and some of them leave the droplet and can be detected by mass spectroscopy. Thus, the presence of detached He atoms signals the presence of absorption at the respective laser frequency. Since the temperature of He droplets is less than 1K, the molecules inside are in their vibrational ground state. In this sense there is resemblance to matrix isolation. On the other hand one can also observe rotational excitation what is possible only in gas phase. Since a mass spectrometer can be made very sensitive one could observe absorption by only one molecule, i.e. as single-molecule spectroscopy seems to be in reach. So far, however, nobody made spectroscopy of carbon molecules in helium nanodroplets.

1.1.3 Matrix Isolation

Matrix isolation is the technique of isolating reactive molecules and atoms from each other by embedding them in an chemically non-reactive solid. Condensed rare gases (Ne, Ar, Kr) are commonly applied for this purpose. The ices of such rare gases are quite transparent in the infrared, visible and ultraviolet regions of the spectrum. Of course, low temperature is necessary to condense these gases. As a consequence of that feature, a high vacuum is also necessary to keep atmospheric impurities out of

1 Introduction

the matrix. Low temperature does have one important advantage: the molecules in the sample are quenched to their vibrational ground state. Furthermore, the molecules cannot rotate in the matrix. This greatly simplifies the absorption spectra.

In order to achieve low temperatures, the matrix gas is deposited on a substrate with good thermal conductivity. The substrate is cooled by a closed-cycle refrigerator (based on Joule-Thomson effect in expanding helium) to typical minimum temperatures of 7-10 K.

In order to keep the sample molecules well separated in the matrix, the amount of matrix gas ought to be much larger than the amount of vapor of the species under investigation. If warmed up slightly, the matrix may permit diffusion of some of the sample molecules in the matrix. This can lead to chemical reactions between the reactive sample species within the matrix. The rate of these reactions can be controlled by the degree of warming and may be limited by the mobility and reactivity of the various species. Thus, thermal annealing of the matrix can be useful in producing new molecules and at the same time allows studying the abundance dynamics for different species.

Substitution of molecular atoms by their isotopes (such molecules are called isotopomers) leads to the shifts in vibrational frequency. By observing the distribution of isotopomeric peaks for the same vibrational absorption one can gain some information about number of atoms in a molecule and about the molecular symmetry. In matrices containing carbon molecules, the partial ^{13}C substitution is the method generally applied for carrier identification. Combined with calculated isotopomeric patterns of IR lines, several assignments of vibrational absorptions were carried out.

The advantage of the matrix isolation approach in comparison with gas phase measurements is the possibility to accumulate much more molecules in the sample. The already mentioned advantage of a simple spectrum (which contains no rotations and only transitions from the ground state) also has its drawbacks. No information is available about the molecule's moment of inertia - which in case of molecular chains is the key parameter for identifying the absorber.

Another complication introduced by the matrix is the so called *matrix shift*. The trapped molecule interacts with surrounding matrix molecules and this leads to the shift of absorption to lower or higher energies in comparison with gas phase data. Sometimes even several adjacent lines appear for the same vibrational mode. The

reason for this effect is that several distinct positions of a sample molecule with respect to the matrix structure can occur. Matrices usually exhibit poly-crystalline face centered cubic (fcc), monoclinic, hexagonal and other lattices. The peaks, corresponding to the same vibrational mode of the sample molecule are called *site peaks*.

The reason for applying matrix isolation technique in our experiments is the easiness in production of various carbon molecules in quantities sufficient for infrared studies. In our case the host matrix also plays a role as the medium in which controlled diffusion and thus mutual reactions of the carbon molecules can take place.

1.2 Known experimental data

1.2.1 Infrared absorptions of carbon molecules.

The IR-spectrum of matrix isolated carbon species in a Ne-matrix shown on Fig.1.1.

Almost all known information about spectra of carbon species are reviewed in [19, 20, 30]. The most successful methods in carbon molecule identification turned out to be mass selection followed by neutralisation and matrix isolation (IR-spectra of chains up to C₁₁, UV-spectra up to C₂₁) and diode laser spectroscopy in gas phase (IR-spectra of chains up to C₁₃). In mass selection experiments, there is a problem in extending the knowledge about IR-spectra towards longer chains. The reason is the very low abundances of such species. In gas phase measurements the problem is to know the approximate IR-region where an absorption of a molecule is expected to be. The preparation of the long chain molecules in the matrix gives sufficient amount of species for IR-measurement, but on the other hand the problem arises to distinguish between different molecules since they all are present in the matrix at the same time.

The known infrared absorptions of carbon molecules are displayed in Table 1.1 (based on NIST database [30]).

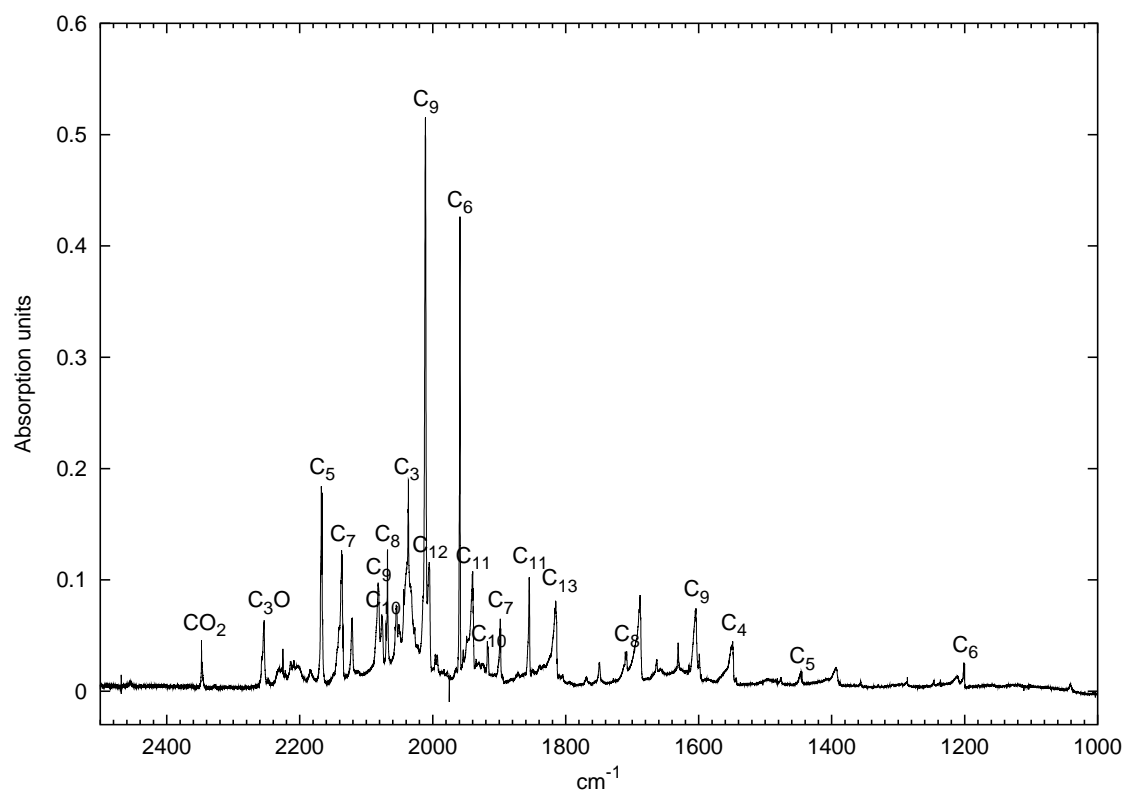


Fig. 1.1: IR-spectrum of matrix-isolated carbon species in Ne at 8K.

Tab. 1.1: IR-absorptions of carbon molecules. Experimental data. (MIS – Matrix Isolation Spectroscopy; DLS – Diode Laser Spectroscopy; TPE – Threshold photoelectron spectroscopy, including zero kinetic energy electron (ZEKE) detection; T – tentative assignment).

Molecule	Absorption, cm^{-1}	Mode	Method	References
C_3	2040.02	ν_3 stretch, Σ_u^+	DLS in gas	[7]
	2042	ν_3 stretch, Σ_u^+	MIS in Ne	[31]
	2038.9	ν_3 stretch, Σ_u^+	MIS in Ar	[31]
	2033.3	ν_3 stretch, Σ_u^+	MIS in Kr	[32]
	2036.0	ν_3 stretch, Σ_u^+	MIS in H_2	[33]
	2031	ν_3 stretch, Σ_u^+	MIS in N_2	[34]
	63.41	ν_2 bend, Π_u^+	DLS in gas	[35, 36]
	70	ν_2 bend, Π_u^+	MIS in Ne	[37]
	70	ν_2 bend, Π_u^+	MIS in Ar, LIF	[38]
C_4	1548.61	ν_3 stretch, Σ_u	DLS in gas	[39]
	1543.4	ν_3 stretch, Σ_u	MIS in Ar	[40]
	1547.0	ν_3 stretch, Σ_u	MIS in Ne	[41]
	1539.5	ν_3 stretch, Σ_u	MIS in Kr	[32]
	160 ± 4	ν_5 bend, Π_u	DLS in gas	[42]
	172.4	ν_5 bend, Π_u	MIS in Ar	[43]
C_5	2169.441	ν_3 stretch, Σ_u^+	DLS in gas	[44, 45]
	2166.4	ν_3 stretch, Σ_u^+	MIS in Ne	[46]
	2164	ν_3 stretch, Σ_u^+	MIS in Ar	[47, 46]
	2157	ν_3 stretch, Σ_u^+	MIS in Kr	[32]
	2164.5	ν_3 stretch, Σ_u^+	MIS in H_2	[33]
	1444.3	ν_4 stretch, Σ_u^+	MIS in Ne	[48]

1 Introduction

Molecule	Absorption, cm^{-1}	Mode	Method	References
C_6	1446.6	ν_4 stretch, Σ_u^+	MIS in Ar	[49]
	1443.2	ν_4 stretch, Σ_u^+	MIS in Kr	[32]
	535 ± 10	ν_6 bend, Π_u	TPE in gas	[27]
	118 ± 3	ν_7 bend, Π_u	TPE in gas	[27]
	1959.86	ν_4 stretch, Σ_u^+	DLS in gas	[50]
	1958.7	ν_4 stretch, Σ_u^+	MIS in Ne	[48]
	1952.0	ν_4 stretch, Σ_u^+	MIS in Ar	[51]
	1951.2	ν_4 stretch, Σ_u^+	MIS in Kr	[32]
	1956.8	ν_4 stretch, Σ_u^+	MIS in H_2	[52]
	1199.4	ν_5 stretch, Σ_u^+	MIS in Ne	[48]
	1197.3	ν_5 stretch, Σ_u^+	MIS in Ar	[47]
	1197.0	ν_5 stretch, Σ_u^+	MIS in Kr	[32]
cyclic C_6	90 ± 50	ν_9 bend, Π_u	TPE in gas	[53]
	1694.9	ν_4, E'	MIS in Ar	[54, 55]
C_7	2138.315	ν_4 stretch, Σ_u^+	DLS in gas	[56]
	2134.6	ν_4 stretch, Σ_u^+	MIS in Ne	[48]
	2127.8	ν_4 stretch, Σ_u^+	MIS in Ar	[57]
	2120.4	ν_4 stretch, Σ_u^+	MIS in Kr	[32]
	1898.376	ν_5 stretch, Σ_u^+	DLS in gas	[56]
	1897.5	ν_5 stretch, Σ_u^+	MIS in Ne	[48]
	1894.3	ν_5 stretch, Σ_u^+	MIS in Ar	[57]
	1889.3	ν_5 stretch, Σ_u^+	MIS in Kr	[32]
C_8	496 ± 110	ν_7 bend, Π_u	TPE in gas	[27]
	2067.9779	ν_5 stretch, Σ_u^-	DLS in gas	[24]
	2067.8	ν_5 stretch, Σ_u^-	MIS in Ne	[17]

1.2 Known experimental data

Molecule	Absorption, cm^{-1}	Mode	Method	References
	2063.9	ν_5 stretch, Σ_u^-	MIS in Ar	[58, 59]
	2065.3(T)	ν_5 stretch, Σ_u^-	MIS in Kr	[32]
	1707.8	ν_6 stretch, Σ_u^-	MIS in Ne	[58, 59]
	1705.6	ν_6 stretch, Σ_u^-	MIS in Ar	[58]
	1706.0(T)	ν_6 stretch, Σ_u^-	MIS in Kr	[32]
cyclic C_8	1844.2	ν_{12} , E_u	MIS in Ar	[60, 61]
cyclic C_8	1818	ν_{12} , E_u	MIS in Ar	[62]
C_9	2079.67	ν_5 stretch, Σ_u^+	DLS in gas	[63]
	2081.1	ν_5 stretch, Σ_u^+	MIS in Ne	[59]
	2078.1	ν_5 stretch, Σ_u^+	MIS in Ar	[32]
	2079.0(T)	ν_5 stretch, Σ_u^+	MIS in Kr	[32]
	2014.28	ν_6 stretch, Σ_u^+	DLS in gas	[64]
	2010	ν_6 stretch, Σ_u^+	MIS in Ne	[59]
	1998	ν_6 stretch, Σ_u^+	MIS in Ar	[51, 65]
	1994.2	ν_6 stretch, Σ_u^+	MIS in Kr	[32]
	2007.3	ν_6 stretch, Σ_u^+	MIS in H_2	[33]
	1602.8	ν_7 stretch, Σ_u^+	MIS in Ne	[32]
	1601.0	ν_7 stretch, Σ_u^+	MIS in Ar	[66]
	1600.8	ν_7 stretch, Σ_u^+	MIS in Kr	[32]
C_{10}	2074.4	stretch, Σ_u^+	DLS in gas	[22]
	2074.5	stretch, Σ_u^+	MIS in Ne	[59]
	1915.4	stretch, Σ_u^+	MIS in Ne	[59]
C_{11}	1938.6	ν_7 stretch, Σ_u^+	MIS in Ne	[59]
	1946.0 ± 0.8	ν_7 stretch, Σ_u^+	MIS in Ar	[67]
	1937.3	ν_7 stretch, Σ_u^+	MIS in Kr	[68]

1 Introduction

Molecule	Absorption, cm^{-1}	Mode	Method	References
C_{12}	1942.6	ν_7 stretch, Σ_u^+	MIS in N_2	[68]
	1853.4	ν_8 stretch, Σ_u^+	MIS in Ne	[59]
	1856.7 ± 0.8	ν_8 stretch, Σ_u^+	MIS in Ar	[67]
	1849.9	ν_8 stretch, Σ_u^+	MIS in Kr	[68]
	1854.8	ν_8 stretch, Σ_u^+	MIS in N_2	[68]
	1357.0	ν_9 stretch, Σ_u^+	MIS in N_2	[68]
	2140.6(T)	ν_7 stretch, Σ_u^+	MIS in Ar	[69]
	2003.9(T)	ν_8 stretch, Σ_u^+	MIS in Ne	[59]
	1997.2	ν_8 stretch, Σ_u^+	MIS in Ar	[69]
C_{13}	1818.0	ν_9 stretch, Σ_u^+	MIS in Ar	[69]
	1808.96	stretch, Σ_u^+	DLS in gas	[23]

1.2.2 Electronic absorptions of carbon molecules.

UV/VIS-absorptions of carbon chain molecules were measured by the group of J.P.Maier [70, 71, 72] in Ne-matrices. The electronic absorptions in Ne are presented in Fig.1.2. The data were provided by T. Wakabayashi [73]. As was mentioned in Ref.[74] there are very strong electronic transition in chain molecules with a singlet electronic ground state. These molecule are the bare C_{2n+1} chains, but also the chain oxides C_{2n+1}O , OC_{2n+1}O .

1.3 Theoretical studies of small carbon molecules

Calculations on small carbon clusters have been performed by many researches. Most of the theoretical results before 1998 are reviewed in [19] and [20].

Ab initio calculations predict two low energy structures for C_4 , C_6 , C_8 and C_{10} ,

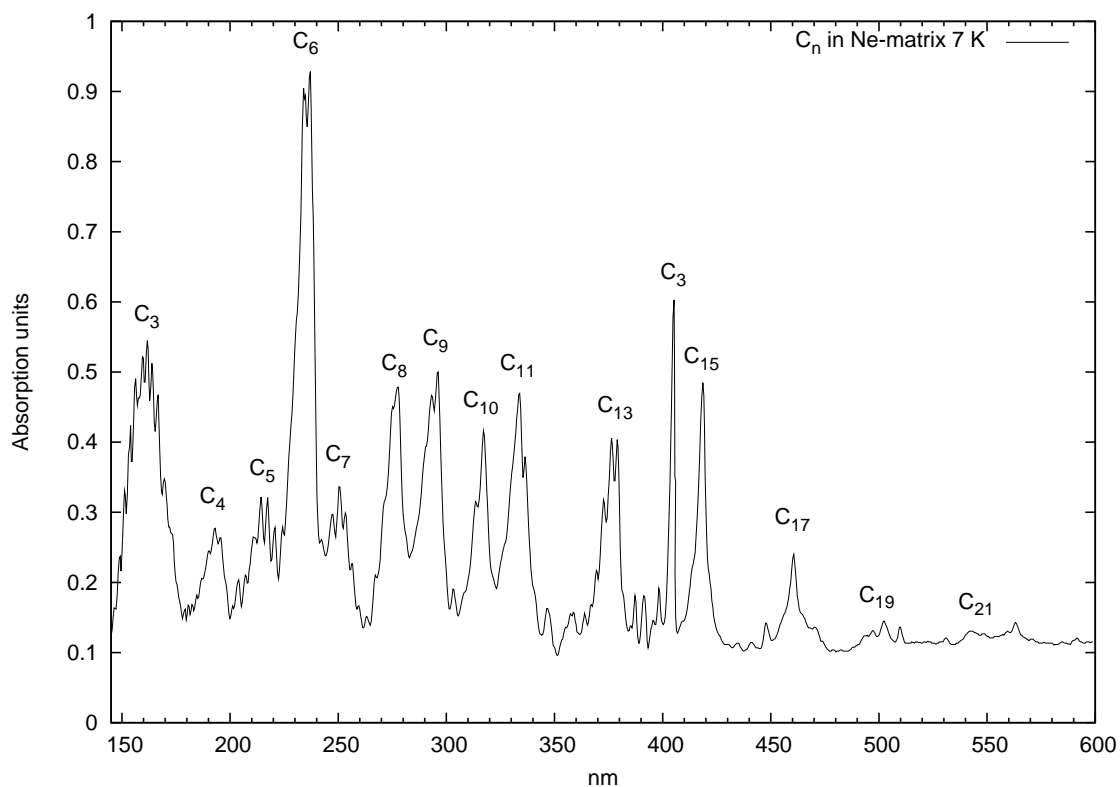


Fig. 1.2: VUV/UV/VIS-spectrum of matrix-isolated carbon species in Ne at 7K. Notice sequencing of the absorptions with increasing of chain length for odd-numbered carbon chains and for even-numbered chains. Data are from [73].

namely linear and cyclic. The geometry of odd carbon chains (up to C_{11} at least) is predicted to be linear. For species with more than 12 atoms, cyclic structures were proposed as more favorable in energy. A singlet electronic ground state was proposed for odd linear C_n and a triplet ground state for even-numbered linear carbon species.

Calculations (and experiments) indicate that long odd-numbered C_n molecules with singlet ground states have big oscillator strengths [74]. The positions of UV/VIS absorptions calculated by applying the configuration interaction (CI) method agree quite well with experimental data. Our CI-calculation of electronic transitions for oxides of carbon chains suggests that the oxides and the pure carbon chains absorb at very similar wavelengths. Thus pure carbon chain spectra and absorptions of oxides may interfere, – an effect which was observed (see chapter 4).

A good agreement with experimental vibrational data of C_5 and C_7 show the large-scale coupled cluster calculations carried out by P. Botschwina [75]. *Ab initio* and DFT calculations of vibrational modes performed for longer chains (C_9 , C_{11} and C_{13}) [76] unfortunately do not agree very well with experimental data. The most reliable CCSD(T) (coupled cluster) calculations for long chain molecules require enormous amounts of computing time. *Bond charge models* were also applied for calculation of vibrational frequencies of various carbon molecules [77].

1.4 Computational methods

For the calculation of different molecular properties we used two software packages: Gaussian 98 [78] and Hyperchem 6 [79]. There are several available computational methods: *ab initio* [80, 81], DFT (density functional theory) [81], CI (configuration interaction) [80] and semi-empirical [81](PM3 [82, 83], for instance). *Ab initio* calculations only have parameters associated with the basis set of the atomic orbitals which are used in linear combination to describe the molecular orbitals. These basis sets are usually associated with shells, such as an s shell, sp shell, etc. The basis set is the only parameter in *ab initio* calculations. The density functional method attempts to describe how the ground state energy of a molecule depends on the electron density of the molecule. Density Functional Theory (DFT) calculations are similar to *ab initio* calculations but have additional parameters depending on

the type of density functional. The later is the principal variable in DFT calculations. Semi-empirical calculations use many empirical parameters associated with the specific molecular atoms. These parameters were obtained and optimized by comparison with experiments. Otherwise these methods apply a rigorous quantum mechanical formulation.

1.4.1 *Ab initio* method.

As a starting point in quantum mechanical calculation the Schrödinger equation is used:

$$\hat{H}\Psi = \varepsilon\Psi, \quad (1.4.1)$$

where the Hamiltonian \hat{H} contains the input information about a molecule. In the considered quantum chemical calculations one is exclusively interested in the molecular ground state, i.e. in the electronic wavefunction which minimizes the energy. Different approximations are commonly used. The Born-Oppenheimer approximation neglects the motion of nuclei, introducing an electronic wavefunction Ψ_{elec} :

$$\hat{H}_{elec}\Psi_{elec} = \varepsilon_{elec}\Psi_{elec}. \quad (1.4.2)$$

Independent electron approximation considers

$$\hat{H}_{elec} = \sum_i \hat{H}_i^{eff}, \quad (1.4.3)$$

where \hat{H}_i^{eff} is an effective one-electron Hamiltonian. Since all electrons are identical particles, the many-electron Schrödinger equation decays into a one-electron problem:

$$\hat{H}_i^{eff}\psi_i = E_i\psi_i, \quad (1.4.4)$$

where the solutions Ψ_i are called *Molecular Orbitals*(MO). The N-electron wavefunction, which satisfies the Pauli exclusion principle can be represented by a *Slater determinants*:

$$\Psi(\vec{r}_1, \dots, \vec{r}_N) = \frac{1}{\sqrt{N!}} \begin{vmatrix} \psi_1(\vec{r}_1) & \dots & \psi_N(\vec{r}_1) \\ \vdots & \vdots & \vdots \\ \psi_1(\vec{r}_N) & \dots & \psi_N(\vec{r}_N) \end{vmatrix} \quad (1.4.5)$$

1 Introduction

The next approximation is a representation of MO as a linear combination of atomic orbitals (AO) ϕ_j :

$$\psi_i = \sum_j C_{ij} \phi_j. \quad (1.4.6)$$

Hence one obtains the matrix equation:

$$\mathbf{HC} = \mathbf{SCE}, \quad (1.4.7)$$

where $H_{ij} = \int \phi_i \hat{H}^{eff} \phi_j d\vec{r}$, C_{ij} are defined in equation 1.4.6, $S_{ij} = \int \phi_i \phi_j d\vec{r}$, and $E_{ij} = E_i \delta_{ij}$. Solving of the equation 1.4.7 for the coefficients C_{ij} requires a matrix diagonalization.

The Hartree-Fock procedure or Self-Consistent Field (SCF) method introduces well defined mathematical approximations to end up with a one-electron eigenvalue problem. This problem must be solved iteratively to achieve self-consistency. In the case of closed-shell system one solves the Roothaan equations, while for the open-shell system Pople-Nesbet unrestricted equations are used.

The Hartree-Fock method introduces an effective one-electron Hamiltonian (as in the equation 1.4.4):

$$\hat{F}\psi_i = E_i\psi_i, \quad (1.4.8)$$

where the Fock operator \hat{F} is a sum of the kinetic energy operator for an electron, and the potential energy of this electron in the average field of the other electrons. \hat{F} depends on solutions Ψ_i , so the equation 1.4.8 requires iterative solution to self-consistency. The solution of Hartree-Fock eigenvalue problem 1.4.8 yields a set of orthonormal spin orbitals. The N lowest spin orbitals are called *occupied* (N is the number of electrons), and the remaining $2K-N$ spin orbitals are called *unoccupied* or *virtual* (K is the number of used spatial basis functions).

Therefore, the matrix equation 1.4.7 turns into the Roothaan equations:

$$\mathbf{F}(\mathbf{C})\mathbf{C} = \mathbf{SCE}, \quad (1.4.9)$$

which can be solved iteratively, starting from the guess matrix \mathbf{C} .

The Pople-Nesbet equations are the generalization of the equations 1.4.9, where the spatial orbitals ψ_i^α (spin up) and ψ_i^β (spin down) are not defined to be identical, but solved independently:

$$\begin{aligned} \mathbf{F}^\alpha(\mathbf{C}^\alpha, \mathbf{C}^\beta)\mathbf{C}^\alpha &= \mathbf{S}\mathbf{C}^\alpha\mathbf{E}^\alpha, \\ \mathbf{F}^\beta(\mathbf{C}^\alpha, \mathbf{C}^\beta)\mathbf{C}^\beta &= \mathbf{S}\mathbf{C}^\beta\mathbf{E}^\beta. \end{aligned} \quad (1.4.10)$$

In a strict sense the later equations violate Kramer's theorem which states that (except in the open shell) each orbital should host two electrons, rather than each electron should move in its own orbital. Since open shell configurations are rather difficult to calculate rigorously, these equations are of some value in an approximate sense.

1.4.2 Configuration Interaction

The self consistent methods so far presented do not take care of any electron-electron correlations besides those imposed by the Pauli-principle. To overcome this limitation, so called "configuration interaction" (CI) calculations can be carried out. The basic idea of this method is a diagonalization of N-electron Hamiltonian \mathbf{H} in a basis of N-electron functions Ψ_i (Slater determinants). In other words, one represents CI wave function as a linear combination of Slater determinants:

$$\Phi_a = \sum_i C_{ia} \Psi_i. \quad (1.4.11)$$

Depending on the required accuracy one takes into account singly, doubly, triply and higher excited Slater determinants (in a *coupled cluster* method doubly and quadruply excited Slater determinants are considered). A singly excited Slater determinant is a Slater determinant, where one electron from an occupied orbital moves to a virtual orbital. In a doubly excited Slater determinant two electrons from occupied orbitals move to virtual orbitals, and so on. $\{\Psi_i\}$ form an orthonormal basis (as Slater determinants), so $S_{ij} = \int \Psi_i \Psi_j d\vec{r} = \delta_{ij}$ and $\det(\mathbf{C}) = 1$. Therefore, one obtains similar to 1.4.7 equation:

$$\mathbf{HC} = \mathbf{CE}, \quad (1.4.12)$$

solutions of which describe not only the ground state but also excited electronic states.

1.4.3 Semiempirical methods.

Semiempirical methods are simplified versions of Hartree-Fock theory using empirical (derived from experimental data) corrections in order to improve performance

and computational speed. These methods are usually named by acronyms encoding some of the underlying theoretical assumptions. The most frequently used methods (MNDO [84, 85, 86, 87], AM1 [88], PM3 [82, 82]) are all based on the Neglect of Differential Diatomic Overlap (NDDO) integral approximation.

A principle difficulty in an attempt to solve Schrödinger equation for molecules is the large number ($\sim N^4$) of two-electron integrals:

$$\langle ij|kl\rangle = \int \frac{\phi_i^A(\vec{r}_1)\phi_j^B(\vec{r}_1)\phi_k^C(\vec{r}_2)\phi_l^D(\vec{r}_2)}{|\vec{r}_1 - \vec{r}_2|} d\vec{r}_1 d\vec{r}_2, \quad (1.4.13)$$

where ϕ_i^A is an atomic orbital centered at atom A. The differential overlap approximation assumes that:

$$\int \phi_i^A(\vec{r}_1)\phi_j^B(\vec{r}_1)d\vec{r}_1 \ll 1, \quad (1.4.14)$$

and NDDO is based on:

$$\phi_i^A\phi_j^B = \phi_i^A\phi_j^B\delta_{AB}. \quad (1.4.15)$$

AM1 (Austin model 1) is a modified MNDO method, and PM3 is a reparametrization of AM1. The parameters for PM3 were obtained by comparing a much larger number of experimental versus computed molecular properties.

Semiempirical methods use tabulated, internally stored pre-calculated data instead of computing them from atomic orbitals in all cases. This parametrization speeds up calculation to such an extent that even larger molecules or molecules with realistic substituents (Phenyl etc.) can be calculated.

1.4.4 Density Functional Theory approach.

The DFT method is based on Hohenberg-Kohn theorem which states[89]: *the energy E of a molecular system is a universal functional of the electron density $E = E(\rho)$. The exact energy is returned only when ρ is exact, and approximate electron density leads to higher energies.*

Certainly, $\rho(\vec{r})$ is a much simpler function than the N-electron wavefunction since it is a function of only 3 variables rather than $3N$ (N is the number of electrons). Therefore one may expect a simplification and acceleration of quantum mechanical calculations.

The expansion of ρ according to effective single-electron wavefunctions followed by a variation of the energy functional leads to the Kohn-Sham equations [90] (similar to 1.4.8):

$$(\hat{T} + V^{eff}[\rho(\vec{r})])\psi_i(\vec{r}) = E_i\psi_i(\vec{r}), \quad (1.4.16)$$

where the effective potential is

$$V^{eff}[\rho(\vec{r})] = V^{ext}(\vec{r}) + \int \frac{2\rho(\vec{r}_1)}{|\vec{r} - \vec{r}_1|} d\vec{r}_1 + \frac{\delta E^{xc}[\rho(\vec{r})]}{\delta \rho(\vec{r})}. \quad (1.4.17)$$

The last term in 1.4.17 is the non-local exchange-correlation potential. So, the difference between DFT and *ab initio* effective single-electron equations is the non-local exchange-correlation potential (instead of HF exchange energy).

The way how one defines the exchange-correlation potential generates different DFT variants. The frequently applied functional is B3-LYP (Becke's 3 parameter hybrid functional using Lee-Yang-Parr correlation functional) [91]. The exchange part of B3-LYP consists of 20% Hartree-Fock exchange, 8% of Slater exchange and 72% of Becke-88 Exchange. The correlation part of B3-LYP contains 19 % VWN III (for Vosko, Wilk and Nusair functional III) Correlation and 81% LYP Correlation.

For more detailed description of the methods see, for example, Ref. [81].

1.5 Definition of goals and outline of the work

The main goal of the work is to develop a method for the identification of the IR lines of a molecular species, of which the UV/VIS absorptions are known. For this purpose a reactive rather than an inert matrix is applied and the changes in the spectra are induced by a photochemical reaction. As a reactive reactant oxygen was chosen. The selectivity of photo-oxidation is provided by laser light exposure at the wavelength of the UV/VIS absorption of the considered species. The outline of the work is as follows.

- In chapter 2 the experimental setup and procedure will be described in detail.
- Since not very much is known about the absorptions of carbon species in oxygen matrices, chapter 3 compares the spectra in oxygen matrices with that of the well known argon matrices. The aim of this chapter is to find the

absorption positions of known carbon species, e.g. by extrapolating the data of rare gas matrices to oxygen matrices.

- Chapter 4 is divided in two parts. In the first part the method of selective laser-induced oxidation of carbon species will be discussed of which UV/VIS as well as IR absorptions are known (C_6 , C_9 – C_{13}). Conclusions concerning the selectivity and applicability of the method will be drawn. The second part contains the description of the selective photo-bleaching experiments of C_{15} . At present the infrared absorptions of the C_{15} molecule are not identified, while the electronic absorption of this molecule has been already measured [72]. The assignment of the C_{15} infrared active absorption in O_2 , Ar and mixed (Ar + 10% O_2) will be made in this chapter. Also the correlations between UV/VIS and IR absorptions of unidentified oxides will be discussed. Attempts will be made to identify the carriers of some of these absorptions.
- In chapter 5 experiments with isotopic oxygen substitution will be described. The goal of these experiments is to find out which IR absorptions in oxygen-containing matrices originate from oxides. For this purpose ^{16}O was substituted by the ^{18}O isotope. $^{18}O_2$ -, (50% $^{18}O_2$ + 50% $^{16}O_2$)-, (Ar + 10% $^{18}O_2$)-matrices were produced and a comparison with similar ^{16}O -containing matrices is performed. The assignment of the C_6O_2 infrared absorption will be described. Implication regarding other carbon chain oxides will emerge.
- Conclusions concerning the laser-induced oxidation technique as a method for carbon species identification and other results of the work will be summarized in chapter 6.

2. Experimental setup and procedure

The whole experimental setup (Fig. 2.1) was designed for measurements of infrared and ultraviolet spectra of matrix isolated carbon clusters [92]. All experiments can be performed under low temperature (usually 7 – 40 K) and vacuum (order of 10^{-7} mbar) conditions. The IR and UV/VIS spectra can be recorded simultaneously from the same matrix sample.

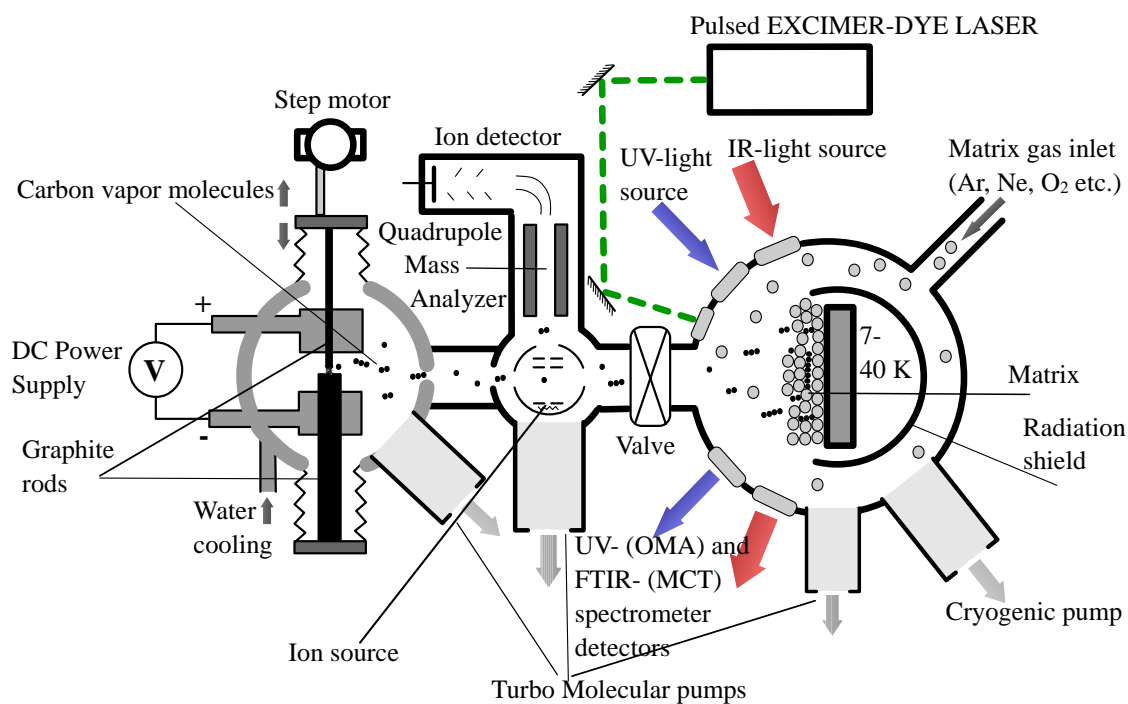


Fig. 2.1: Experimental setup

2.1 Carbon source and quadrupole mass spectrometer

The resistive heating source is used for production of carbon vapor. Between two graphite rods (diameter 3mm and 6mm respectively) a DC voltage is applied. The rods are brought into contact under vacuum conditions ($<10^{-7}$ mbar). The 3mm rod serves as anode and the 6 mm rod as cathode such that the electrons from the thick electrode heat up the thin rod. The voltage can be adjusted in the range 0–15 V. Currents (up to 70 A) heat up the rods to temperatures $>2500\text{K}$ where evaporation of carbon starts. The hottest spot is at the contact point on a thin rod and most carbon molecules are emitted from there.

The graphite rods have <2 ppm of impurities. In order to drive out volatile impurities (as e.g. adsorbed gasses), the carbon rods are baked prior to evaporation for about 3 hours at $\sim 1000\text{K}$ under vacuum.

The rods are inserted in two water-cooled copper contacts in such a way that it is possible to move them along their axes. The motion of a 3mm rod is controlled by a step motor. During evaporation the speed of a thin rod is usually 2–3 mm/sec. Such motion provides quasi uniform evaporation of a thin rod.

Carbon vapor contains mostly small molecules: C(20–50%), C_2 (10–30%), C_3 (50–70%). The abundance of different species can be controlled by the current through the rods. High currents (with high temperature as a consequence) provide more atomic carbon while at low currents one can observe also larger molecules like C_5 . The pressure in the oven during evaporation rises to about 10^{-5} mbar.

The composition of the carbon vapor and impurity gases in the vacuum we monitor by Balzers quadrupole mass spectrometer QMG421. The available range of masses is 0–1024 amu with maximal resolution 0.03 amu.

The impurity gases in our oven chamber are H_2O , N_2 , O_2 , CO_2 and some hydrocarbons. During carbon evaporation, the abundance of CO_2 , C_3O and CO in the oven compartment increases. In order to prevent matrix contamination from these molecules an additional turbo molecular pump installed between the oven and the matrix isolation chamber [93].

2.2 Matrix isolation chamber

This chamber is made of one block of aluminium with several openings for windows. On the axis with the molecular carbon beam coming from the oven, a matrix substrate is installed. As a substrate a rhodium coated sapphire front mirror is used. The reason for taking sapphire is a good thermal conductivity of this material. The Rh-coating is hard enough against wiping and has a good reflectivity in UV/VIS: >50% for wavelengths >200nm and >80% for wavelengths >380nm.

The substrate is cooled by DE-204SL two-stage helium expander (APD Cryogenics Inc). The lowest reachable temperature of the substrate is $\sim 7\text{K}$. On the back side of the substrate a transistor (BUZ45A) is attached which is used as a heater. One can keep the definite temperature of the substrate during entire experiment or change it to predefined values. A thermal contact between substrate, cryostat and transistor provides a layer of indium. The temperature of the substrate is measured by a gold-chromium thermocouple, attached to Lake Shore 330 temperature controller.

To protect the substrate from thermal radiation of the environment, a radiation shield is installed. An additional mechanical shutter protects the substrate from deposition of impurities (H_2O mostly). The shutter can be closed when no spectral measurements are carried out.

The vacuum in the chamber is provided by a turbo molecular pump and a cryo pump (Displex HV202-8C, Air Products). The quality of the vacuum in the matrix isolation chamber is $\sim 10^{-7}$ mbar.

For producing matrices we used different gases: Ar (99.9999%, Messer Griesheim), $^{16}\text{O}_2$ (99.998%, Messer Griesheim), $^{18}\text{O}_2$ (99%, Isotec), Ne (99.9999%, Messer Griesheim), Kr (99.99%, Messer Griesheim), Xe (99.99%, Messer Griesheim), N_2 (99.9999%, Messer Griesheim), CO (99.997%, Messer Griesheim) and their mixtures. An additional oxygen filter was installed to increase gas quality (except for O_2 -matrices, of course). If mixtures of gases were needed, the gases were premixed in a separate tank before deposition. Residual water vapor and CO_2 impurities from a matrix gas were captured in a metal porous trap, cooled with liquid nitrogen. The gas flow for the matrix was controlled by mass flow controller (Tylan General FC-280). The gas speed was usually adjusted to get $\sim 10^{-4}$ mbar pressure in the matrix

2 Experimental setup and procedure

isolation chamber during matrix deposition.

For IR light transmission through the matrix chamber, NaCl windows are used. The input/output windows for UV/VIS light are of quartz glass.

2.3 Infrared spectrometer

Our lab is equipped with the Fourier-Transform Infrared (FTIR) spectrometer (IFS 113v, Bruker), which operated under vacuum condition $\sim 10^{-2}$ mbar.

The Bruker 113v FTIR spectrometer is coupled with a visible bench and is designed to work over the frequency region 20 cm^{-1} to 20000 cm^{-1} with an instrumental resolution down to 0.03 cm^{-1} . It is equipped with three light sources (a mercury arc-lamp, a silicon carbide globar (from "glow bar") and a tungsten halogen lamp). It has 6 detectors (Silicon bolometer for FIR, DTGS/PE for FIR, DTGS/KBr for MIR, MCT for MIR, InSb for NIR, Si diode for VIS) and 6 beamsplitters (Si/CaF₂, Ge/KBr, 3.5 m Mylar, 6 m Mylar, 23 m Mylar and 50 m Mylar). The instrument is carefully aligned to optimize far infrared measurements.

In our experiments we used a "Globar MIR" light source and a Ge/KBr beamsplitter. The available range of the liquid nitrogen cooled MCT (Mercury Cadmium Tellurite) detector is $400 - 4000\text{ cm}^{-1}$. Most of the recorded IR-spectra have a resolution 0.3 cm^{-1} .

For the matrix-isolation measurements we used a reflection-transmission mode: light from the globar source goes through a matrix layer, is reflected by the mirror, goes a second time through the matrix layer and then reaches the detector. The IR light angle of incidence is 65° .

2.4 UV/VIS spectrometer

All UV/VIS-spectra were recorded by an Optical Multi-channel Analyzer (OMA) (Model 1236, EG&G). It consists of *Czerny-Turner* monochromator with 50 cm focal length, and a multichannel plate intensifier coupled by a fiber optics to a silicon photodiode array with 1024 elements (Model 1456R-990-HQ). The photodiode array is cooled to 233K by a two-stage Peltier element in order to decrease the noise.

The monochromator has 3 different gratings (147, 600 and 1200 grooves/mm).

The available range of measurements is 180 – 900 nm. The resolution is defined by the grating and the width of the monochromator's input slit. The maximal resolution with the third grating (1200 g/mm) is 0.1 nm (50 μ m input slit width). With the same slit width the second grating allows measurements with 0.2 nm resolution, and the first one gives 1.6 nm.

Before recording a spectrum, we calibrated the spectrometer, using mercury and argon calibration lamps.

For the absorption measurements an UV/VIS light source is required. We applied a deuterium lamp (30 W, Hamamatsu L1626) and for the longer wavelengths in visible range — a tungsten halogen lamp (50 W). The light from a lamp to the matrix isolation chamber and from the chamber to the spectrometer is transmitted through optical fibers. The UV/VIS light has an angle of incidence of 25°

2.5 Excimer-Dye Laser

The pulsed Excimer (XeCl) laser (EMG 210MSC, Lambda Physik) generates an output beam at 308 nm (average power \sim 2 W). The laser pulse duration is about 20 ns at 50 Hz repetition rate.

In order to get other wavelengths, a Dye Laser (FL3002, Lambda Physik) is used, which is pumped by the 308 nm beam from the Excimer laser. Applying different dye solutions one can obtain any wavelength in the range 332–970 nm. The yield of different dyes can be found in [94]. Usually, it is about 10–20%. The bandwidth of the output beam is 0.2 cm⁻¹ and wavelength accuracy is 1 Å.

The use of frequency-doubling KPB (KPb₂Cl₅) crystal (FL-32) allows also to get shorter wavelengths 230–275 nm, and for the KDP (Potassium Dihydrogen Phosphate) crystal FL-30 – 280–348 nm.

The Dye Laser can be operated in the scanning mode. In this mode the wavelength of the output beam continuously changes within a predefined range. This range is limited by a applied dye.

The laser beam, after being reflected by two mirrors reaches the substrate with an incidence angle of 25°.

2.6 Experimental procedure

Normally the procedure of an experiment is as follows:

- Pumping all chambers of the experimental setup to about $\sim 10^{-7}$ mbar.
- Cooling down a substrate for a matrix.
- Recording of IR and UV/VIS background spectra.
- Codeposition of matrix gas and carbon vapor molecules from the oven. During the deposition we monitor matrix growing process by IR and UV/VIS spectra measurements.
- Measuring final UV/VIS and IR spectra of a prepared matrix sample.
- Subjecting the matrix to different processes as e.g. temperature cycling (annealing), laser irradiation, continuous UV-light.
- Measuring of UV/VIS and IR spectra again and comparing with the previous spectra.

3. Comparison of C_n absorption spectra in solid Oxygen and Argon

3.1 Introduction

Electronic absorptions of carbon chains in Ne-matrices were assigned by employing of mass selection technique [70, 71, 72]. In Ar-matrices, the absorption lines are shifted to somewhat lower energies.

Infrared active vibrations of carbon molecules are studied extensively by many research groups. Most of known the information is reviewed in [20].

In studies of carbon molecules so far mainly unreactive matrices were employed. The introduction of reactive matrices considerably changes the situation. In this case a matrix plays a role not only as a host medium, where molecules are trapped, can diffuse and conjugate, but also as a reactant. Two general complications arise:

- the diffusion and reaction between carbon molecules competes with chemical reactions with matrix material; as a consequence
- the already complex C_n spectra become even more complicated due to the presence of reaction products with matrix molecules.

As a reactant matrix oxygen can be applied. It is known that carbon molecules like polyynes can be easily oxidized. Another reason is that oxygen condenses in vacuum at relative high temperatures (less than 51K), and that it is transparent in the infrared and most of UV/VIS region. Furthermore, the study of oxides of carbon can be interesting in the astrophysics of the interstellar medium since oxygen is a similar abundant element in space as carbon, as was already mentioned in the introduction.

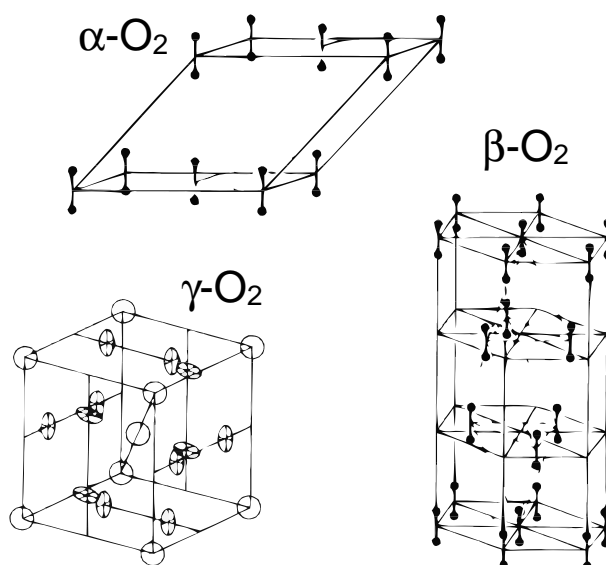


Fig. 3.1: Crystal structures of solid Oxygen (after Ref. [99]).

Matrix isolation spectroscopy in oxygen was applied in studies of different molecules and clusters: i.e. NO, N₂O₄ [95], Cu_n [96], O₃ [97], SO₂ [98], and many others.

Oxygen is an exceptional molecule since it has a triplet ground state, i.e. has two valence electrons with parallel spin. This feature makes O₂ paramagnetic. As a solid at equilibrium vapor-pressure oxygen can form 3 different crystalline structures. At low temperatures (less than 23.8K) it assumes the α -phase with a monoclinic lattice. The β -phase with a rhombohedral lattice occurs between 23.8 and 43.8K. The γ -phase (43.8K–51K) possesses a slightly disordered cubic lattice with 8 molecule in a unit cell (Fig.3.1). α - and β -phases reveal antiferromagnetic properties, while γ -oxygen is paramagnetic [99]. By trial and error we have found that the optimal deposition temperature for our experiments is 25K, i.e. the matrix has the β -phase. At such temperature one can produce enough long chains and the IR absorption lines have no splitting as in the α -phase. Furthermore, under these conditions the matrices are sufficient homogeneous, i.e. transparent and nearly free of scattering.

3.2 Experiment details

The experimental setup was described in chapter 2. As a carbon source the resistive heating source was used. The carbon molecules were co-deposited with pure oxygen (99.998%) on cold substrates at different, but during the process fixed temperatures ranging from 8K to 36K. The approximate ratio of carbon to oxygen atoms was kept at about 1:1000. Infrared and UV/VIS spectra were measured from the same sample. Different mixtures of Ar and O₂ were also used as matrices, IR- and UV/VIS- spectra of carbon and carbon oxides molecules in those matrices were measured at 25K.

3.3 Results and Discussion

In Fig.3.2 one can see the sequence of almost equidistant absorption features in UV/VIS which corresponds to singlet-singlet electronic transitions of long linear odd chains C_n ($^1\Sigma_u \leftarrow X^1\Sigma_g$) in an inert Ar matrix. Such sequencing with the number of carbon atoms is also known for the chains of hydrocarbons [100]. In an oxygen matrix we also observe a progression of absorptions (Fig.3.2) like in argon. Their positions are close to those in an Ar-matrix. The similarity indicates that pure carbon species at least partly survive in an oxygen surrounding. Nevertheless one has to be careful in absorption assignments since the sample definitely contains also oxides of carbon. The oxide absorptions may be masked by the carbon features. As was mentioned in [74] there is an electronic transition with very big oscillator strength for chain molecules with a singlet electronic ground state. These molecule are C_{2n+1}, C_{2n+1}O, OC_{2n+1}O. Our configuration interaction calculation also indicates that long C_n chain molecules with singlet ground state have big oscillator strength (for example, C₉ – 300.6 nm with oscillator strength 5.9, C₁₅ – 434 nm with oscillator strength 8.5). The calculated absorption positions agree quite good with experimental data. CI-calculation of electronic transitions for oxides of carbon chains suggests that these oxides absorb in the same region where pure carbon chains do. From our calculations the absorption of a monoxide of a carbon chain is shifted about 10 nm to longer wavelengths (for example, C₉O – 307.8 nm with oscillator strength 5.8, C₁₅O – 443.5 nm with oscillator strength 7.5).

Analysis of IR-spectra of C_n in Ar- and O₂-matrices reveals more differences

3 Comparison of C_n absorption spectra in solid Oxygen and Argon

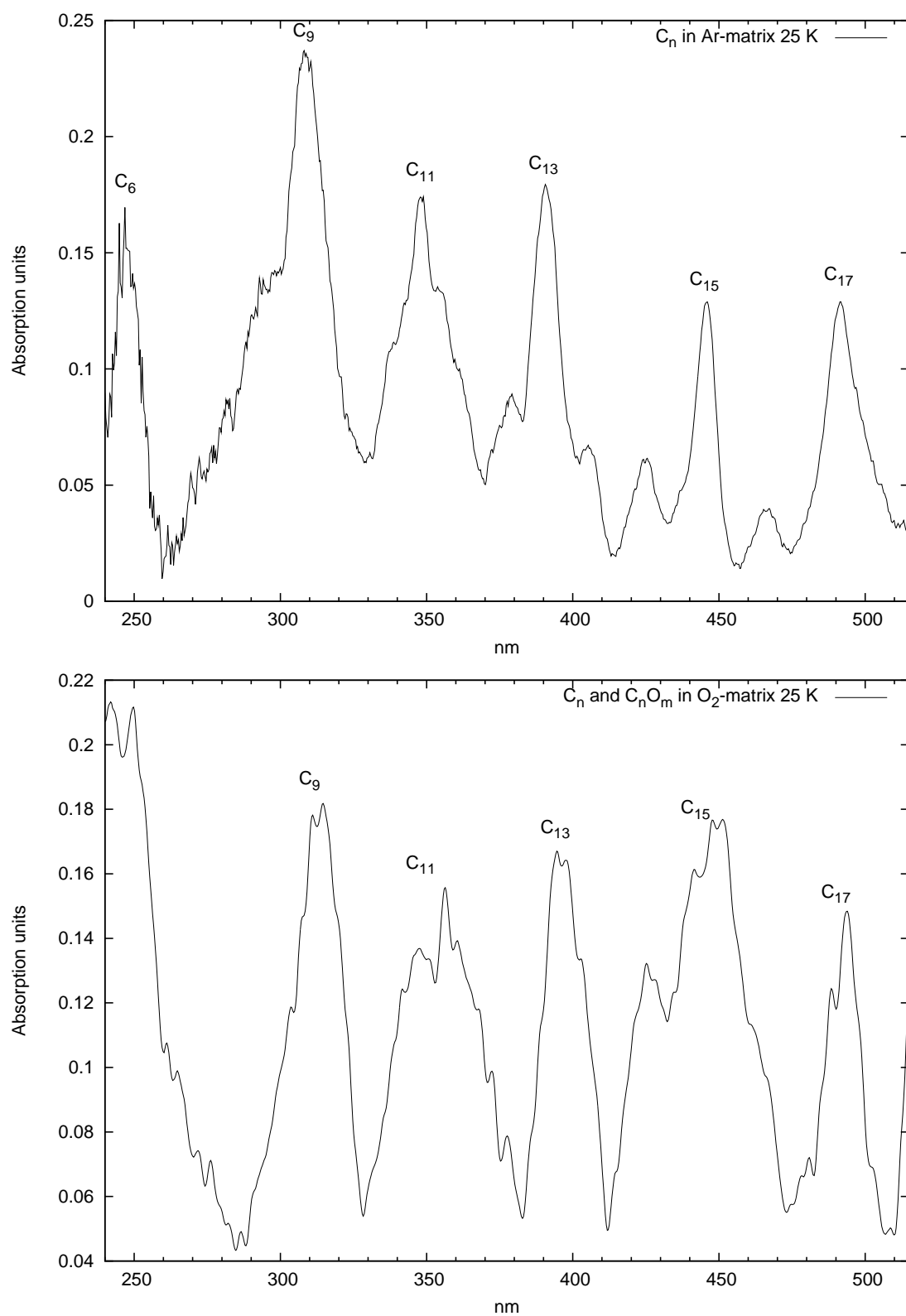


Fig. 3.2: Baseline-corrected UV/VIS-spectrum of carbon chains in Argon and Oxygen matrices after annealing to 25K. Absorption features of C_n in O_2 are almost unshifted relative to C_n in Ar.

(Fig.3.3). First, we have a matrix shift which varies from -10 to +10 cm^{-1} relative to an Ar-matrix. Second, we have new lines which consequently should be assigned to carbon oxides (absorptions of known and unidentified carbon oxides are reviewed in chapter 5). Nevertheless IR-active vibrational absorptions of pure carbon molecules are still in the O_2 -matrix .

Different mixed (Ar + O_2) matrices were created and smooth transitions of IR-lines from 100% Ar-matrix to 100% O_2 -matrix were observed (Fig. 3.4,3.5). On one hand this provides information about positions of carbon molecules absorptions in a pure O_2 -matrix and on the other hand this is one more evidence that pure carbon species exist in an oxygen matrix.

An interesting feature in oxygen matrices is the intense absorptions at 1800 and 1840 cm^{-1} . Corresponding lines in an Ar-matrix located at 1803 and 1844 cm^{-1} and are very small. Addition of oxygen leads to considerable increase of these two absorptions. So, this is the first indication that these absorptions may be oxides. In matrix studies of other researches these two absorptions at 1803 and 1844 cm^{-1} in argon were tentatively assigned as C_{13} (by [62]). At the same time the infrared absorption at 1844 cm^{-1} was assigned as a cyclic C_8 molecule [60, 61]. In order to figure out whether or not the absorptions at 1803 and 1844 cm^{-1} in Ar are oxides, ^{18}O isotopic substitution of oxygen was made. The shifts of these lines observed after ^{18}O substitution, support our assignment of these absorptions as oxides. The experiment and results described in the chapter 5.

The probable reason for the low abundance of even carbon chains in an oxygen matrix is the triplet ground state of these species. The oxidation of molecules in a triplet state goes much faster than the oxidation of singlets. The relative absorptions of C_6 , C_8 , C_{10} to the absorption of C_9 (with singlet ground state) are smaller in an oxygen than in an argon matrix.

The obtained IR-spectrum of matrix isolated carbon molecules in the α -phase oxygen matrix at 8K presented on Fig. 3.6. The prominent absorption belongs to C_3 which is the most abundant molecule in carbon vapor. Upon annealing of matrices or deposition at elevated temperatures C_3 is consumed to form large chains. The molecular absorption lines experience broadening and splitting. There is an interesting feature in the spectrum – the presence of the Raman-active O_2 -line at 1550 cm^{-1} .

3 Comparison of C_n absorption spectra in solid Oxygen and Argon

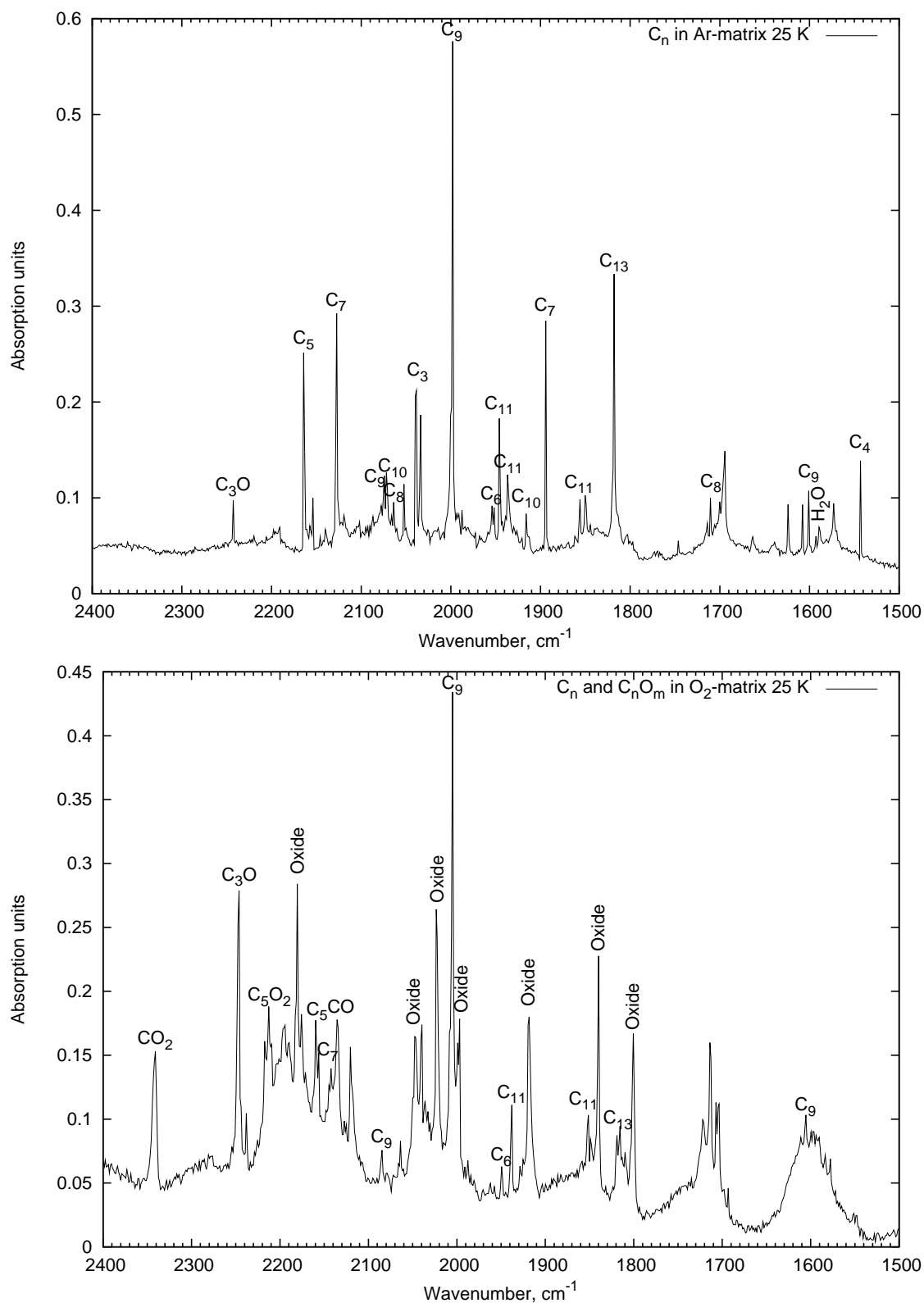


Fig. 3.3: IR-spectrum of carbon chains in Argon and Oxygen matrices after annealing to 25K. Low abundance of even-numbered carbon chains in O₂ is due to a triplet electronic ground state and high reactivity as a consequence.

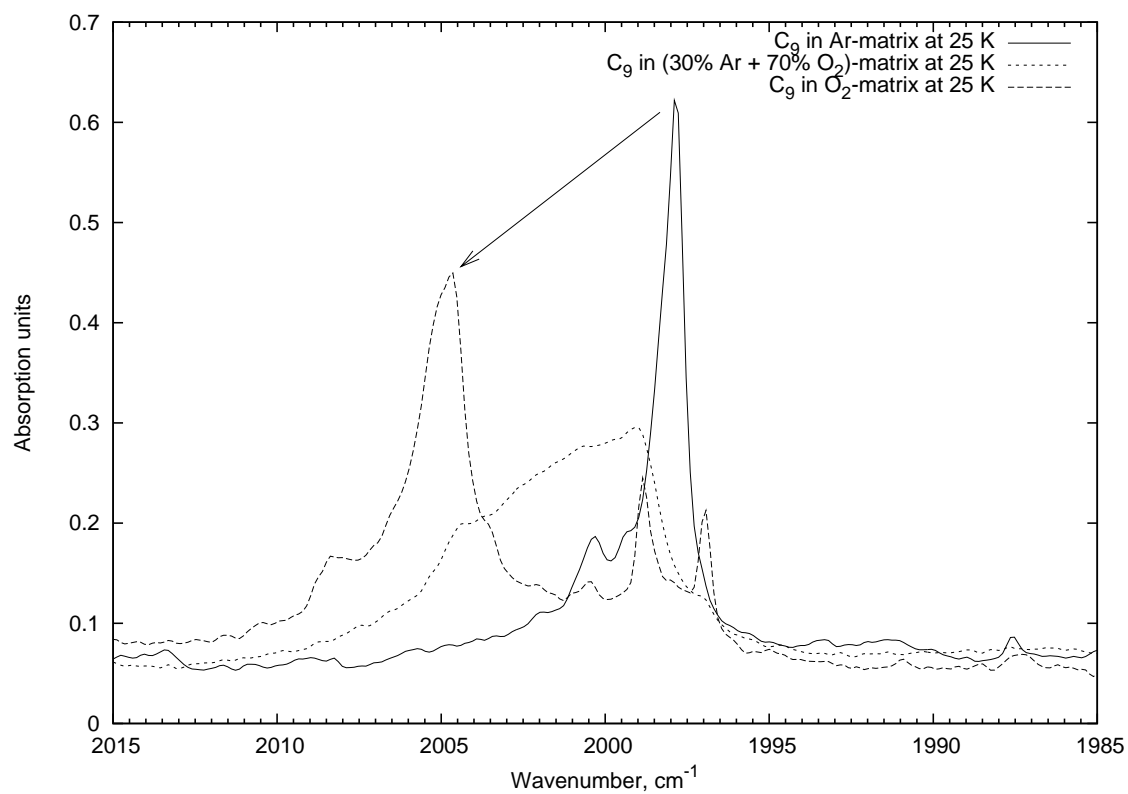


Fig. 3.4: C₉ IR-absorption in Ar-, O₂- and mixed matrices. The mixed matrix (30% Ar + 70 % O₂) probably has no regular crystal structure, therefore absorptions in this matrix are broad and have no well defined position.

3 Comparison of C_n absorption spectra in solid Oxygen and Argon

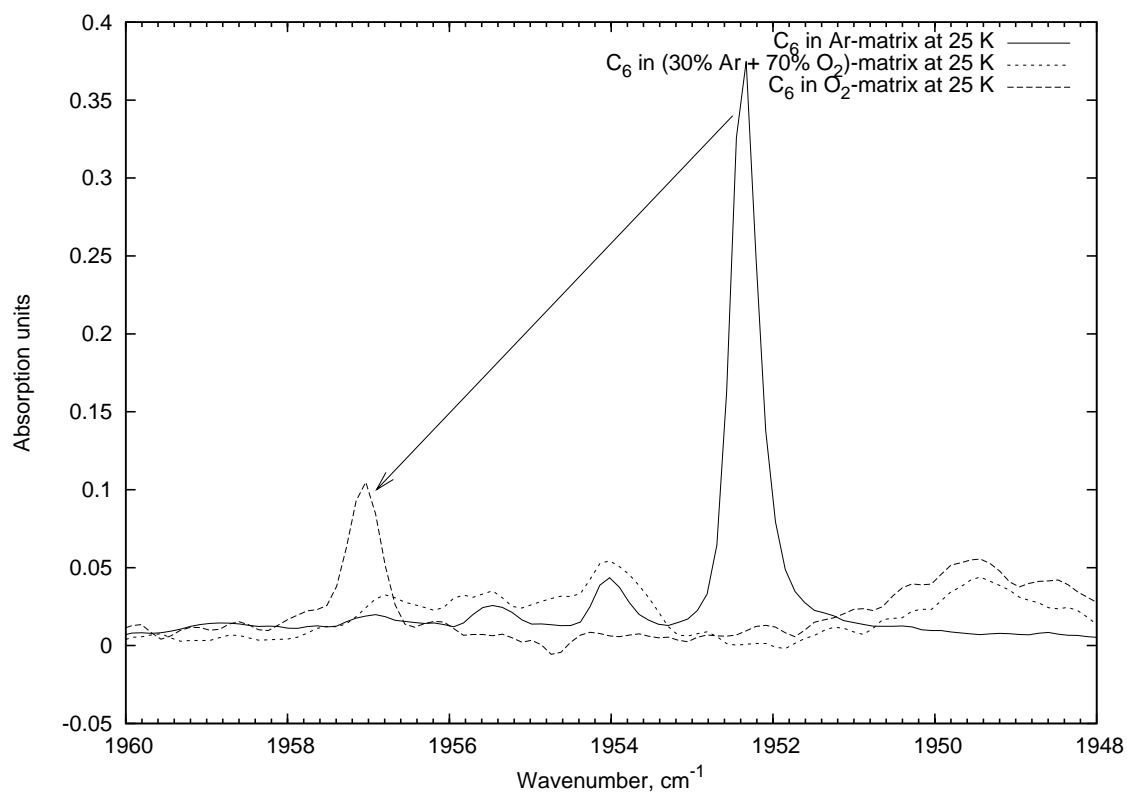


Fig. 3.5: C_6 IR-absorption in Ar-, O_2 - and mixed matrices. In the mixed matrix the C_6 absorption can be hardly seen probably due to the absence of regular matrix structure and low abundance of C_6 as a reactive molecule with a triplet ground state.

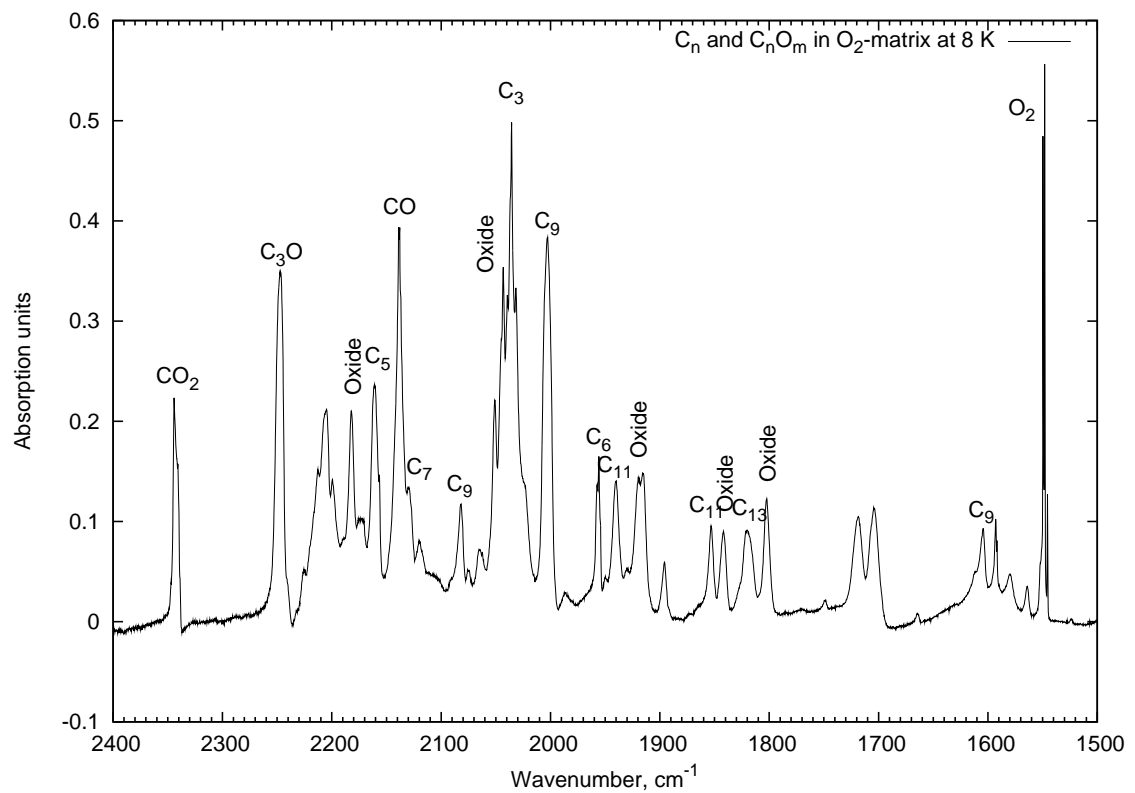


Fig. 3.6: C_n IR-absorptions in α -phase O_2 -matrix. The interesting feature in the spectrum – a raman-active O_2 -line at 1550 cm^{-1} .

3 Comparison of C_n absorption spectra in solid Oxygen and Argon

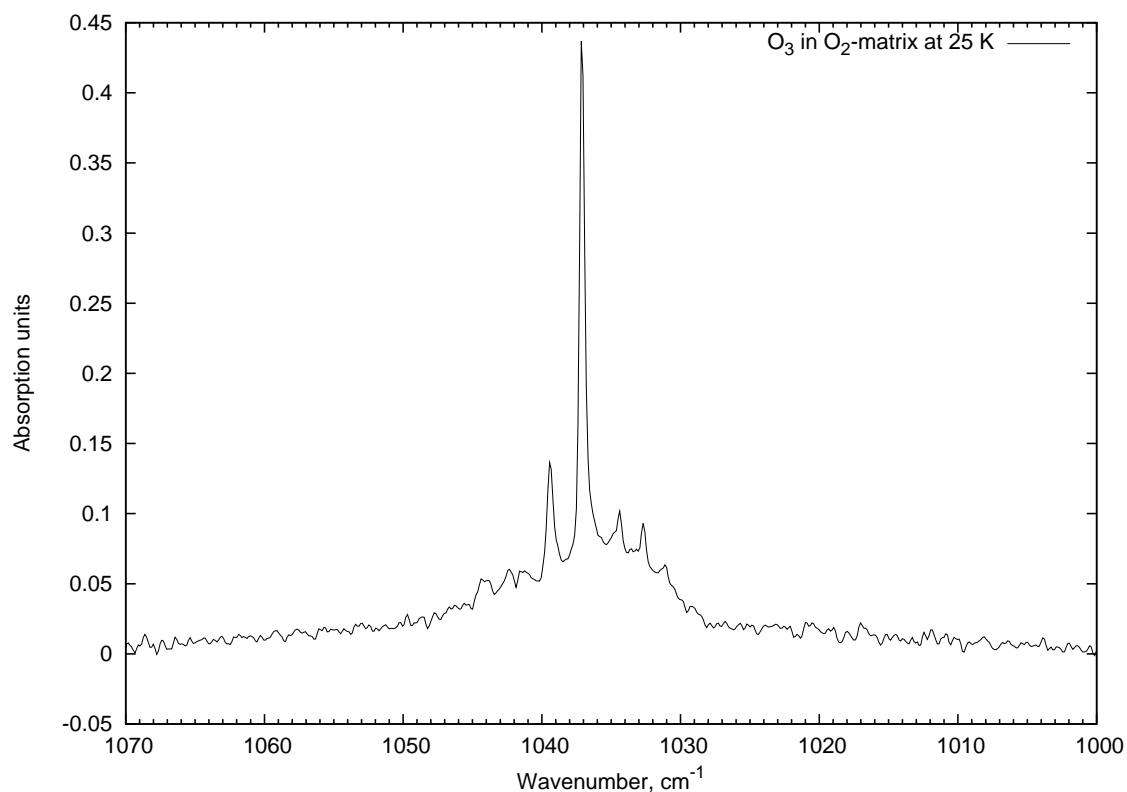


Fig. 3.7: O_3 IR-absorption in an O_2 -matrix. The distribution of peaks is not only due to site effects, but also due to ozone dimers, trimers and depends on O_3 concentration in the matrix [101].

Another remarkable feature in an O_2 -matrix is the O_3 absorption at 1040 cm^{-1} (Fig. 3.7). It is mostly produced in chemical reactions of carbon molecules and oxygen, leading to atomic oxygen which forms O_3 .

So, pure carbon molecules survive after oxygen addition to the rare-gas matrix and still exist in pure oxygen matrices. The mixed matrices ($Ar+O_2$) provide information about absorptions of carbon molecules in a pure oxygen matrix.

4. Selective laser-induced oxidation of carbon molecules

4.1 Introduction

There are several known types of photochemical reactions: simple fragmentation, isomerization, photo-ionization, photoinduced addition, fragmentation followed by reaction, atom transfer reaction, photo-electron transfer reactions, and intermolecular complex formation [102]. Many photochemical reactions with oxygen in cryogenic matrices were investigated. For example, photolysis of *cis*-2-butene C_4H_8 gives products such as *trans*-2-butene, CH_3CHO , CO_2 , CO and O_3 [103]. Another example is photo-oxidation of $(SO_2)_2$ in an oxygen matrix [98] with SO_3 as a product. The reaction mechanism involves excitation to a *charge-transfer* state which may react to form photoproducts [102]. Many inorganic species show charge-transfer absorption and are called charge-transfer complexes. For a complex to demonstrate charge-transfer behavior, one of its components must have electron donating properties and another component must be able to accept electrons. Absorption of radiation then involves the transfer of an electron from the donor to an orbital associated with the acceptor. The large molar absorptivities of these transitions are due to the large electric dipole moment changes resulting from the electrons transfer across relatively large regions of a complex.

Irradiation with the laser at a definite wavelength (corresponding to known electronic absorption of C_n) in UV sometimes leads to a decreasing of absorption lines in IR-spectra. For the first time it was observed for linear C_6 in solid Ne [104]. This molecule was the only carbon chain which was successfully depleted in that matrix. There is no common accepted explanation for this observation. The C_6 depletion may occur by multi-photon absorption, leading to an excited energy-state in which

the molecule can be "broken" and parts of it could react with neighbor-molecules. One may speculate about oxide formation by oxygen impurities, but no increase of oxides was observed. Another, however insufficient, explanation is changing of the molecular orientation in a matrix, i.e. changing of sites [104]. In any case, electronic excitation from the ground state leads to the "expansion" of the electron wavefunction and a reactive surrounding like oxygen can be very helpful to stimulate chemical reactions. Indeed, the experiments with O₂-matrices have shown that it is also possible "to kill" selectively carbon molecules others as C₆. In this case we have carbon oxides as a reaction products.

So, the strategy of IR-lines identification can be as follows:

1. Tuning the laser frequency to a known UV-absorption of a specific carbon cluster, and irradiating the matrix sample.
2. Looking for correlation in changes between UV/VIS and IR spectra of that known species.
3. Test of selectivity and efficiency of the method.
4. Selective oxidation of carbon species with known UV-absorption, but unknown IR-absorption. Identification of vibrational transitions.

The photooxidation experiments in the O₂-matrices were made in the β -phase at 25K for reasons, discussed on page 30.

4.2 Test of the method on known carbon chains

Concerning the selectivity of photooxidation, there is a difficulty which has to be considered: we have a mixture of different C_n molecules in our matrices, and the strong $^1\Sigma_u \leftarrow X^1\Sigma_g$ electronic absorption profiles of C_n-species move with n into the red. There are usually weak absorptions at the red portion of such strong transitions [72]. The detailed absorption of C_n are not well known in Ar and O₂ matrices. Therefore, in irradiating a particular C_n molecule one may accidentally excite a cluster C_m with m < n. We thus applied a strategy of "killing" shorter carbon chains before we irradiated longer C_n molecules.

4.2.1 Experimental details

The experimental setup was described in chapter 2. For the experiments reported here the carbon molecules were co-deposited with either a pure oxygen (99.998%) or with an argon-oxygen mixture (90% Ar + 10% O₂) on a cold substrate at 25K. The ratio of carbon to oxygen atoms was kept at about 1:1000. Infrared and UV/VIS spectra were measured from the same sample. The UV/VIS spectrum was recorded during 60 sec in order to minimize the effect from UV-irradiation by the deuterium lamp. The first grating was used (147 g/mm) with a slit width 350 μm , yielding a spectral resolution of 4.6 nm. The measurement of the IR-spectra were made with a resolution 0.3 cm^{-1} and 1000 scans were accumulated.

After deposition, the matrix was exposed to laser irradiation at different wavelengths. The sequence of irradiations in every matrix sample is shown in the Table 4.1.

For photooxidation of C₉ the attenuated pump beam from XeCl laser with 308 nm wavelength was used. For other molecules, the dye-laser with different dye solutions was applied: DMQ (LC3590) for C₁₁, QUI (LC3690) and PBBO (LC4000) for C₁₃, Coumarin 2 (LC4500) for C₁₅. Data on the yields of the different dyes can be found in Ref. [94].

C₉: Irradiation of C₉ was performed during 1 hour in an Ar-O₂-matrix and during 80 min in an O₂-matrix. The strong laser pump beam was attenuated in order to avoid substrate damage. The approximate average power was 10 mW.

C₁₁: The UV-absorption of C₁₁ is located at 340 – 370 nm in an O₂-matrix. The pure O₂-matrix, which was already treated with 308 nm laser exposure, was again irradiated by laser in the scanning mode at wavelengths 350 – 364 nm during 160 min.

The mixed matrix (90% Ar + 10% ¹⁸O₂) was irradiated at the fixed wavelength 357 nm during 80 min. The matrix had been previously irradiated with 308 nm laser for 50 min.

1800/1840-oxide(s): In case of the pure O₂-matrix laser exposures at 397 nm were carried out during 140 min. The matrix was previously irradiated at 308 nm for 80 min and at 350 – 364 nm for 160 min.

C₁₃: For photobleaching of C₁₃ in a pure oxygen matrix, the laser was applied

4 Selective laser-induced oxidation of carbon molecules

Matrix	Excitation wavelength, nm	Duration, min	Molecule
Ar + 10% $^{16}\text{O}_2$	308	60	C_9
$^{16}\text{O}_2$	308	80	C_9
	350–364	160	C_{11}
	397	140	1800/1840-oxide(s)
$^{16}\text{O}_2$	308	120	C_9
	350–364	160	C_{11}
	397	140	”1800/1840” -oxide(s)
	438–455	330	C_{15} and ”1704”-oxide
	400–406	240	C_{13}
Ar + 10% $^{18}\text{O}_2$	308	50	C_9
	357	80	C_{11}

Tab. 4.1: Irradiation sequence in laser induced oxidation experiments. Four different matrices with different compositions were used.

in the scanning mode at 400–406 nm for 240 min . The matrix had been previously irradiated at 308 nm for 120 min, 350 – 364 nm for 160 min, 397 nm for 140 min, 438 – 455 nm for 330 min. For a better overview the exposure histories are displayed in Table 4.1.

4.2.2 Results and Discussion

The concentration of C_6 in an O_2 -matrix decreases spontaneously without any additional treatments like laser radiation. There are also small changes in other carbon species, but only C_6 decreases almost completely. Laser irradiation with different UV-frequencies or irradiation with a deuterium lamp just accelerates the process of C_6 depletion. The Fig.4.1 shows infrared spectra before and after 10 min irradiation with a deuterium lamp. The absorption of C_9 at 2005 cm^{-1} was decreased by 20%, the C_6 absorption at 1659 cm^{-1} was decreased by 89%. The changes of other known pure carbon molecules are negligible.

The barrier for reaction of C_6 with oxygen seems to be the lowest among infrared active carbon clusters. The high reactivity of this molecule may originate from its triplet ground state (all C_n with even n have triplet electronic ground states). That the other even species (C_8 , C_{10}) are low abundant in oxygen may have the same reason.

C_9 : For the first time we observed a selective photo-bleaching effect for this molecule trapped in an Ar- O_2 -matrix after irradiation with 308 nm laser light (Fig. 4.2). The abundance of C_9 was considerably decreased (91% in the IR, $85 \pm 10\%$ in the UV). But there are not only changes of the C_9 bands. C_6 was depleted by 97% and C_3 by 15%. The photooxidation of C_9 in a pure oxygen matrix is shown on Fig.4.3 The decrease of C_9 in the infrared spectrum was 94%. In the UV region the evaluation of decrease percentage could not be performed accurately because of baseline changes. Roughly, it is $80 \pm 15\%$ which is close to the data observed in the infrared spectrum. We also observe a increasing of CO_2 , C_3O , C_5O_2 and absorptions of some other unidentified oxides, which are absent in the rare gas matrices.

More than 90% decrease of C_9 is a very good indication of selective photooxidation reaction for this molecule. The C_3 -decrease is probably coming from a weak C_3 -absorption at the oxidation wavelength of 308 nm [72]. Possible products of the

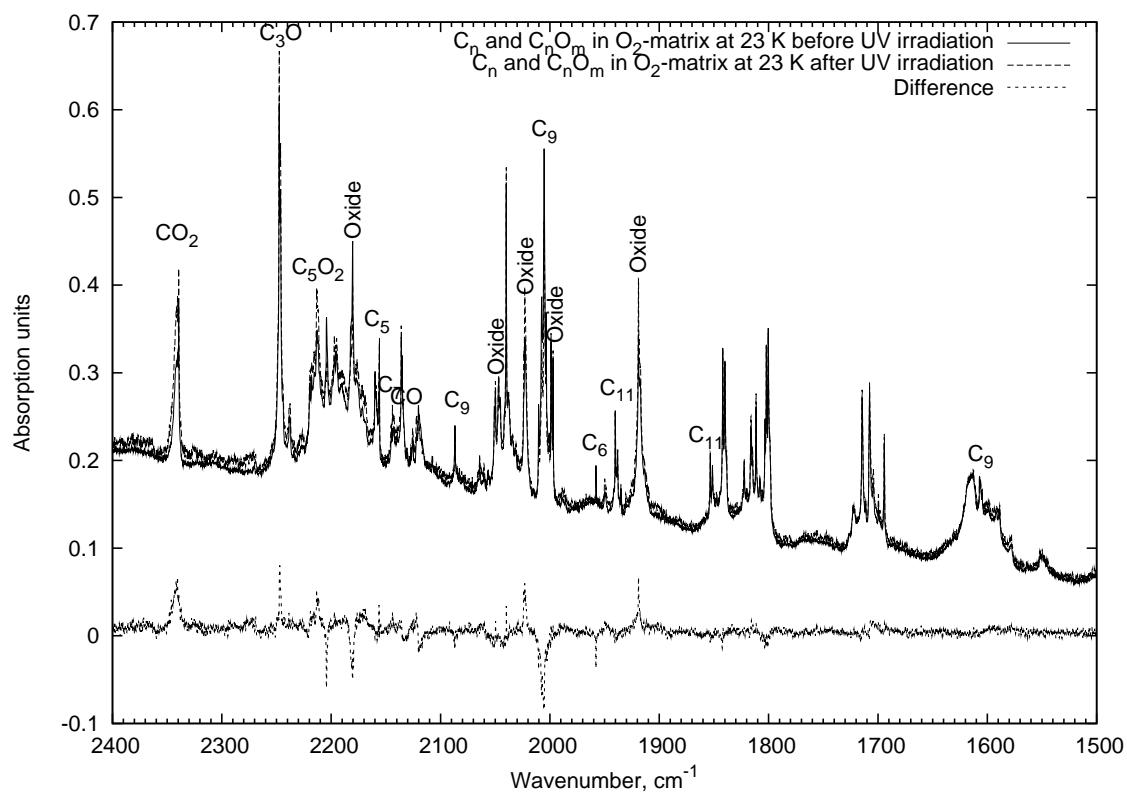


Fig. 4.1: IR-spectrum of carbon species in an O₂-matrix before and after irradiation with UV/VIS light from a deuterium lamp during 10 min at T=23K (α -phase). Notice the decrease of C₉ and that of the already depleted C₆

4.2 Test of the method on known carbon chains

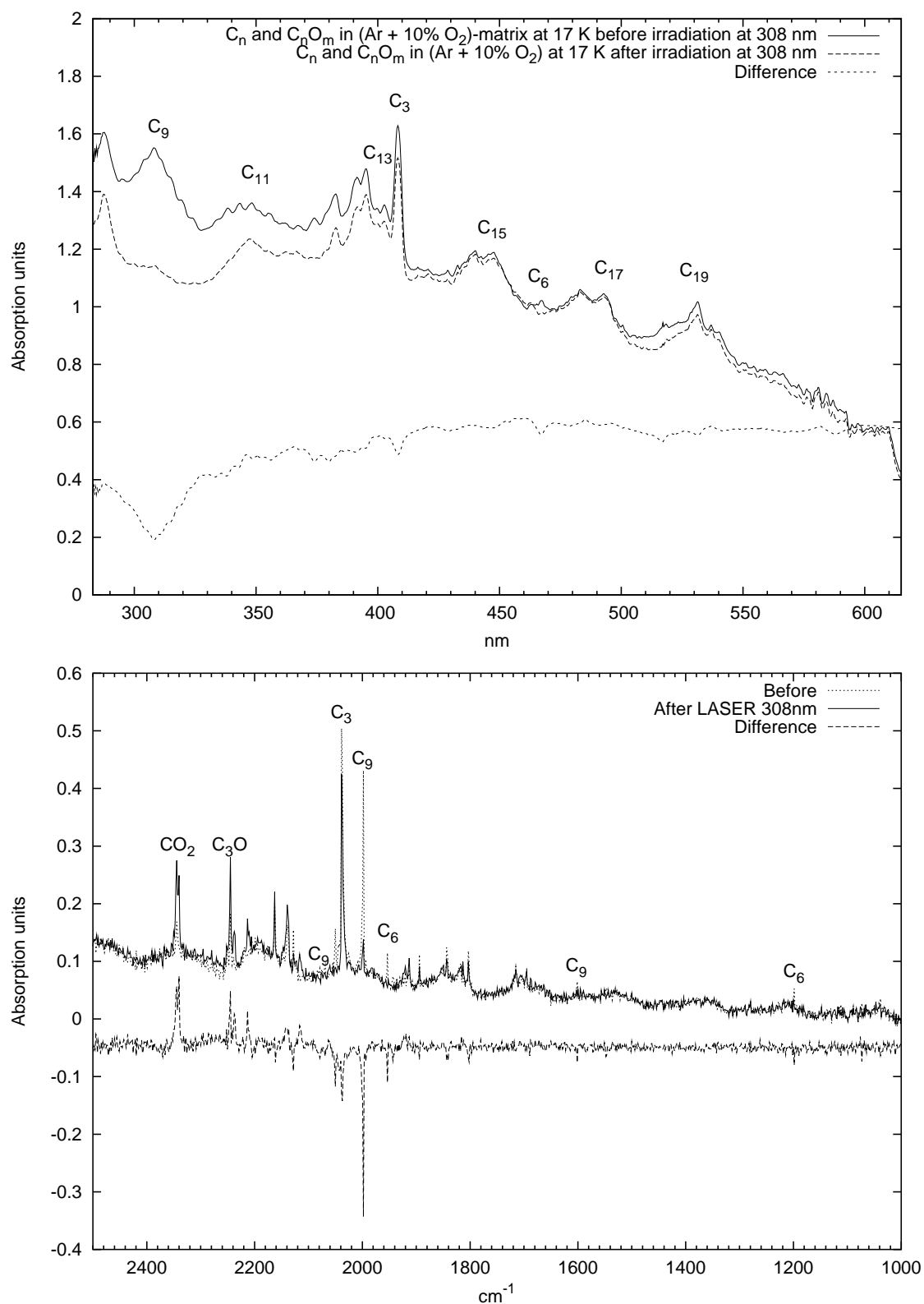


Fig. 4.2: UV/VIS and IR-spectrum. "Killing" of C₉ in Ar + 10% O₂ matrix during 1 hour at T=17K. Decrease of C₆ is due to high reactivity of this molecule with triplet ground state. Considerable increase of CO₂ and C₃O indicates that these molecules probably are the main products.

4 Selective laser-induced oxidation of carbon molecules

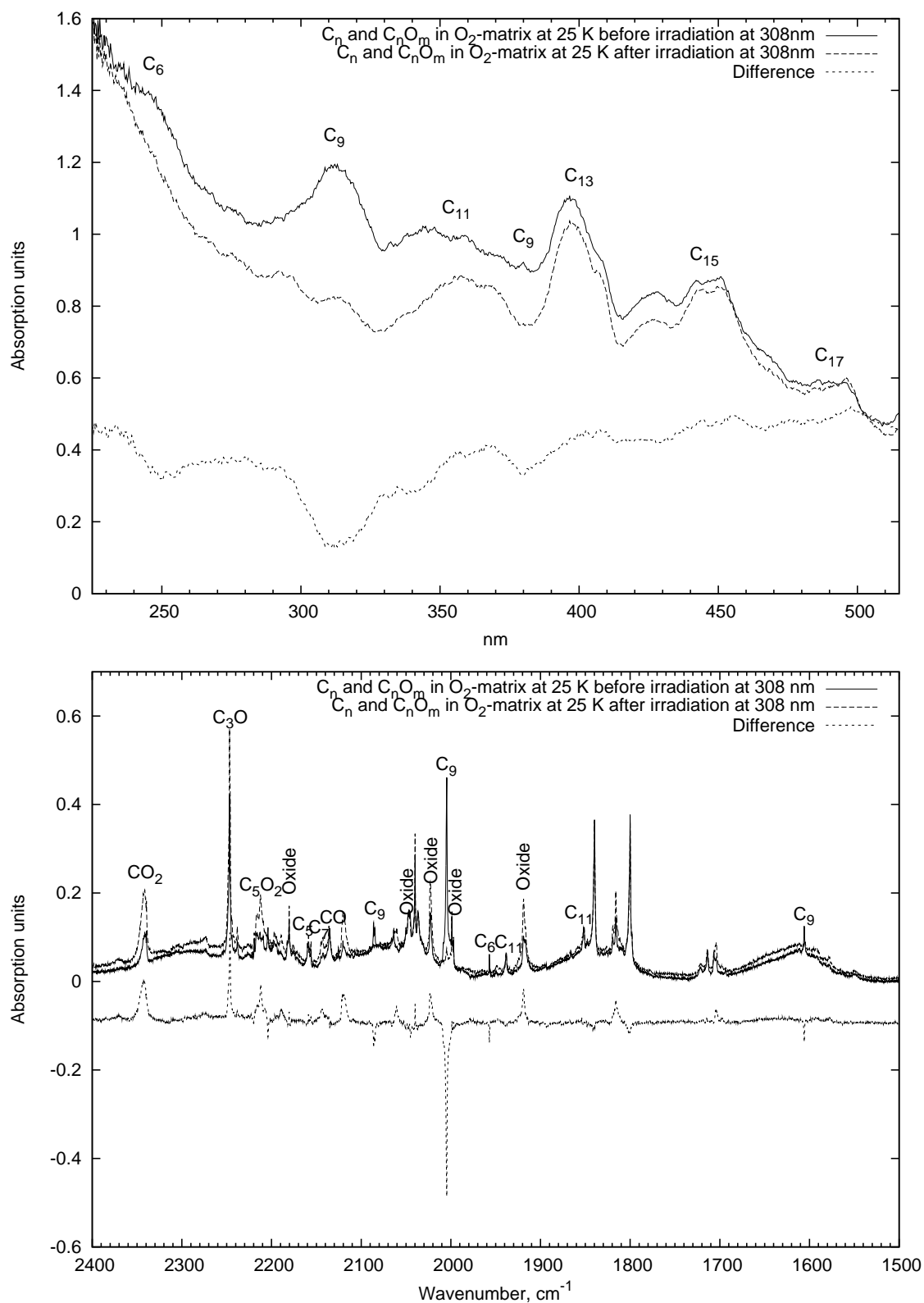


Fig. 4.3: UV/VIS and IR-spectrum. "Killing" of C₉ by 308 nm laser in a pure O₂ matrix during 80 min at T=25K. Almost complete decrease of C₉ indicates good selectivity of its photooxidation.

reaction of C_3 with O_2 are the oxides C_3O and CO_2 . All increased unidentified lines in the infrared spectrum probably belong to oxides of carbon since they do not appear in rare gas matrices. Among the known increased absorptions are that of CO_2 , C_3O and C_5O_2 . Probably, there are several possible reactions of C_9 with O_2 . It is most important and interesting for us that the other long carbon chains remained unchanged. The photooxidation of C_9 thus is sufficiently selective.

C_{11} : The infrared and UV/VIS spectra before and after irradiation in a pure oxygen matrix are presented in Fig.4.4. Differences of infrared absorptions after laser irradiation are summarized in the table 4.2. The most strongly decreased IR lines belong to C_5 , C_7 and C_{11} . In the UV we observe a broad feature decreasing in the range from 300 to 480 nm with maximal decrease at the C_{11} position (350–364 nm).

The spectra before and after laser treatment in a mixed matrix (90% Ar + 10% $^{18}O_2$) are shown on Fig.4.5. The only decreased lines in the infrared spectrum belong to C_{11} (-50%), C_6 (-25%) and C_9 (-10%). In the UV/VIS spectrum we observe again a decrease of a broad feature with pits at 357 (C_{11}), 380 and 409 nm (C_3). The decreasing of C_{11} (330 – 370 nm) is 30%.

In all bleaching experiment with pure oxygen matrices only the lines of C_{11} could be depleted entirely, i.e. by 100%. The simultaneous depletion of C_5 , C_7 , C_3O , C_9 and some other unidentified molecules means that several reactions of carbon species take place. The possible reason is the presence of weak electronic absorptions of these species in the region of excitation. Usually most relaxations in a matrix are radiationless, but the excitation may be transported otherwise to neighbor molecules. This can induce the oxidation of those neighbor molecules. So, the photooxidation in the case of C_{11} in an oxygen matrix has a poor selectivity. Nevertheless, only C_{11} was depleted completely after laser irradiation.

The laser induced oxidation of C_{11} in a mixed matrix (90% Ar + 10% $^{18}O_2$) has shown better selectivity in comparison with a pure oxygen matrix. Only C_{11} , C_9 and C_6 were depleted. Decreasing of C_9 is due to the existing C_9 absorption at the irradiation wavelength. 50% decrease of C_{11} indicates sufficient selectivity of the photooxidation of this molecule. Increased absorptions of CO_2 and C_{10} after oxidation of C_{11} may originate from the chemical reaction $C_{11} + O_2 \xrightarrow{h\nu} C_{10} + CO_2$. Surprisingly, the produced triplet C_{10} seems to be stable in the matrix.

4 Selective laser-induced oxidation of carbon molecules

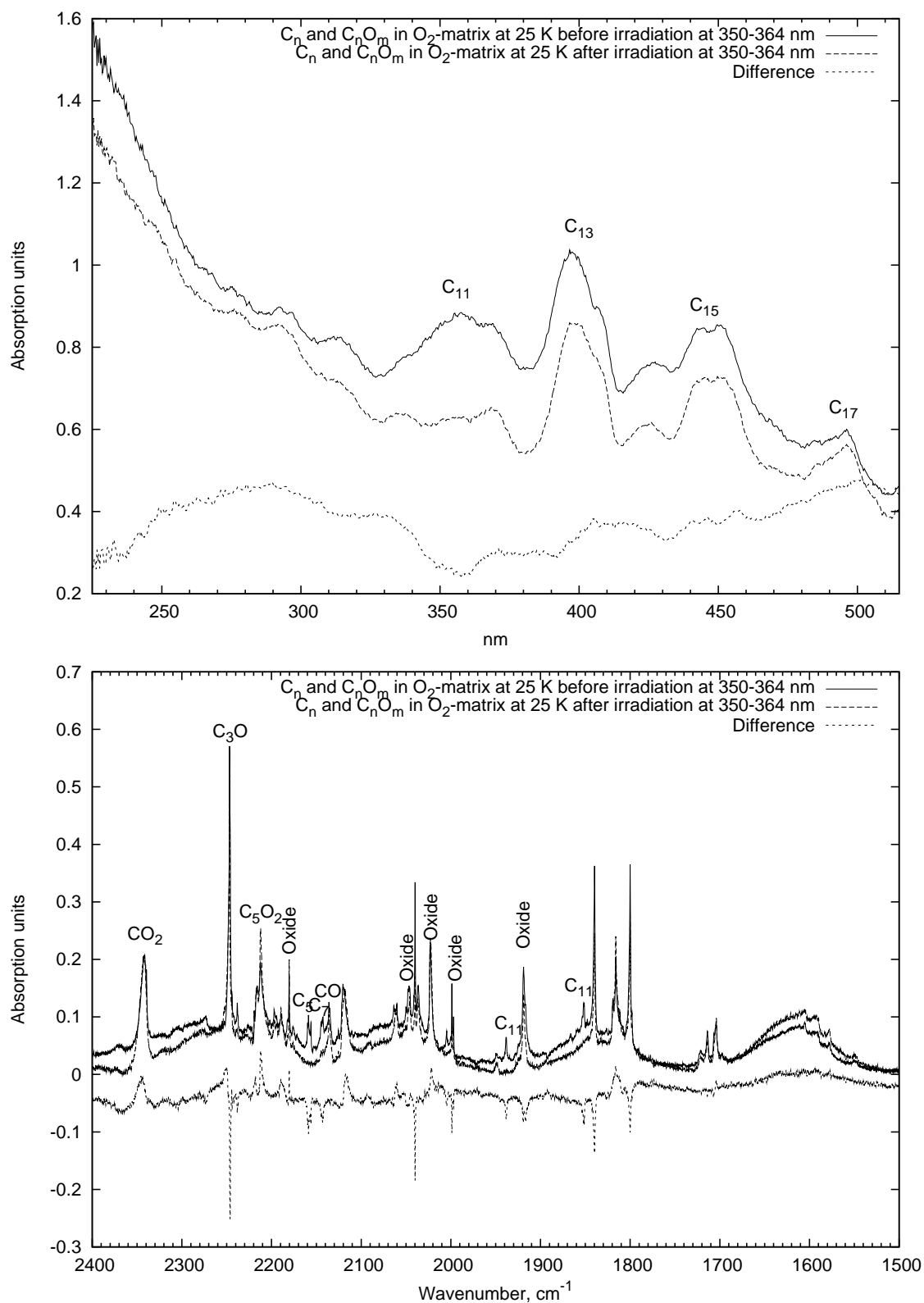


Fig. 4.4: UV/VIS and IR-spectrum. "Killing" of C_{11} by 350–364 nm laser in a pure O_2 matrix during 160 min at $T=25K$. Only C_{11} absorptions in infrared were completely depleted.

4.2 Test of the method on known carbon chains

Absorption, cm^{-1}	Difference, %
2343 (CO_2)	56
2247 (C_3O)	-12
2212 (C_5O_2)	25
2180	-7
2159 (C_5)	-96
2143 (C_7)	-84
2135 (CO)	-3
2040 ($\text{C}_3?$)	-68
2020	29
1998	-39
1938 (C_{11})	-99
1918	-34
1851 (C_{11})	-100
1844	-40
1803	-34
1820	48
1721	-22
1714	-9
1707	-18
1703	28
1037 (O_3)	-14

Tab. 4.2: Difference after laser irradiation at 350–364 nm during 160 min.

4 Selective laser-induced oxidation of carbon molecules

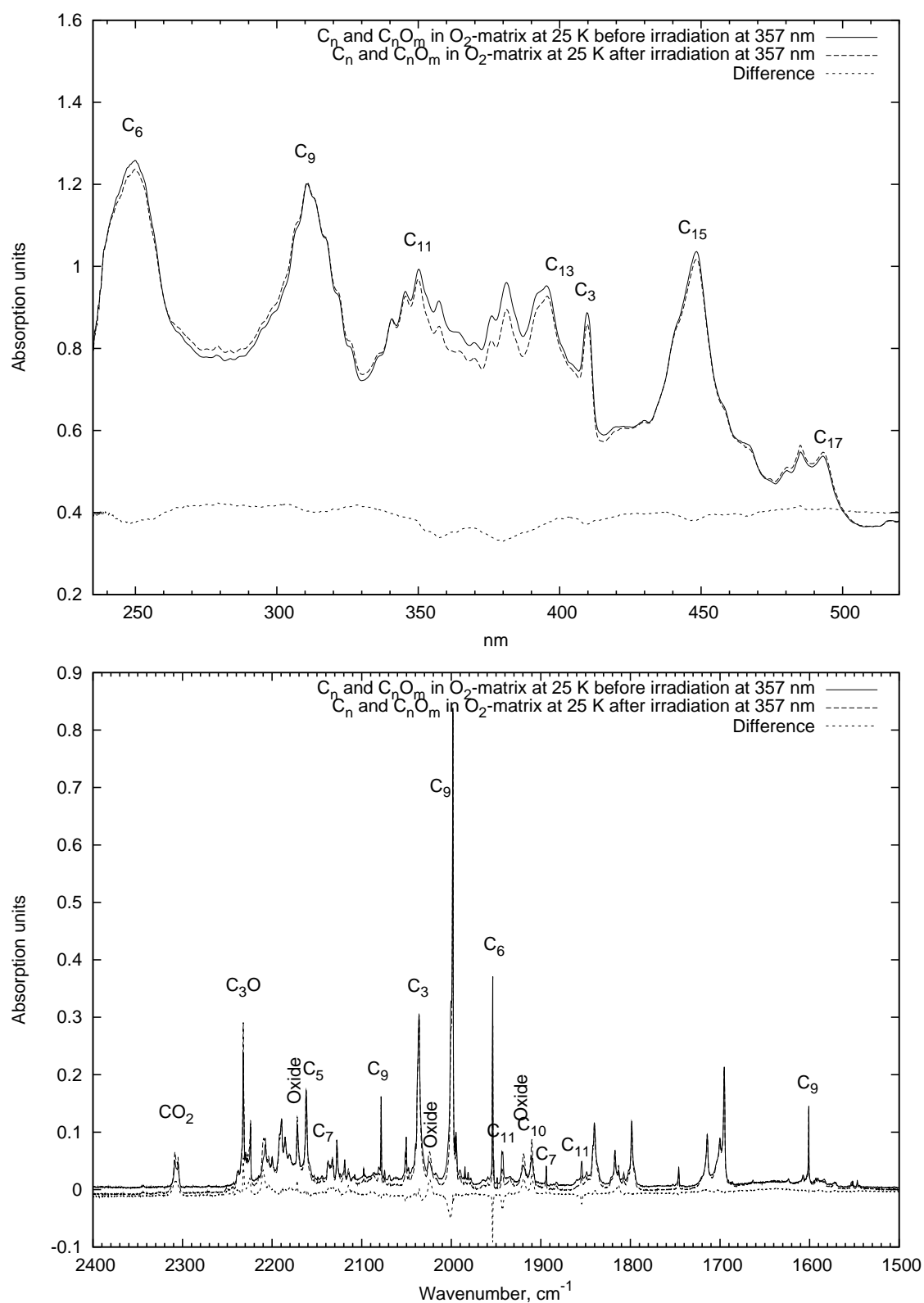


Fig. 4.5: UV/VIS and IR-spectrum. "Killing" of C₁₁ by 357 nm laser in a mixed 90% Ar + 10% ¹⁸O₂- matrix during 80 min at T=25K. Relative decrease of C₁₁ absorptions is about 50%. Other molecules were not strongly affected.

C₁₃ and the 1800/1840-oxide(s). Irradiation at 397 nm leads to decreasing of two lines in the infrared spectrum: 1800 (82%) and 1840 cm⁻¹ (78%) (Fig.4.6). Increased lines are oxides: CO₂, C₃O, C₅O₂ and other unidentified oxide species.

In the UV/VIS we observe the decrease of the absorption at 397 nm. The feature has a width of 20 nm.

A more detailed analysis of the electronic absorption around 400 nm reveals a double structure. One can distinguish two maxima located at 396 nm and 404 nm. Laser irradiation in the scanning mode at 400–406 nm leads to the decrease of IR-lines at 1819 and 1816 cm⁻¹ by 43 % (Fig. 4.7). Other decreased absorptions belong to oxides: around 2200 cm⁻¹ and 2117 cm⁻¹ (absent in rare-gas matrices and strong in oxygen, 2117 cm⁻¹ absorption may belong to C₇O₂, see tables 5.1 and 5.3 in chapter 5). The absorption of CO₂ was increased and the line at 1704 cm⁻¹ also increased (by 22%). As will be shown later in chapter 5, the absorption at 1704 cm⁻¹ belongs to a dioxide of a long carbon chain. In the UV/VIS spectrum two absorption bands decreased – 404 nm (C₁₃) and 422 nm. At the same time the absorption at 452 nm increased.

As was already mentioned in chapter 3 (page 33) and will be discussed later in chapter 5, two absorptions at 1803 and 1844 cm⁻¹ in an Ar-matrix (1800 and 1840 cm⁻¹ in O₂) belong to oxides of carbon. We have found that the corresponding electronic absorption of the 1800/1840-oxide(s) lies at 397 nm in an oxygen matrix, which is very close to the C₁₃ absorption. According to our estimate the absorber can be an oxide of a long carbon chain: C₁₃O, C₁₃O₂, C₁₁O or C₁₁O₂. The reason why we assume an odd number of carbon atoms is a strong UV absorption that is typical for a singlet ground state of a chain molecule (oxides of carbon with an odd number of carbon atoms have singlet ground states) [74]. The reason for assuming 11 or 13 carbon atoms comes from configuration interaction calculations we performed for the electronic transitions yielding 402 nm for C₁₃O₂ and 357 nm for C₁₁O₂.

The 1819, 1816 cm⁻¹ pattern of absorptions in O₂ (1818 cm⁻¹ in Ar) probably belongs to the IR-active C₁₃ stretching mode. There are no other candidates in the region around 1809 cm⁻¹ — the band position reported for C₁₃ in gas-phase [23]. The assignment by Ref. [62] of cyclic C₈ absorption at 1818 cm⁻¹ in Ar is in conflict with assignments by Ref. [60, 61] and our C₁₃ assignment. Indeed, irradiation at 400–406 nm leads to a decrease of the 1819 and 1816 cm⁻¹ line pattern.

4 Selective laser-induced oxidation of carbon molecules

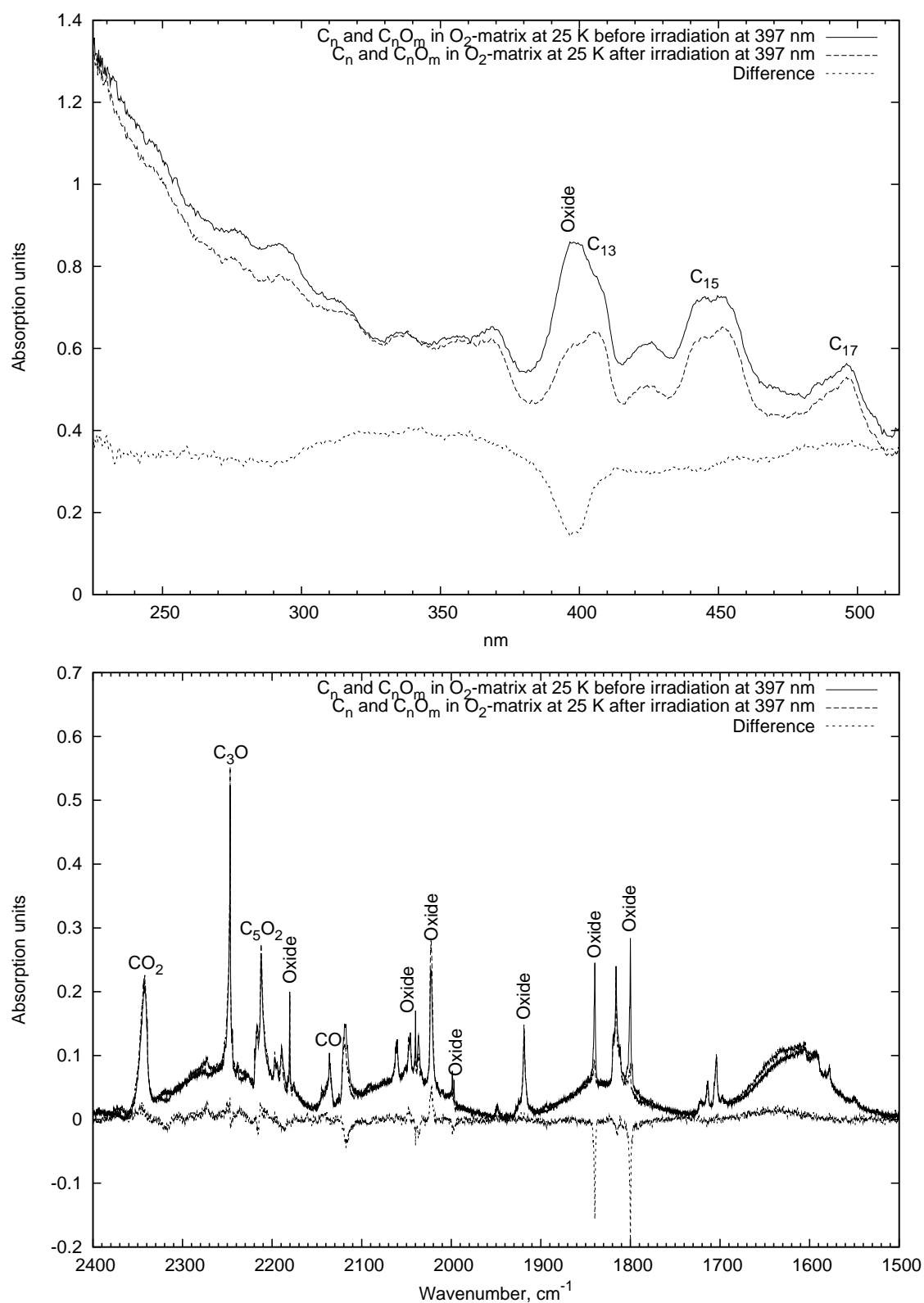


Fig. 4.6: UV/VIS and IR-spectrum. "Killing" of "1800/1840-oxide(s)" by 397 nm laser in a pure oxygen matrix during 140 min at $T=25K$. Electronic absorption of the "1800/1840-oxide(s)" partly overlaps with the C_{13} absorption.

4.2 Test of the method on known carbon chains

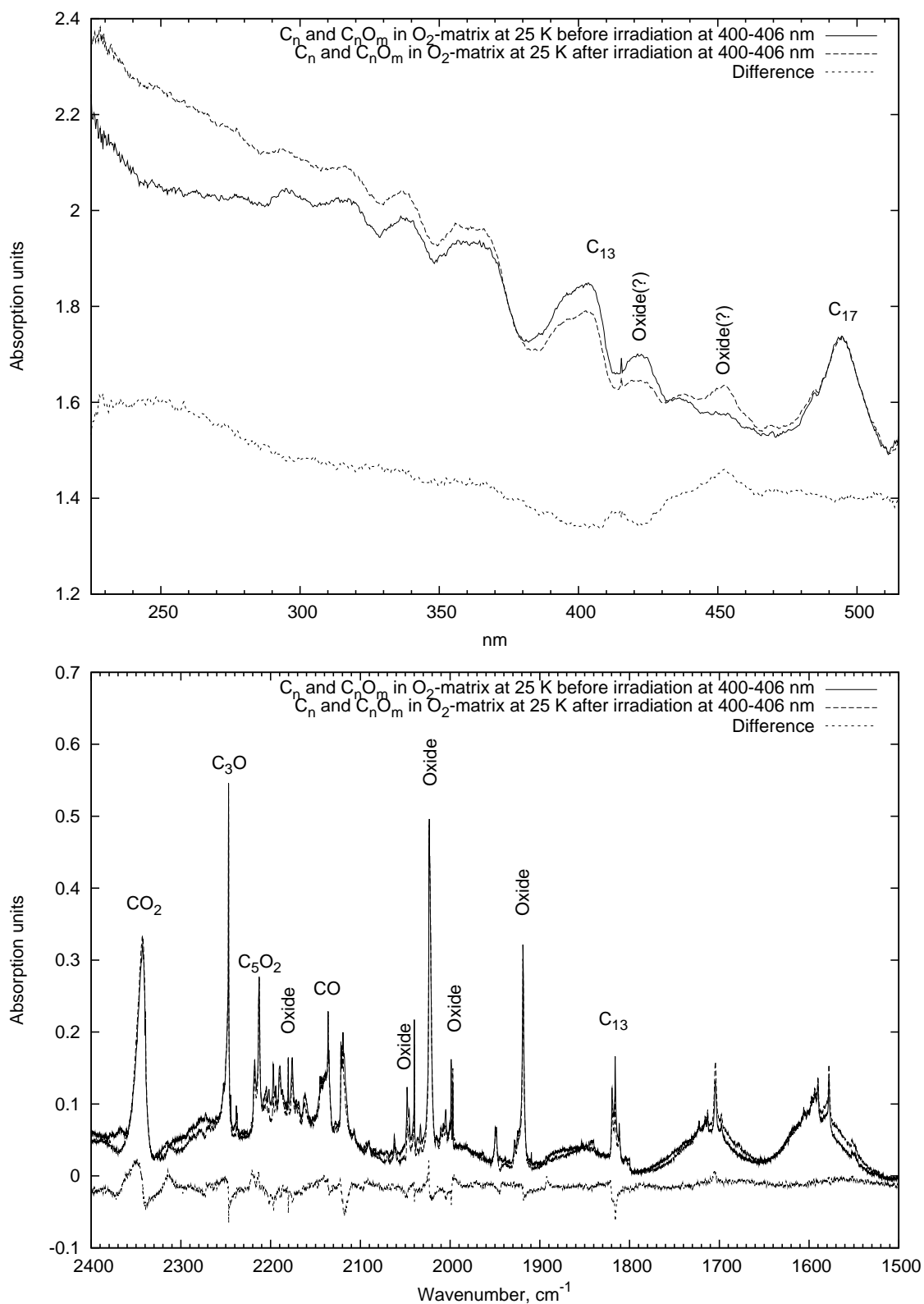


Fig. 4.7: UV/VIS and IR-spectrum. "Killing" of C_{13} by 400–406 nm laser in a pure oxygen matrix during 240 min at $T=25K$. Missing absorptions of C_9 , C_{11} , C_6 , "1800/1840-oxide(s)" have been already photobleached.

4 Selective laser-induced oxidation of carbon molecules

UV/VIS absorption, nm	IR-absorption, cm^{-1}	Molecule
308	2086, 2005, 1606 (in O_2)	C_9
308	2078, 1998, 1601 (in Ar + 10% O_2)	C_9
350–364	1938, 1852 (in O_2)	C_{11}
357	1943, 1855 (in Ar + 10% O_2)	C_{11}
400–406	1819, 1816 (in O_2) (1818 in Ar)	C_{13}
397	1800, 1840 (in O_2)	Oxide (C_{13}O_2 , C_{13}O , C_{11}O_2 or C_{11}O ?)
452	1704 (in O_2)	Oxide (C_{15}O_2 , C_{15}O , C_{13}O_2 or C_{13}O ?)

Tab. 4.3: Correlated UV/VIS and IR-absorptions in the laser-induced oxidation experiments.

Hence, the UV/VIS absorption at 404 nm must belong to C_{13} and the other one at 422 nm which is very tiny in an Ar matrix probably belongs to an oxide. The increased absorption at 452 nm probably also belongs to an oxide of a long carbon chain. C_{13}O_2 , C_{13}O , C_{15}O_2 or C_{15}O are possible candidates for this absorption with corresponding vibrational absorption at 1704 cm^{-1} ("1704 oxide"). The estimate of the number of carbon atoms is again based on configuration interaction calculations.

The results of our tests of the laser-induced oxidation method are summarized in the table 4.3 and shown in Fig.4.11.

In conclusion, the photooxidation method applied on carbon molecules C_9 , C_{11} , C_{13} and "1800/1840-oxide(s)" is sufficiently selective for identification purposes and we are confident that it can be applied for the molecules with known electronic absorptions but unknown vibrational transitions.

Matrix	Excitation wavelength, nm	Duration, min	Molecule
¹⁶ O ₂	308	120	C ₉
	350–364	160	C ₁₁
	397	140	”1800/1840”-oxide(s)
	438–455	80	C ₁₅ and ”1704”-oxide
	436–444	240	C ₁₅
	450–455	270	”1704”-oxide
Ar + 10% ¹⁸ O ₂	308	50	C ₉
	357	80	C ₁₁
	448	80	C ₁₅
	441	240	C ₁₅

Tab. 4.4: Irradiation sequence in the C₁₅ laser induced oxidation experiments. Two different matrices with different compositions were used.

4.3 Depletion of C₁₅

While the electronic absorption of C₁₅ is at 440 nm, the vibrational IR-active absorptions of this carbon chain are unknown. The width of the UV line is about 10 nm.

4.3.1 Experimental details

Laser irradiation of the C₁₅ electronic absorption region was made in two different types of matrices – a pure O₂-matrix and in an Ar + 10% ¹⁸O₂-matrix, both at 25K. Again we followed the strategy of ”killing” shorter carbon chains before longer ones.

At the beginning of the experiment in a pure oxygen matrix other carbon chain molecules were photobleached: C₉ – by 308 nm for 120 min, C₁₁ – by 350–364 nm for 160 min, ”1800/1840-oxide” – by 397 nm for 140 min. After that, infrared and

UV/VIS spectra were measured, the laser exposure was applied at 438–454 nm in the scanning mode during 80 min. Then IR and UV/VIS spectra were measured again. The laser at 436–444 nm was applied during 240 min, followed by IR, UV/VIS spectra measurement. Then photobleaching of the "1704 oxide" was made by laser at 450–455 nm during 270 min, IR and UV/VIS spectra were measured.

In a mixed (Ar + 10% $^{18}\text{O}_2$)-matrix long C_n molecules were also irradiated before C_{15} -"killing". The laser was applied at 308 nm for 50 min, at 357 nm for 80 min. The UV/VIS and infrared spectra were recorded. For the "killing" of C_{15} the laser irradiation at 448 nm was applied for 80 min, followed by spectra measurements. After that the same matrix was irradiated by 441 nm laser light during 240 min. The final infrared and UV/VIS spectra were recorded.

For clarity, Table 4.4 displays the irradiation sequence.

4.3.2 Results and Discussion

C_{15} in a pure O_2 -matrix: After irradiation at 438 – 454 nm we observed a decrease of the C_{15} electronic absorption (Fig. 4.8) with a peak at 442 nm. The oxide absorption with a maximum at 452 nm slightly decreased. The C_{15} decrease in the visible spectrum is roughly 40–80%. Such a big uncertainty originates from the base line change and overlap with the oxide absorption at 452 nm. In the IR-spectrum, significantly decreased lines are C_5O_2 (30%), the oxide at 2180 cm^{-1} (52%), the oxide at 1704 cm^{-1} (25%) and lines at 1721 , 1714 , 1707 cm^{-1} ($40\pm 10\%$). Among increased lines are C_3O (6%), the oxide at 1998 , 1997 cm^{-1} (35%), CO_2 (roughly 4%). All other changes in the infrared spectrum are negligible. Therefore, the only decreased lines in the infrared, which could belong to a pure carbon molecule (no shift in an $^{18}\text{O}_2$ -matrix, see chapter 5) are 1721 , 1714 , and 1707 cm^{-1} .

As one can see in Fig.4.8, there are two peaks in the UV/VIS spectrum after irradiation: 439 nm and 452 nm. The second round of laser irradiation at 436 – 444 nm during 140 min was performed on the same matrix sample. Recorded infrared and UV/VIS spectra are shown on Fig. 4.9. In the UV/VIS spectrum we observe the decrease of C_{15} absorption at 439 nm on $38\pm 15\%$. In the infrared most of the increased lines are in the region of oxides ($>2100\text{ cm}^{-1}$). The oxides at 2047 and 2023 cm^{-1} also increased. Among decreased absorptions are the rest of C_9 at

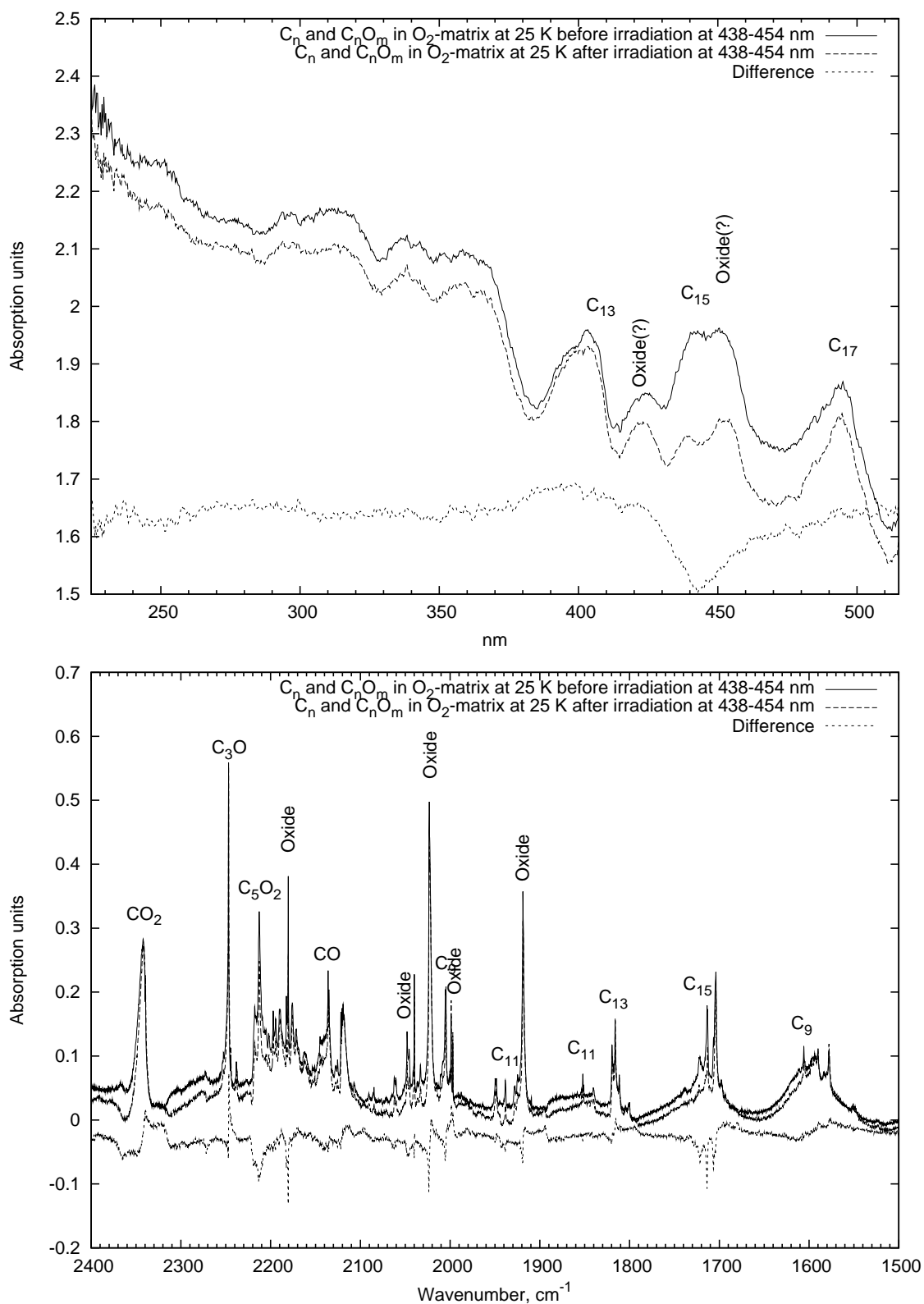


Fig. 4.8: UV/VIS and IR-spectrum. "Killing" of C₁₅ by 438–454 nm laser in a pure oxygen matrix during 80 min at $T=25\text{K}$. Decreased absorption lines at 1721, 1714, 1707 cm^{-1} we assign as site peaks of C₁₅ in a β -phase solid oxygen.

4 Selective laser-induced oxidation of carbon molecules

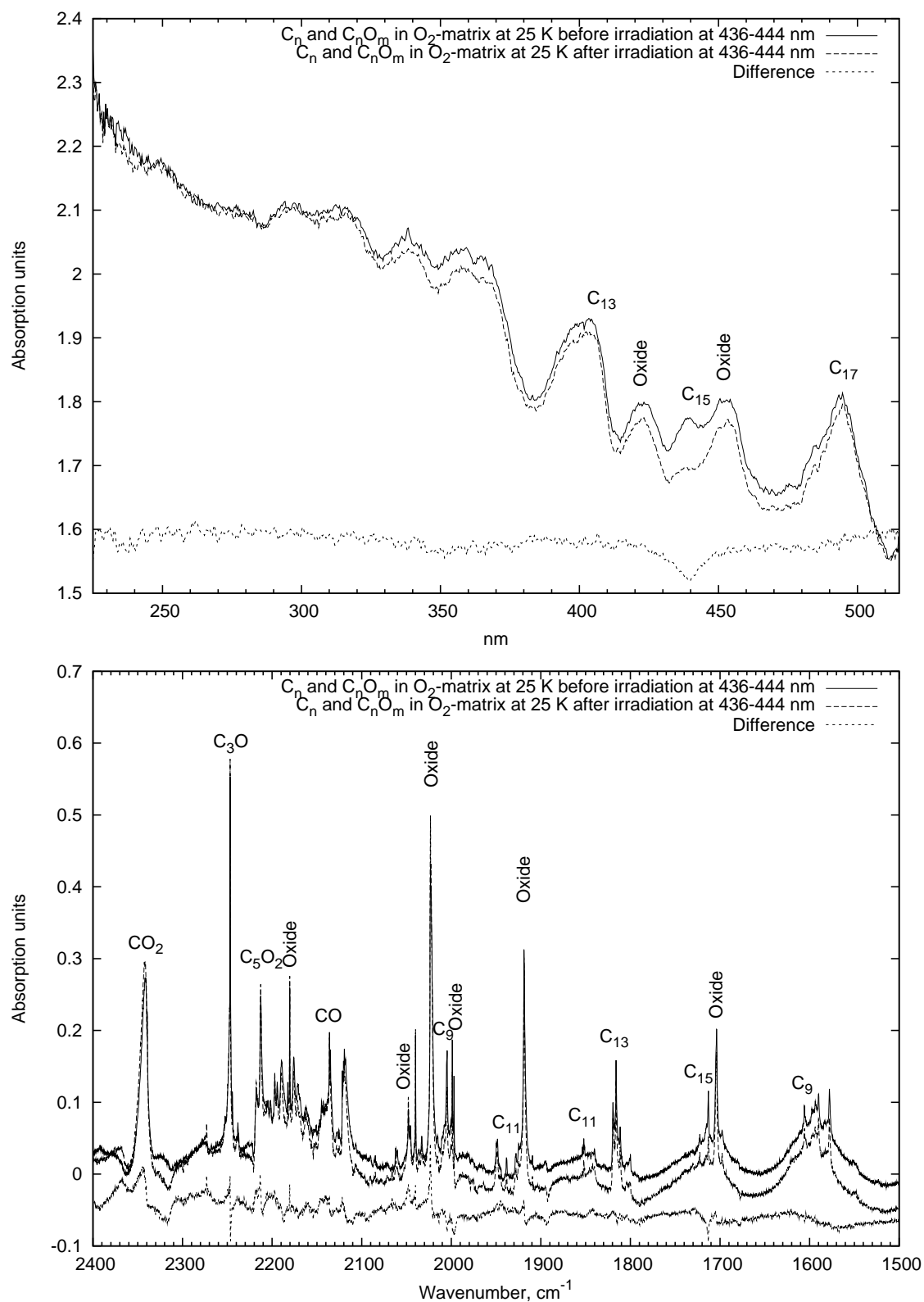


Fig. 4.9: UV/VIS and IR-spectrum. "Killing" of C₁₅ by 436–444 nm laser in a pure oxygen matrix during 240 min at $T=25\text{K}$. The remained site peak of C₁₅ at 1714 cm^{-1} was depleted.

2005 cm⁻¹ (by 16%), the oxide at 1999, 1997 cm⁻¹ (by 20%) and the absorption at 1713 cm⁻¹ (by 40%). Again, the only possible candidate for C₁₅ is the line at 1713 cm⁻¹.

In order to confirm the correlation between IR-absorption of the oxide at 1704 cm⁻¹ and the electronic absorption at 452 nm (see page 54) the same matrix was irradiated with laser light at 450–455 nm. The measured spectra are presented in Fig.4.10. One clearly sees the decrease of the absorption at 452 nm. Simultaneously, the electronic absorption at 250 nm decreased. The decreased lines in the infrared spectrum are the oxide at 1704 cm⁻¹ (30%), C₃O (4%) and the oxide at 2180 cm⁻¹ (50%). We assigned the oxide at 2180 cm⁻¹ to C₆O₂ (see chapter 5).

The appropriate UV/VIS positions, where we have performed laser excitation of different carbon species and observed correlations with infrared absorptions in oxygen matrices are shown in Fig.4.11.

The analysis of the UV/VIS and infrared spectra before and after laser irradiations revealed that the only possible absorptions, which can belong to C₁₅ in a β -phase O₂-matrix are the absorptions close to 1700 cm⁻¹. Three lines at 1721, 1714 and 1707 cm⁻¹ we assign as site peaks of C₁₅ absorption in a β -phase oxygen matrix. There is one more site peak of C₁₅ at 1695 cm⁻¹ in an α -phase oxygen matrix (Fig. 4.1). This peak considerably decreases after transition to a β -oxygen, but it is very strong in an Ar-matrix.

The correlation of 1704 cm⁻¹ vibrational absorption and 452 nm electronic absorption was confirmed. As was already discussed above (page 54), the possible candidates are C₁₃O₂, C₁₃O, C₁₅O₂ or C₁₅O.

C₁₅ in a mixed Ar + 10% O₂-matrix: For supporting the identification of the C₁₅ infrared absorption a mixed matrix of Ar and 10% ¹⁸O₂ was produced. The exposure history displayed in Table 4.4. After irradiation at 448 nm during 80 min some changes were observed (Fig.4.12). In the UV/VIS spectrum the C₁₅ absorption at 448 nm decreased by 13 %. The decreased absorptions in the infrared are: 2172 cm⁻¹ (12% – C₆¹⁸O₂, see chapter 5), 2162 cm⁻¹ (4% – C₅), 1998 cm⁻¹ (2% – C₉), 1953.6 cm⁻¹ (3% – C₆), 1700 cm⁻¹ (19%) and 1695 cm⁻¹ (2%). Among increased lines are only oxides (CO₂, C₃O and some others).

As one can see in the UV/VIS spectrum (Fig.4.12) the C₁₅ absorption has a shoulder at 441 nm, probably belonging to a site of C₁₅ in a mixed (Ar + 10% ¹⁸O₂)-

4 Selective laser-induced oxidation of carbon molecules

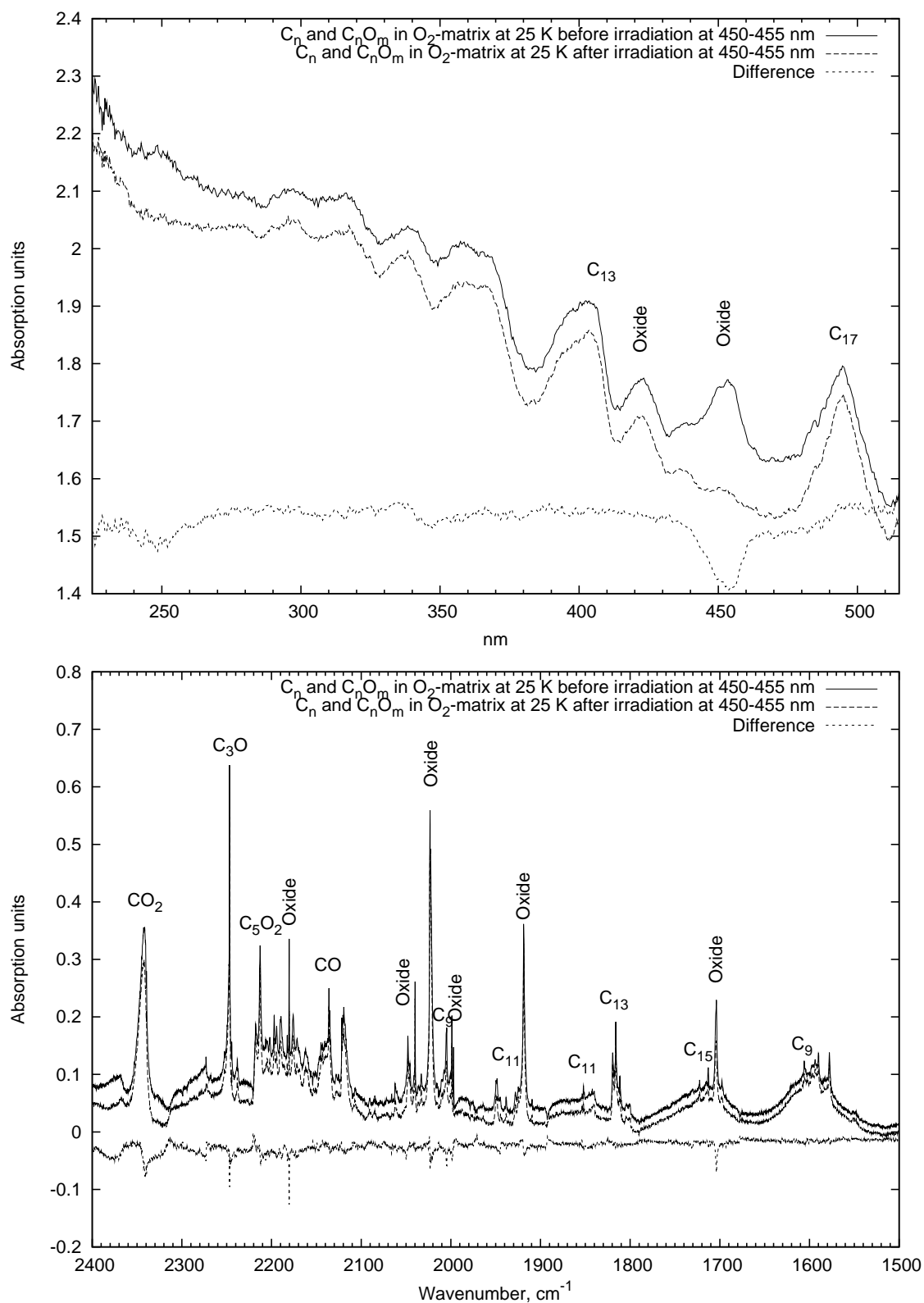


Fig. 4.10: UV/VIS and IR-spectrum. "Killing" of "1704 oxide" by 450–455 nm laser in a pure oxygen matrix during 270 min at $T=25\text{K}$. The increase of this oxide was observed after C₁₃-"killing", see Fig.4.7.

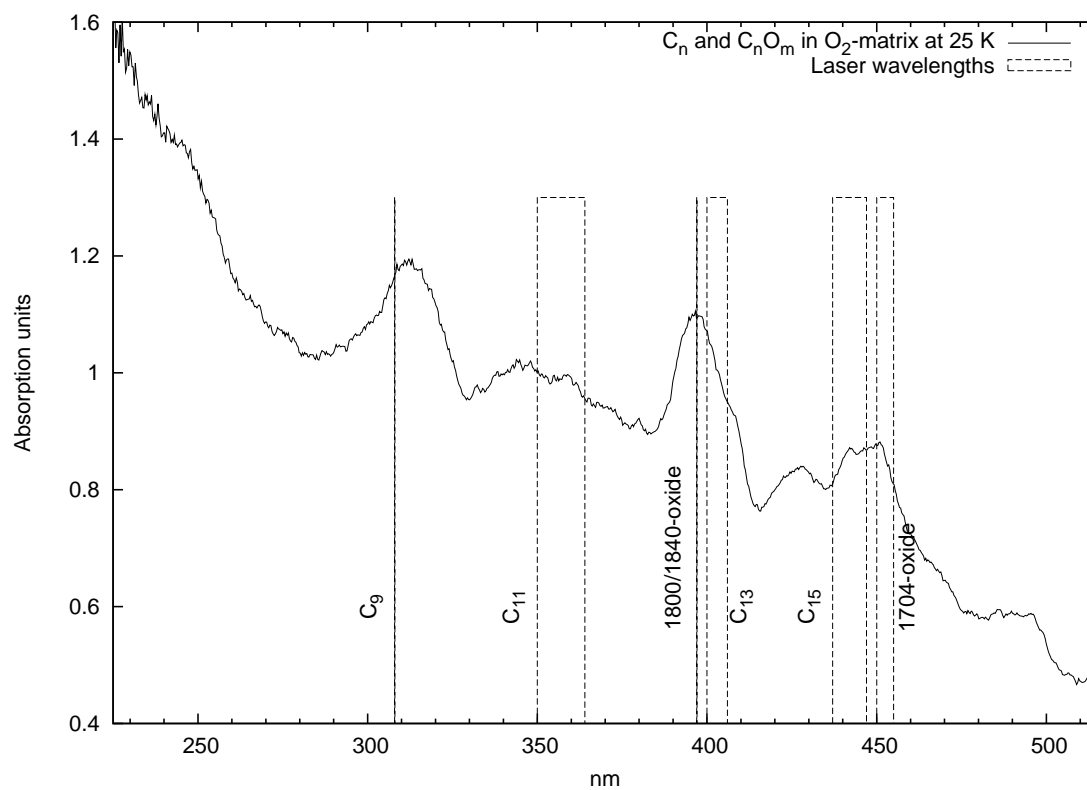


Fig. 4.11: UV/VIS absorptions of carbon molecules and oxides of carbon in an O₂-matrix at 25K. The ranges where the laser excitation of the molecules was applied are plotted with empty bars.

4 Selective laser-induced oxidation of carbon molecules

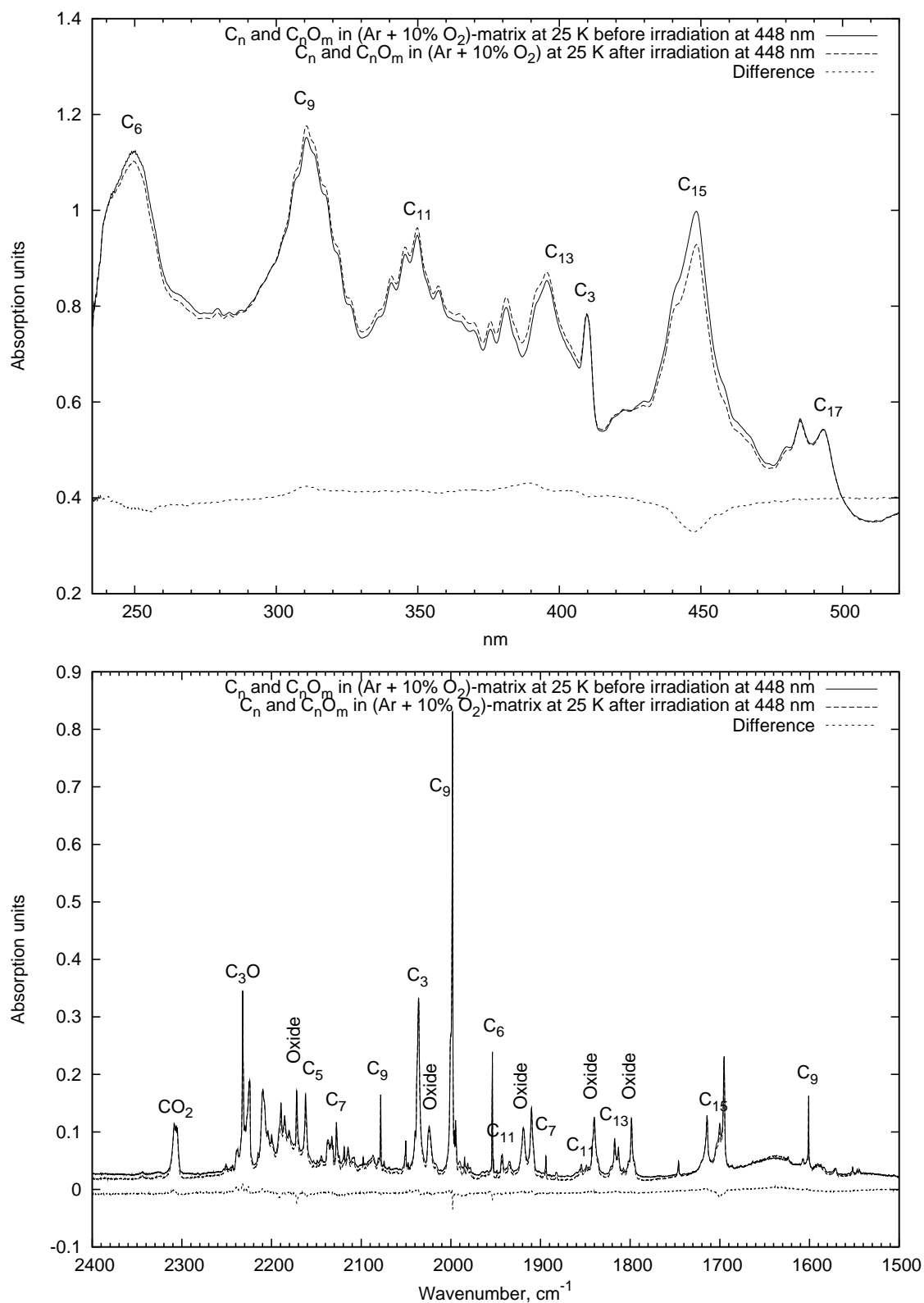


Fig. 4.12: UV/VIS and IR-spectrum. "Killing" of C₁₅ by 448 nm laser in a mixed Ar + 10% ¹⁸O₂-matrix during 80 min at T=25K. The most strongly affected infrared absorption is at 1700 cm⁻¹: 20% decrease.

matrix. We irradiated the same matrix sample as before with 441 nm laser light during 240 min. The recorded UV/VIS and infrared spectra presented on Fig.4.13. In the UV/VIS we observed a considerable decrease of C₁₅ (25%) and C₆ (30%). The absorption of C₉ decreased by 6%. In the infrared spectrum considerably decreased lines are: 1713 cm⁻¹ (18%), 1700 cm⁻¹ (30%), 1695 cm⁻¹ (22%), C₆ (29%), C₉ (6%), C₃¹⁸O (26%), C₅ (14%), C₇ (37%). Absorption lines of some oxides increased: C¹⁸O₂ (19%), 2024 cm⁻¹ (16%), 1919 cm⁻¹ (8%).

The infrared absorptions of C₁₅ in an (Ar + 10% ¹⁸O₂)-matrix are 1713, 1700 and 1695 cm⁻¹. In a pure Ar matrix the absorption at 1713 cm⁻¹ is very weak. Most probably it is a site peak of C₁₅ in the oxygen surrounding. The absorptions at 1700 and 1695 cm⁻¹ in pure Ar matrices are more distinct after annealing to less than 40K (the sublimation temperature of solid Ar).

Our assignment of the 1695 cm⁻¹ absorption as belonging to C₁₅ contradicts previous assignments of this line. The authors of Ref. [54] and [55] claim that this line originates from the cyclic (D_{3h}) C₆ molecule. Both assignments were based on Ar matrix isolation experiments in which carbon molecules were created with mixed ¹²C, ¹³C isotopes. Comparison of the experimental vibrational isotopomer frequencies with calculated frequencies (DFT method) was made and seemed to support the conclusion concerning the carrier molecule. Such a method does not provide unique results in assignment when the number of carbon atoms is large. From isotopic replacement experiments the author of Ref.[105] suggested the number of carbon atoms to be greater than 10 for this carrier. The spectrum from [105] is shown on Fig.4.14. At a ratio ¹³C/¹²C=0.11 the most probable isotopomers have only a single carbon atom substituted. We estimated the positions of singly substituted isotopomeric lines of C₁₅ using semi-empirical PM3 calculations. The calculated line positions are shown on the same Fig.4.14. We see good coincidence of experimental and calculated absorptions for singly substituted isotopomer of C₁₅. The line at 1687.5 cm⁻¹ (noted by an *) may not be related to 1694.9 cm⁻¹ absorption, as was mentioned by Ref.[54], because of different behavior during annealing. So, the isotopic replacement experiments do not contradict the assignment of 1695 cm⁻¹ line as linear C₁₅.

4 Selective laser-induced oxidation of carbon molecules

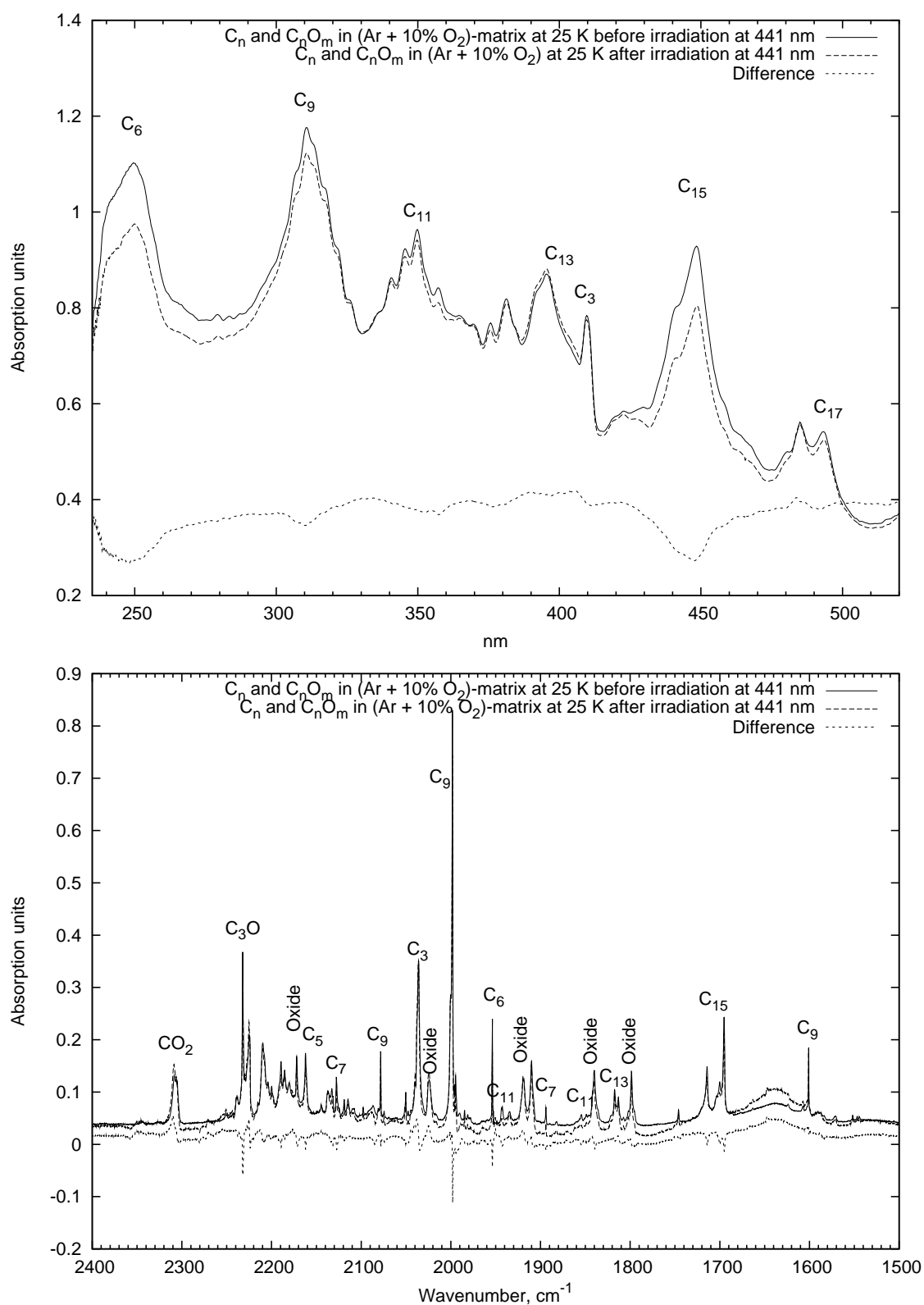


Fig. 4.13: UV/VIS and IR-spectrum. "Killing" of C₁₅ by 441 nm laser in a mixed Ar + 10% ¹⁸O₂-matrix during 240 min at T=25K. In this case three site peaks of C₁₅ were depleted: 1713 cm⁻¹ (18%), 1700 cm⁻¹ (30%), 1695 cm⁻¹ (22%). However, some other known absorptions also decreased (see text).

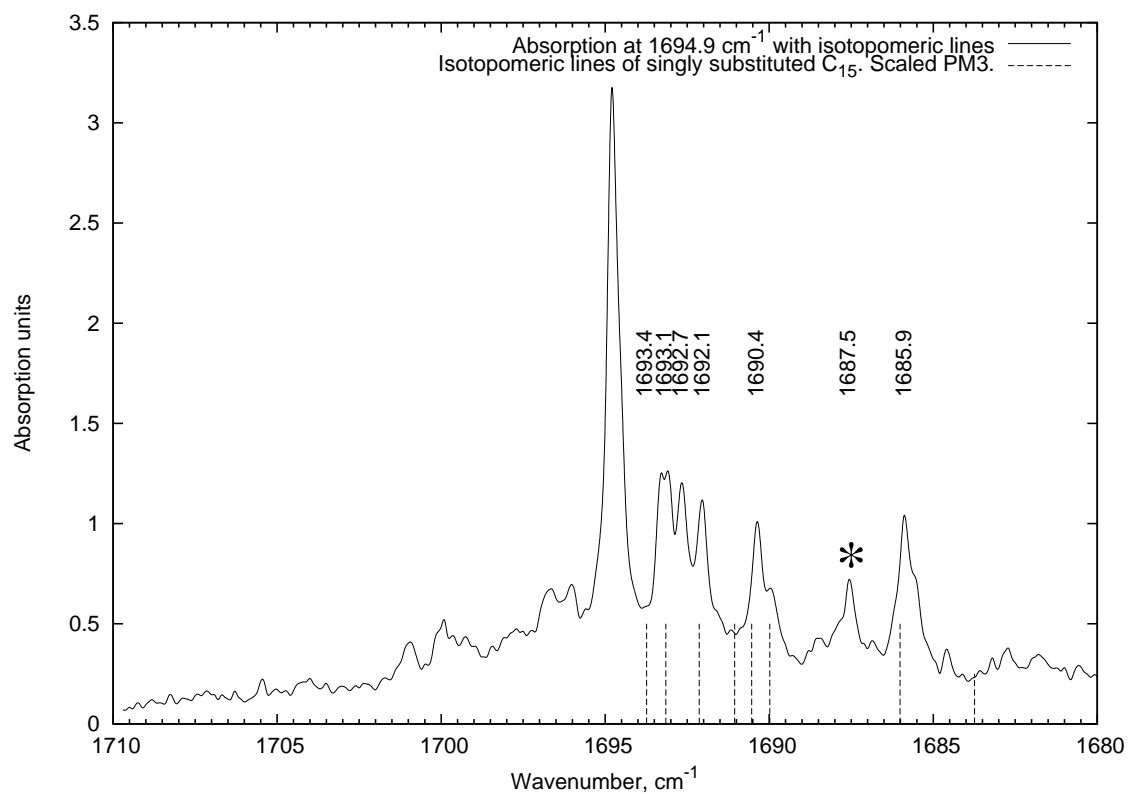


Fig. 4.14: The 1694.9 cm^{-1} absorption with isotopomeric lines. Calculated frequencies (PM3) of singly substituted isotopes are scaled in such a way that $^{12}C_{15}$ absorption is at 1694.9 cm^{-1} . The line (*) at 1687.5 cm^{-1} may not be related to 1694.9 cm^{-1} absorption [54].

Molecule	DFT, cm^{-1}	PM3, cm^{-1}	Exp., cm^{-1}
C ₉	1996 (4136), 1922 (5903)	2107 (22941)	2004
C ₁₁	1917 (14578) , 1755 (2127)	1922 (45134)	1944, 1851
C ₁₃	1840 (20182)	1729 (77821)	1816
C ₁₅	1804 (26842)	1502 (129379)	1721, 1714, 1707
C ₁₇	-	1215 (206426)	-
C ₁₉	-	788 (318451)	-

Tab. 4.5: IR-frequencies of the most intense mode of long carbon chains: calculation and experiment. Calculated by DFT frequencies are scaled by factor 0.9. Experimental data is for oxygen matrix at 25 K. The intensities of calculated vibrations are given in brackets.

4.4 Discussion

4.4.1 Comparison of experimental and calculated IR-absorption frequencies.

A chain molecule C_n has $n - 1$ stretching modes of which 1/2 are IR active. For long chains one expects lots of lines, but as it appears only a few are intense. In order to understand this feature quantum mechanical calculations were made.

DFT (B3LYP/6-31G(d), [106]) and PM3 quantum-mechanical calculation predict positions of IR-active vibrational modes, which are displayed in Table 4.5. The frequencies calculated by DFT are scaled by factor 0.9. Experimental data are for an oxygen matrix at 25 K.

It is interesting to note that according to calculation there is only one very intense absorption of a long odd carbon chain (in particular in case of C₁₅). The position of this most intense absorption shifts with increasing chain length to longer wavelengths, forming a regular sequence. This absorption corresponds to the totally antisymmetric stretching mode which produces a maximal change of the dipole moment. The atomic displacement pattern of this mode is shown in Fig.4.15.

One can try to understand this by taking into consideration the eigenvectors of the normal modes and the Mulliken atomic charges, as calculated by the DFT and

PM3 method.

Atomic charges are not a measurable properties of a molecule, because molecules consist of nuclei and distributed electrons. Some arbitrary decisions have to be taken, on how to distribute the calculated electron density between atoms. Let us consider a molecular orbital made of two atomic orbitals: $\psi = c_1\phi_A + c_2\phi_B$, where ϕ_A and ϕ_B are atomic orbitals of atoms A and B respectively. The integral of the electron density ψ^2 is:

$$\int \psi^2 d\vec{r} = c_1^2 \int \phi_A^2 d\vec{r} + c_2^2 \int \phi_B^2 d\vec{r} + 2c_1c_2 \int \phi_A\phi_B d\vec{r}$$

The part of electron(s) $c_1^2 \int \phi_A^2 d\vec{r}$ belongs to atom A and the part of electron(s) $c_2^2 \int \phi_B^2 d\vec{r}$ belongs to atom B. In the Mulliken population analysis the overlap electron population $2c_1c_2 \int \phi_A\phi_B d\vec{r}$ is divided equally between the two partner atoms. For more detailed description of Mulliken population analysis see Ref.[107]. Even though it may appear that the Mulliken charges have a formal character, their physical importance emerges in explaining the strength of the IR absorptions.

From the quantum mechanical calculations it turns out that the approximate Mulliken charges pattern in a linear chain with an odd number of carbon atoms alternates in the following way:

$$\left(+\frac{q}{2}\right) (-q) (+q) (-q) \dots (+q) (-q) \left(+\frac{q}{2}\right),$$

where the charge $q/2$ is located at the ends of a molecule. The integrated vibrational absorption coefficient can be estimated as ([108], p.79):

$$I \sim \frac{1}{m_{red.}} \left(\frac{d\mu}{ds}\right)_{s=0}^2, \quad (4.4.1)$$

where $m_{red.}$ – reduced mass, μ – dipole moment, s – normal coordinate. As soon as all atoms in a chain have the same weight, $m_{red.}$ is the same for all vibrational modes.

$$\frac{d\mu}{ds_k} = \sum_{i=1}^N \frac{\partial\mu(x_1, \dots, x_N)}{\partial x_i} \frac{\partial x_i}{\partial s_k} = \sum_{i=1}^N \frac{q_i dx_i}{dx_i} L_{i,k} = \sum_{i=1}^N q_i L_{i,k}, \quad (4.4.2)$$

where N – number of atoms, x_i – Cartesian coordinate of i^{th} atom, q_i – Mulliken charge of i^{th} atom, k – number of a normal mode, L – matrix of vibrational eigenvectors as columns ($\vec{s} = L^{-1}\vec{x}$). This means that if there is a totally alternation

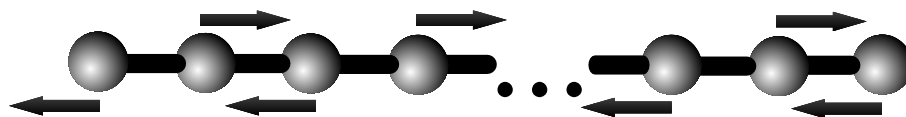


Fig. 4.15: The most intensive IR-mode of a long carbon chain is the totally alternating vibration, in which the displacement turns around in going from one atom to the next.

mode, then it would have the highest intensity, because Mulliken charges alternate in the same way: all atoms with charges of one sign move against all others with the opposite sign.

The strength of this vibration increases with increasing of the molecular chain length ($\sim N^2$, according to PM3 and $\sim N$, according to DFT, where N is the number of atoms). This explains why the absorptions of long chains are observable in spite of their low abundance.

4.4.2 Theoretical view on laser-induced reactions.

Experiment shows that a carbon molecule in a cold oxygen surrounding can exist without immediate oxidation. This means that there is a reaction barrier against oxidation. The barrier differs for different carbon molecules being particularly small for C_6 . As was already mentioned in the introduction to this chapter, the reaction mechanism of photooxidation at cryogenic temperatures involves excitation to a *charge-transfer* state which may react to form photoproducts [102]. The fact that the oxidation takes place even without excitation (one observes slow decreasing of other pure carbon species, order of 1% per day) suggests triggering of this reaction by electron tunneling. In an ensemble of electrons in a "boxes" (carbon molecules) certain number of electrons can tunnel through the barrier and that will create a transition complex of a carbon chain and oxygen atom(s). The transition complex decays then to the product(s), i.e. carbon oxides.

Now one can electronically excite some type of molecules by light. This will decrease the reaction barrier and oxidation will go faster only for that selected type of molecules.

An electronically excited molecule during relaxation can go into vibrationally

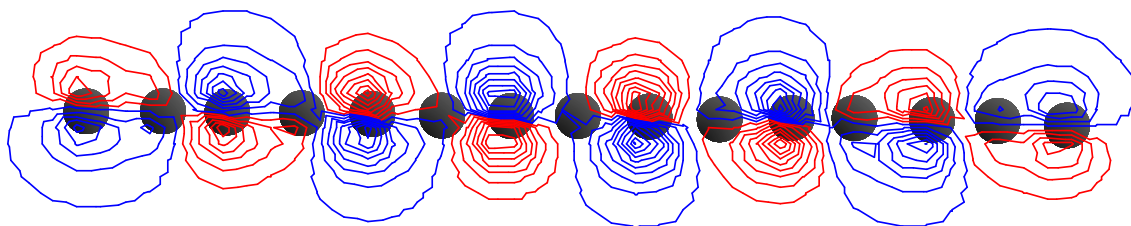


Fig. 4.16: Highest occupied molecular orbital of the excited C_{15} molecule. PM3 model. Average bond length 1.28 Å. (The HOMO of the excited C_n is in fact the LUMO of the C_n in the ground state).

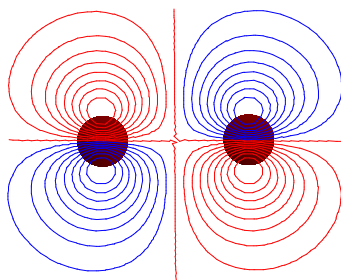


Fig. 4.17: Highest occupied molecular orbital of the O_2 molecule in the ground state. PM3 model. Bond length 1.7 Å.

excited states. This may lead to atomic tunneling and also may play a role in the reaction mechanism [109].

We now may turn to the question at which place in a chain an oxygen will be attached or inserted? It seems to be that this is a statistical process, because we did not observe increasing of only one product. Usually CO_2 and C_3O absorption increase after irradiation. The formalism of frontier orbitals (i.e. the interaction of the highest occupied molecular orbitals – HOMOs and the lowest unoccupied molecular orbitals – LUMOs) gives some ideas about the most probable reaction points on a carbon molecule. In our case the important interactions are the interaction of the HOMO of the electronically excited carbon chain (Fig.4.16) with the HOMO of molecular oxygen (Fig.4.17) in the ground state and the LUMO/LUMO interaction of the excited C_n with O_2 (see [110]). There is no preferential place on a carbon chain for oxidation as we see from the Fig. 4.16 and Fig. 4.17. Therefore, probably there are several possible channels for this reaction with different products as C_nO and C_mO_2 . An insertion of O into the chain would lead to a break-up of the molecule: $C-C-O-C-C \dots \longrightarrow C-C-O + C-C \dots$.

5. Isotopic substitution of oxygen. Implications regarding carbon chain oxides.

5.1 Introduction

In our "killing" experiments in oxygen matrices different oxides were produced, that caused the appearance of additional absorptions in the infrared and the UV/VIS-spectra. For the purpose of oxides identification and distinguishing between oxides and pure carbon molecules several experiments were performed using $^{18}\text{O}_2$ matrices. The expected qualitative effect is the shift of oxides infrared absorptions to the red. Furthermore, mixtures of $^{16}\text{O}_2$ and $^{18}\text{O}_2$ can provide information about the number of oxygen atoms in the molecule and the magnitude of the shift allows to estimate the number of carbon atoms in the oxide molecule, assuming that the vibrational mode is known.

Infrared absorptions of some of the carbon oxides were already measured by several research groups. Mostly, these are monoxides and dioxides of short carbon chains. C^{16}O (2135 cm^{-1} in O_2) and C^{16}O_2 (2343 cm^{-1} in O_2) molecules are classical examples in spectroscopy and reviewed in Herzberg textbooks [111, 112]. The known infrared absorptions of the other carbon oxides are displayed in Table 5.1. The authors of [113, 114, 115] produced carbon oxides from various precursors like diazoketone ($\text{C}_5\text{N}_4\text{O}_3$), 2,4,6-tridiazao-1,3,5-cyclohexantrion ($\text{C}_6\text{N}_6\text{O}_3$), anhydride of mellitic acid (C_{12}O_9) by photolysis. Another approach is to use pure carbon molecules as precursors together with oxygen containing molecules like H_2O . The authors of Ref.[116] added H_2O to an argon matrix, containing C_n molecules which led to the formation of complexes between C_n and H_2O . After irradiation with

UV light hydrogen atoms were detached and oxides formed.

Tab. 5.1: IR-absorptions of carbon oxides. If matrix isolated IR-spectrum is known, then only matrix data is shown. (MIS – Matrix Isolation Spectroscopy, DLS – Diode Laser Spectroscopy, T – tentative assignment).

Molecule	Absorption, cm^{-1}	Mode	Method	References
CO_3	2053	ν_1 CO stretch, A_1	MIS in Ar	[117]
	1070	ν_2 OO stretch	MIS in Ar	[117]
	975	ν_5 CO stretch, B_2	MIS in Ar	[117]
	564	ν_6 OCO bend	MIS in Ar	[117]
C_2O	1969	ν_1 CO stretch, Σ^+	MIS in Ar	[118]
	1978	ν_1 CO stretch, Σ^+	MIS in Ar	[118]
	1064	ν_3 CC stretch, Σ^+	MIS in Ar	[118]
	381	ν_2 bend, Π	MIS in Ar	[118]
C_3O	2243	ν_1 , Σ^+	MIS in Ar	[119, 120, 121]
	1907	ν_2 , Σ^+	MIS in Ar	[120, 121]
	939.1	ν_3 , Σ^+	MIS in Ar	[121]
C_3O_2	2258	ν_3 CO stretch, Σ_u^+	DLS in Gas	[122]
	1573	ν_4 CC stretch, Σ_u^+	DLS in Gas	[122]
C_4O	2221.7		MIS in Ar	[114]
	1922.7		MIS in Ar	[114]
	1431.5		MIS in Ar	[114]
	774.8		MIS in Ar	[114]
	484.0		MIS in Ar	[114]

5 Isotopic substitution of oxygen. Implications regarding carbon chain oxides.

Molecule	Absorption, cm^{-1}	Mode	Method	References
C_4O_2	2130.3		MIS in Ar	[113]
	1276.9		MIS in Ar	[113]
	467.1		MIS in Ar	[113]
C_5O	2251.7 (T)		MIS in Ar	[116]
C_5O_2	2213	ν_4, Σ_u^+	MIS in Ar	[114]
	2058.7	ν_5, Σ_u^+	MIS in Ar	[114]
	1144.1	ν_6, Σ_u^+	MIS in Ar	[114]
	539	ν_9, Π_u	MIS in Ar	[114]
	470	ν_{19}, Π_u	MIS in Ar	[114]
C_6O	2163.8	Σ^+	MIS in Ar	[115]
	1447.8	Σ^+	MIS in Ar	[115]
C_7O	2244.2 (T)		MIS in Ar	[116]
	2198.3 (T)		MIS in Ar	[116]
C_7O_2	2187.4	ν_5, Σ_u^+	MIS in Ar	[115]
	2118.5	ν_6, Σ_u^+	MIS in Ar	[115]
	1696.1	ν_7, Σ_u^+	MIS in Ar	[115]
	856.3	ν_8, Σ_u^+	MIS in Ar	[115]
C_9O	2239.5 (T)		MIS in Ar	[116]
	2040.7 (T)		MIS in Ar	[116]

5.2 Experimental details

The experimental setup was described in chapter 2. To observe isotopic shifts several matrices were applied: a pure $^{16}\text{O}_2$ (99.998%), a pure $^{18}\text{O}_2$ (99.998%), a mixed (50%

Molecule	$C_n^{16}O_m$ absorption, cm^{-1}	$C_n^{18}O_m$ absorption, cm^{-1}	Calculated position of $C_n^{18}O_m$, cm^{-1}
CO ₂	2342	2306	2306
C ₃ O	2247	2234, 2228	2230
CO	2135	2084	2084
O ₃	1037	980	978

Tab. 5.2: Positions of various carbon oxide molecules and O₃ in ¹⁶O₂ and ¹⁸O₂ matrices. Comparison with calculated frequency for $C_n^{18}O_m$.

¹⁶O₂ + 50% ¹⁸O₂), a mixed (90% Ar + 10% ¹⁶O₂), and a mixed (90% Ar + 10% ¹⁸O₂). For the experiments reported here the carbon molecules were co-deposited with matrix molecules on a cold substrate at the temperature 25K. The matrix composition of 10% O₂ and 90% Ar at 25K causes the hexagonal close packed (hcp) crystal structure of the matrix, while a pure Ar matrix has a face centered cubic (fcc) lattice [123]. The approximate ratio of carbon to oxygen atoms was kept at about 1:1000. The measurements of the IR-spectra were made with resolution 0.3 cm^{-1} and 1000 scans were accumulated.

5.3 Results and Discussion

¹⁸O₂-matrix. In the pure (99.9%) ¹⁸O₂-matrix (Fig.5.1) one can observe redshifts of IR-active vibrational modes of the oxides. The PM3 calculation, followed by scaling to an experimental value for a ¹⁶O-containing molecule, gives good agreement for several known ¹⁸O-containing molecules (Table 5.2).

One interesting feature in the infrared spectrum is the C₃O absorption in ¹⁸O₂- and ¹⁶O₂-matrices. A single line appears in ¹⁶O₂-matrices at 2247 cm^{-1} whereas two lines appear in ¹⁸O₂ at 2234 and 2228 cm^{-1} . At present we have no explanation for this effect. A possibility is the presence of different sites in ¹⁸O₂ matrix.

The list of the infrared absorptions, shifted after isotopic substitution is presented in the Table 5.3. Some of the lines which are not shifted in an ¹⁸O₂-matrix are

5 Isotopic substitution of oxygen. Implications regarding carbon chain oxides.

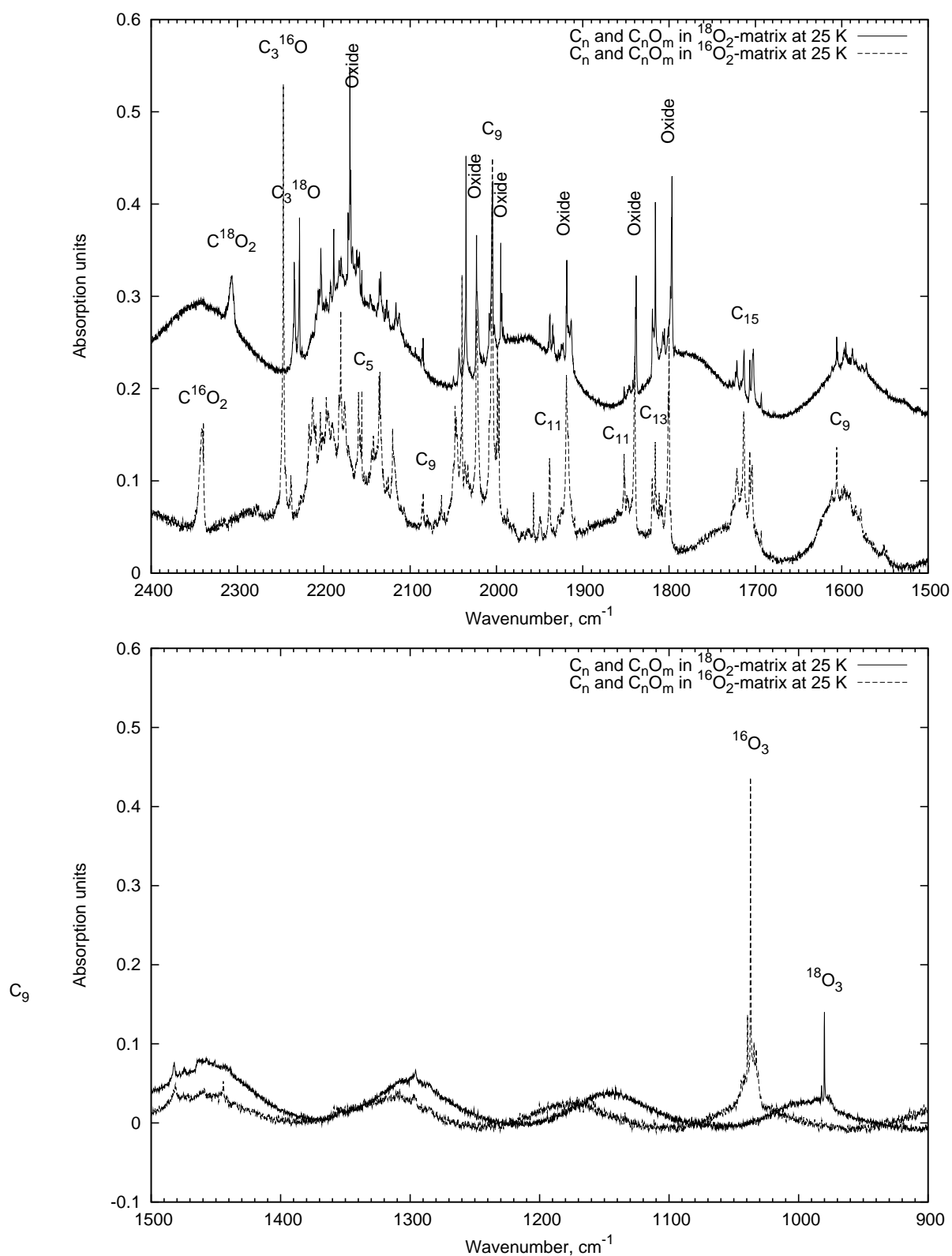


Fig. 5.1: IR-spectrum of carbon species in a pure ¹⁸O₂-matrix and in a pure ¹⁶O₂-matrix at T=25K. The wiggles in the infrared spectra originate from interference on a matrix layer.

Absorption, cm^{-1}	Molecule	Absorption, cm^{-1}	Molecule
2343	CO_2	2135	CO
2240	C_3O	2120	-
2217	-	2063	-
2213	C_5O_2	2047	-
2204	-	2040	-
2202	-	1998	-
2197	-	1997	-
2195	-	1840	-
2194	-	1811	-
2190	-	1809	-
2180	-	1807	-
2175	-	1800	-
2171	-	1704	-
2158	-	1600	-
2145	-	1578	-
2142	-	1037	O_3

Tab. 5.3: Absorptions of oxides in $^{16}\text{O}_2$ -matrix, shifted after oxygen isotopic replacement.

nevertheless definitely oxides, namely the lines at 2020 and 1918 cm^{-1} . The reason that these lines should be oxides is their absence in other matrices like Ar, Ne, Kr, N_2 . According to the qualitative estimates from PM3 calculation such lines (which show very small shifts) may belong to monoxides of long chains, i.e. C_9O , C_{11}O , etc.

(50% $^{16}\text{O}_2$ + 50% $^{18}\text{O}_2$)-matrix. The method of oxygen isotopic substitution in principle should yield information about the number of oxygen atoms in a molecule. In the mixed matrix of 50% $^{16}\text{O}_2$ and 50% $^{18}\text{O}_2$ one can observe a distribution of isotopic peaks of oxides (Fig. 5.2). Basically, molecules containing two

5 Isotopic substitution of oxygen. Implications regarding carbon chain oxides.

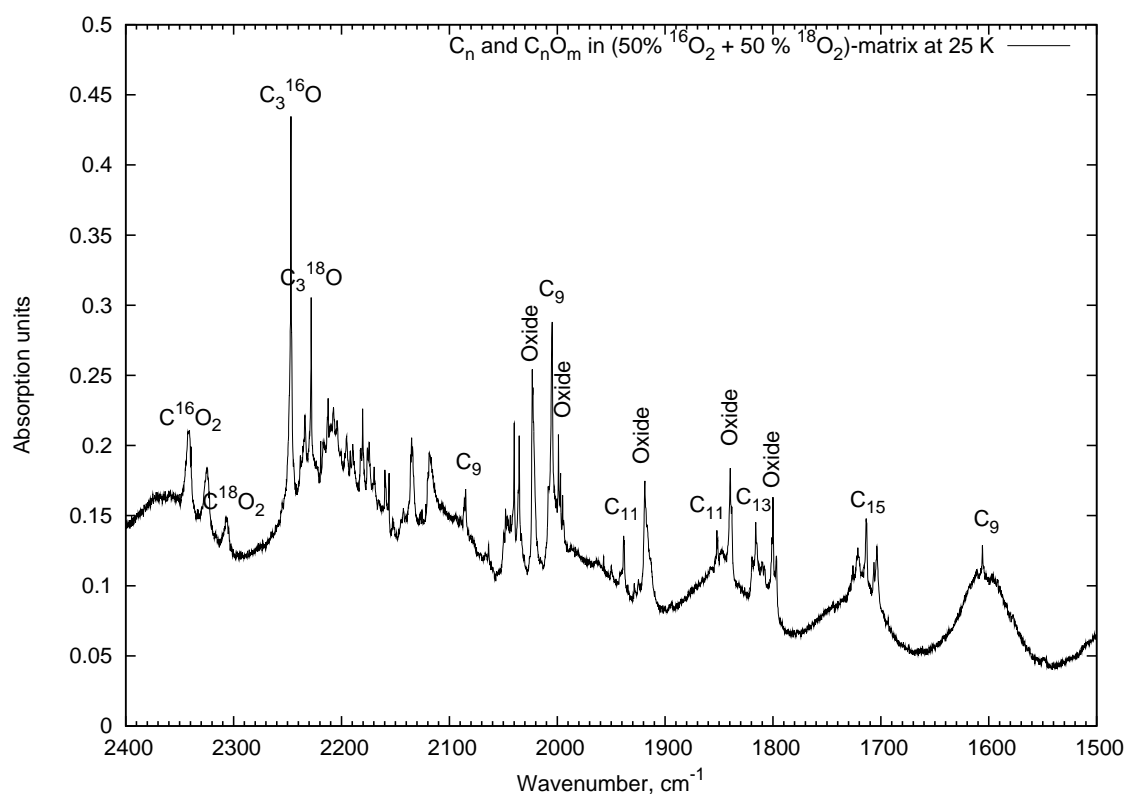


Fig. 5.2: IR-spectrum of carbon species in a mixed (50% $^{18}\text{O}_2 + 50\% \text{}^{16}\text{O}_2$)-matrix at $T=25\text{K}$.

oxygen atoms should give 3 peaks ("16-16", "16-18" and "18-18") for the same vibrational mode in the case when oxygen atoms terminate a carbon chain $\text{O}-(\text{C})_n-\text{O}$ with $D_{\infty h}$ symmetry. Such picture we observe for known molecules, i.e. CO_2 (see Fig. 5.2). Another example is provided by the sharp line at 2180 cm^{-1} (Fig.5.3) which splits to three lines in a mixed matrix: $2180, 2174.3, 2169.7 \text{ cm}^{-1}$. This is a clear indication of a dioxide. Since many IR-absorptions of carbon oxides are already known, we expect that this dioxide has more than 5 carbon atoms. In order to deduce the number of carbon atoms in this dioxide, PM3 calculation was made. For such a molecule PM3 predicts a strong IR-active stretching mode. The position of this absorption considerably shifts to the red with increasing n in odd C_n . Another common feature is that the shift of "18-18" molecule relative to "16-16" molecule becomes smaller with increasing chain length. The results of calculation and experimental data are presented in the Table 5.4. From all unknown dioxides of carbon, C_6O_2 fits quite accurate to the experimental data. So, we assign the

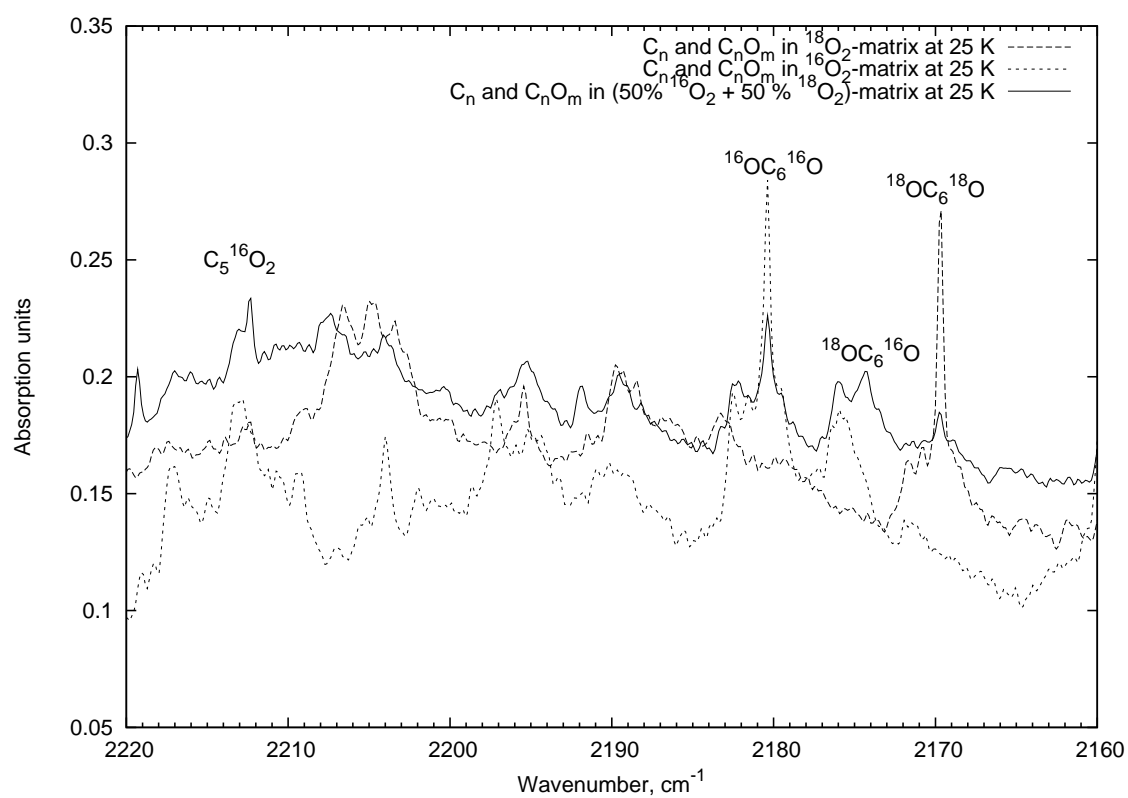


Fig. 5.3: Isotopic distribution of C₆O₂ peaks. IR-spectrum of a mixed (50% ¹⁸O₂ + 50% ¹⁶O₂)-matrix, a pure ¹⁶O₂-matrix and a pure ¹⁸O₂-matrix at T=25K.

5 Isotopic substitution of oxygen. Implications regarding carbon chain oxides.

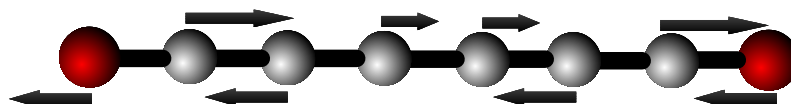


Fig. 5.4: IR-active vibrational mode of C_6O_2 .

absorption line 2180 cm^{-1} in an $^{16}O_2$ -matrix to asymmetric stretching of C_6O_2 (Fig. 5.4). Other researches attempted to synthesize this oxide by pyrolysis of dicarbonic acid chloride and dimethylester [124], but without unambiguous result. No evidence of the presence of C_6O_2 was found.

Molecule	Exp., cm^{-1}	PM3 16-16, cm^{-1}	PM3 18-18 cm^{-1} *	PM3 16-18 cm^{-1} *
C_3O_2	2258, 1573(Gas, [122])	-	-	-
C_5O_2	2213 (Ar, [114]), 2242.13 (Gas, [125])	-	-	-
C_7O_2	2279(T), 2187(w), 2118(vs), 1696(s) (Ar, [115])	-	-	-
C_9O_2	-	2045	2175	2179
$C_{11}O_2$	-	1867	2173	2176.5
C_4O_2	2130 (Ar, [113])	-	-	-
C_6O_2	-	2395	2169.4	2174.8
C_8O_2	-	2311	2176.2	2178.1
$C_{10}O_2$	-	2237.6	2176.8	2179.3

Tab. 5.4: Absorptions of oxides in an $^{16}O_2$ -matrix. *The calculated data for $^{18}OC_n^{18}O$ and $^{16}OC_n^{18}O$ scaled in such a way that $^{16}OC_n^{16}O$ absorption is at 2180 cm^{-1} . The dioxides of odd carbon chains are singlets and the dioxides of even carbon chains have a triplet ground state.

Analysis of the peaks distribution in the mixed matrix allows also to distinguish oxides which most probably are monoxides from other oxides in case of sufficient isotopic shift for our resolution of 0.3 cm^{-1} (IR-spectra were recorded with this resolution and we can not detect shifts less than 0.1 cm^{-1}). The Table 5.5 contains

Absorption in $^{16}\text{O}_2$, cm^{-1}	Absorption in $^{18}\text{O}_2$, cm^{-1}
2039.8	2035.2
1998.7	1995
1996.9	1993.7
1800	1796.6

Tab. 5.5: *Infrared absorptions of unidentified oxides, having only two peaks in the mixed matrix. Most probably these absorptions belong to monoxides.*

absorptions, which have only two peaks in the mixed matrix, so probably belonging to monoxides. However, there is a possibility that a dioxide has also only two peaks in a mixed matrix if the terminating carbon chain oxygen atoms originally are from the same oxygen molecule (the matrix consists of $^{16}\text{O}_2$ and $^{18}\text{O}_2$ molecules). The reaction of such a dioxide formation is $\text{C}_n + \text{O}_2 \longrightarrow \text{OC}_n\text{O}$.

(Ar + 10% $^{18}\text{O}_2$)-matrix. In order to confirm our oxides assignments and measure the positions of oxides in an Ar-matrix, 10% of $^{18}\text{O}_2$ was mixed with Ar (Fig. 5.5). Comparing an (Ar + 10% $^{18}\text{O}_2$)-matrix and (Ar + 10% $^{16}\text{O}_2$)-matrix one can find shifted oxides absorptions (Table 5.6).

As was already mentioned in chapters 3 and 4, absorptions at 1803 and 1844 cm^{-1} in an Ar-matrix are from oxides. Indeed, substitution of $^{16}\text{O}_2$ by $^{18}\text{O}_2$ caused the redshift of these absorptions (Fig.5.6). The exact positions of these lines in a mixed (Ar + 10% $^{16}\text{O}_2$)-matrix are 1802.1 and 1841.9 cm^{-1} . As possible carriers for these two absorptions we suggest C_{13}O , C_{13}O_2 , C_{11}O or C_{11}O_2 . The assumed number of carbon atoms is based on the position of electronic absorption and configuration interaction calculations (see page 51). In the literature the infrared absorptions at 1803 and 1844 cm^{-1} were tentatively assigned to C_{13} [62]. The absorption at 1844 cm^{-1} was also assigned to cyclic C_8 [60, 61]. We have shown that these absorptions are oxides, so the presence of 1803 and 1844 cm^{-1} lines in Ar-matrix is probably due to oxygen impurities.

5 Isotopic substitution of oxygen. Implications regarding carbon chain oxides.

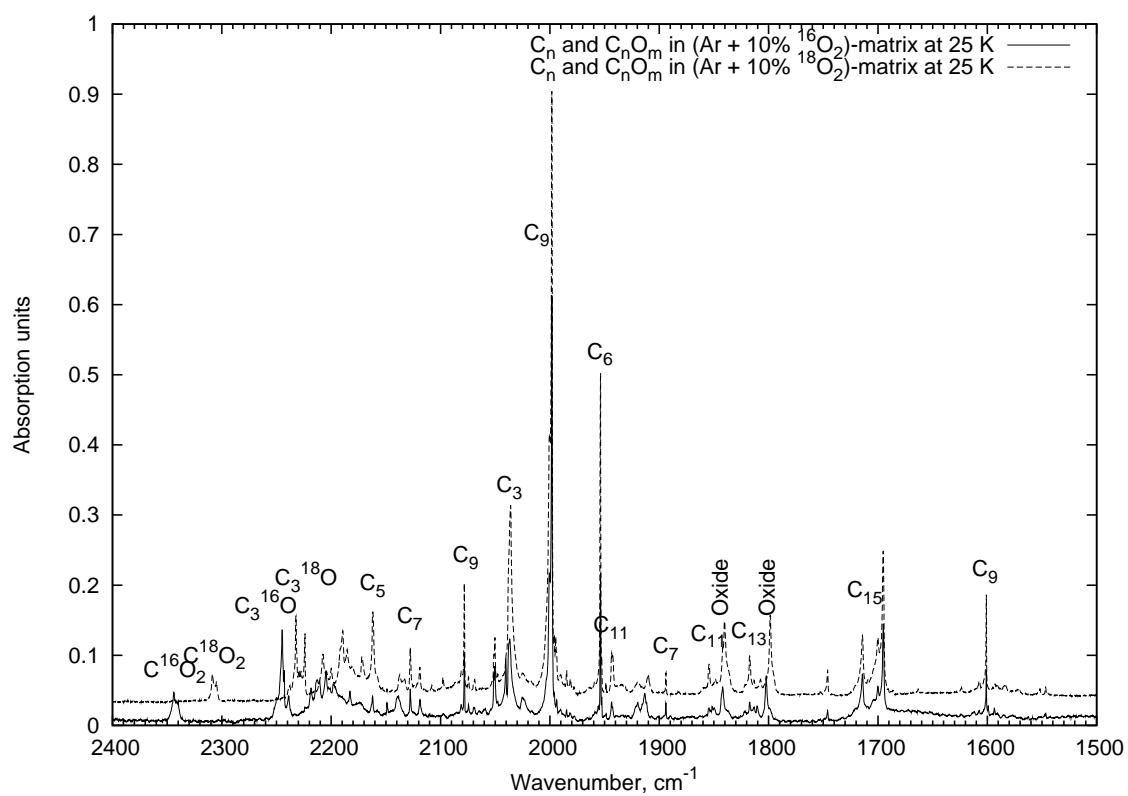


Fig. 5.5: IR-spectra of carbon species in a (Ar + 10% ¹⁸O₂)-matrix and in a (Ar + 10% ¹⁶O₂)-matrix at $T=25\text{K}$. All known absorptions of pure carbon molecules are unshifted.

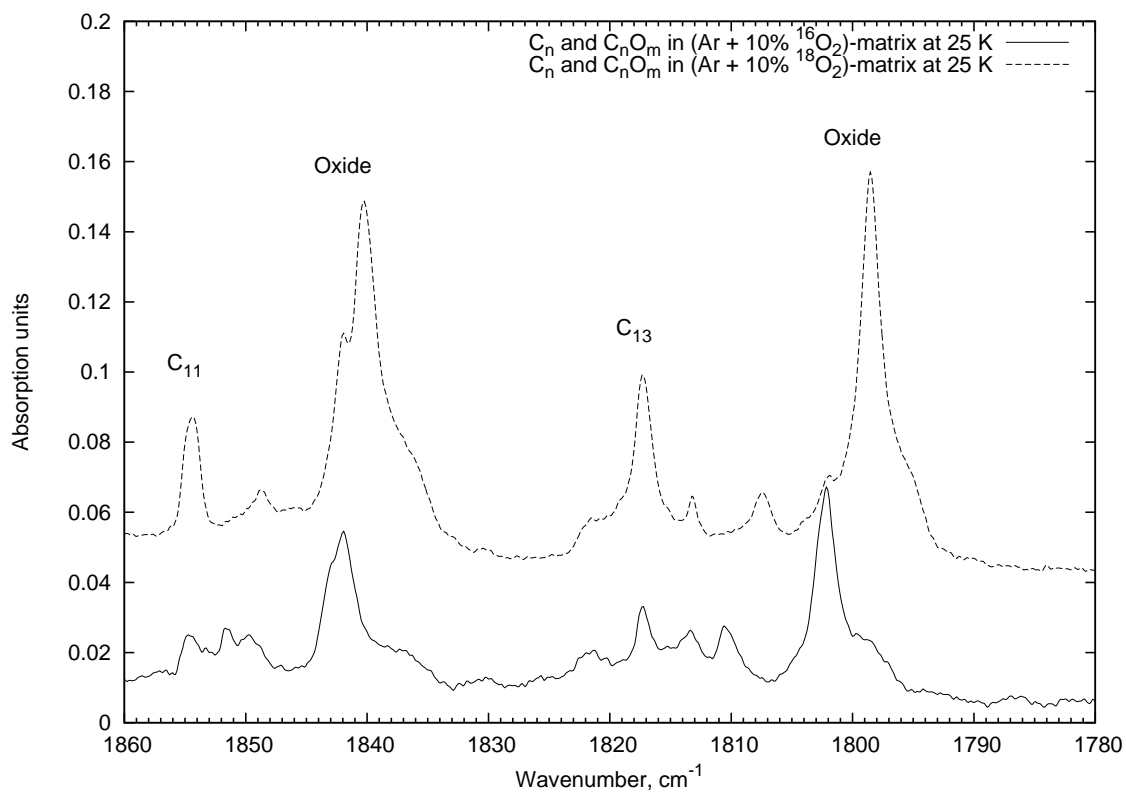


Fig. 5.6: IR-spectra of carbon species in a (Ar + 10% ¹⁸O₂)-matrix and in a (Ar + 10% ¹⁶O₂)-matrix at $T=25\text{K}$. The substantial shift of the absorptions at 1842 and 1802 cm^{-1} indicates that the carrier of this features is/are (an) oxide(s).

5 Isotopic substitution of oxygen. Implications regarding carbon chain oxides.

Absorption, cm^{-1}	Molecule	Absorption, cm^{-1}	Molecule
2343.7	CO_2	2040.4	-
2244.8	C_3O	1993.7	-
2218	-	1913.2	-
2213	C_5O_2	1841.9	-
2210.7	-	1810.3	-
2204.8	-	1802.1	-
2182.8	C_6O_2^*	1593.5	-
2173.6	-	1585	-
2139	CO	1039	O_3
2110	-		

Tab. 5.6: Absorptions of oxides and O_3 in $(\text{Ar} + {}^{16}\text{O}_2)$ -matrix, shifted after oxygen isotopic replacement. * Our identification.

6. Conclusions and Outlook

The positions of the absorptions of known carbon species in oxygen, argon and in argon-oxygen mixed matrices were compared. The data were used to extrapolate the line positions in pure oxygen matrices. We have found that pure carbon molecules at least partly survive after oxygen addition to the rare-gas matrices and still exist in pure oxygen matrices. The reason for the low abundance of even-numbered carbon chains in oxygen matrices is their high reactivity which probably originates from their triplet electronic ground state.

The laser-induced oxidation method was successfully tested on linear C_9 , C_{11} , C_{13} molecules, confirming the existing data about the IR absorptions of these species.

We searched for the IR absorption of C_{13} in O_2 matrices in vicinity of the known frequency of the of this band in gas-phase [23]). The 1819, 1816 cm^{-1} pattern of absorptions in O_2 (1818 cm^{-1} in Ar) we assign to the IR-active C_{13} stretching mode. The assignment of the 1818 cm^{-1} absorption in Ar to cyclic C_8 [62] seems to be in error.

Application of the oxidation method to linear C_{15} has provided new information about the infrared active transition of this molecule. The adjacent absorption lines at 1721, 1714 and 1707 cm^{-1} we assigned as site peaks of the C_{15} absorption in the β -phase of an oxygen matrix. Another line at 1695 cm^{-1} was assigned to a site peak of C_{15} in an Ar- O_2 mixed matrix. The existing literature assignment of the 1695 cm^{-1} as absorption of cyclic C_6 [54, 55] seems to be wrong.

A strong correlation of the 1704 cm^{-1} vibrational absorption and the 452 nm electronic absorption in O_2 -matrix was found. We propose $C_{13}O_2$, $C_{13}O$, $C_{15}O_2$ or $C_{15}O$ as possible carrier of this absorptions.

The isotopic substitution of oxygen has revealed that two absorptions at 1803 and 1844 cm^{-1} in an Ar-matrix (1800 and 1840 cm^{-1} in O_2) belong to oxides of carbon.

6 Conclusions and Outlook

We have found that the corresponding electronic absorption of the "1800/1840-oxide(s)" lies at 397 nm in an oxygen matrix. According to our estimate the absorber can be an oxide of a long carbon chain: $C_{13}O$, $C_{13}O_2$, $C_{11}O$ or $C_{11}O_2$. Therefore, tentative assignment of these two absorptions to C_{13} [62] and the assignment of 1844 cm^{-1} line to cyclic C_8 [60, 61] seem to be in error.

The ^{18}O isotopic substitution has provided information about positions of IR absorptions of carbon oxides in O_2 - and $(Ar+10\%O_2)$ - matrices. The absorption at 2180 cm^{-1} in a $^{16}O_2$ matrix was assigned to the C_6O_2 molecule.

The laser-induced oxidation method for the identification of IR-absorptions of carbon molecules was successfully tested and applied. This method may prove useful also for the characterization of still larger linear chains and cyclic carbon species.

From our data it appears that the IR absorptions of very long odd chains are very intense and the power of absorption is concentrated in a single vibrational mode. The frequency of this vibration seems to decrease steadily with the number of carbon atoms in the chain, yielding a strikingly simple sequence of IR lines.

Bibliography

- [1] G.H. Herbig. The diffuse interstellar bands. *Annual Review of Astronomy and Astrophysics*, 33:359, 1995.
- [2] A.E. Douglas. Origin of diffuse interstellar lines. *Nature*, 269:130–132, 1997.
- [3] A.E. Douglas. Laboratory studies of the λ 4050 group of cometary spectra. *Nat. Res. Council*, 2503:466–468, 1951.
- [4] R. Gredel, E.F. van Dishoeck, and J.H. Black. Fluorescent vibration-rotation excitation of cometary C_2 . *Astrophysical Journal*, 338:1047–1070, 1989.
- [5] D.L. Lambert and A.C. Danks. High-resolution spectra of C_2 swan bands from comet west 1976 VI. *Astrophysical Journal*, 268:428–446, 1983.
- [6] D.L. Lambert, Y. Sheffer, and S.R. Federman. Hubble space telescope observations of C_2 molecules in diffuse interstellar clouds. *Astrophysical Journal*, 438:740–749, 1995.
- [7] K.H. Hinkle, J.J. Keady, and P.F. Bernath. Detection of C_3 in the circumstellar shell of IRC+10216. *Science*, 241:1319–1322, 1988.
- [8] G. Wallerstein and G.R. Knapp. Carbon stars. *Annual Review of Astronomy and Astrophysics*, 36(1):369–433, 1998.
- [9] H.W. Kroto, R.J. Heath, S.C. Brien, R.F. Curl, and R.E. Smalley. C_{60} : Buckminsterfullerene. *Nature*, 318(6042):162–163, 1985.
- [10] W. Krätschmer, L.D. Lamb, K. Fostiropoulos, and D.R. Huffman. Solid C_{60} : a new form of carbon. *Nature*, 347(6291):354–358, 1990.

- [11] S. Ijima. Helical microtubules of graphitic carbon. *Nature*, 354(6348):56–58, 1991.
- [12] G. von Helden. *Investigation of the structure and energetics of gas phase cluster ions using ion chromatography*. PhD thesis, Santa Barbara, 1993.
- [13] T. Wakabayashi and Y. Achiba. A model for the C₆₀ and C₇₀ growth mechanism. *Chem. Phys. Lett.*, 190:465–468, 1992.
- [14] Y.-M. Koo, Y.-K. Choi, K.H. Lee, and K.-W. Jung. Mass spectrometric study of carbon formation in laser ablation of graphite at 355 nm. *Bull. Korean Chem. Soc.*, 23(2):309–314, 2002.
- [15] L.A. Bloomfield, M.E. Geusic, R.R. Freeman, and W.L. Brown. Negative and positive cluster ions of carbon and silicon. *Chemical Physics Letters*, 121:33–37, 1991.
- [16] P. Freivogel, J. Fulara, D. Lessen, D. Forney, and J.P. Maier. Absorption spectra of conjugated hydrocarbon cation chains in neon matrices. *Chemical Physics*, 189:335–341, 1994.
- [17] D. Forney, J. Fulara, P. Freivogel, M. Jakobi, D. Lessen, and J. P. Maier. Electronic absorption spectra of linear carbon chains in neon matrices. I. C₆⁻, C₆, and C₆H. *Journal of Chemical Physics*, 103:48–53, 1995.
- [18] F. Cataldo. Polyynes production in a solvent-submerged electric arc between graphite electrodes. I. Synthesis and spectroscopy. *Fullerenes, Nanotubes, and Carbon Nanostructures*, 12:603–617, 2004.
- [19] W. Weltner and R.J. Van Zee. Small carbon clusters. *Chemical Reviews*, 89:1713–1747, 1989.
- [20] A. Van Orden and R. Saykally. Small carbon clusters. *Chemical Reviews*, 98(6):2314–2357, 1998.
- [21] J.R. Heath and R.J. Saykally. The C₉ cluster: Structure and infrared frequencies. *J. Chem. Phys.*, 93:8392–8394, 1990.

-
- [22] T.F. Giesen, U. Berndt, K.M.T. Yamada, G. Fuchs, R. Schieder, G. Winnewisser, R.A. Provencal, F.N. Keutsch, A. Van Orden, and R.J. Saykally. Detection of the linear carbon cluster C₁₀: rotationally resolved diode-laser spectroscopy. *Chem. Phys. Chem.*, 2:242–247, 2001.
- [23] T.F. Giesen, A. Van Orden, H.J. Hwang, R.S. Fellers, R.A. Provencal, and R.J. Saykally. Infrared laser spectroscopy of the linear C₁₃ carbon cluster. *Science*, 265:756–759, 1994.
- [24] P. Neubauer-Guenther, T. F. Giesen, U. Berndt, G. Fuchs, and G. Winnewisser. The cologne carbon cluster experiment: ro-vibrational spectroscopy on C₈ and other small carbon clusters. *Spectrochimica Acta Part A: Molecular and Biomolecular Spectroscopy*, 59:431–441, 2003.
- [25] P. Birza, T. Motylewski, D. Khoroshev, A. Chirokolava, H. Linnartz, and J. P. Maier. Cw cavity ring down spectroscopy in a pulsed planar plasma expansion. *Chem. Phys.*, 283:119–124, 2002.
- [26] R. Engeln, G. von Helden, A.J.A. van Roij, and G. Meijer. Cavity ring down spectroscopy on solid C₆₀. *J. Chem. Phys.*, 110:2732–2733, 1999.
- [27] D.W. Arnold, S.E. Bradforth, T.N. Kitsopoulos, and D.M. Neumark. Vibrationally resolved spectra of C₂–C₁₁ by anion photoelectron spectroscopy. *J. Chem. Phys.*, 95:8753–8764, 1991.
- [28] S. Goyal, D.L. Schutt, and G. Scoles. Vibrational spectroscopy of sulfur hexafluoride attached to helium clusters. *Phys. Rev. Lett.*, 69:933–936, 1992.
- [29] S. Goyal, D.L. Schutt, and G. Scoles. Infrared spectroscopy in highly quantum matrixes: vibrational spectrum of sulfur hexafluoride ((SF₆)_{n=1,2}) attached to helium clusters. *J. Phys. Chem.*, 97:2236–2245, 1993.
- [30] NIST Chemistry WebBook. <http://webbook.nist.gov>.
- [31] W.Jr. Weltner, P.N. Walsh, and C.L. Angell. Spectroscopy of carbon vapor condensed in rare-gas matrices at 4 and 20K. I. *Journal of Chemical Physics*, 40(5):1299–1305, 1964.

- [32] J. Szczepanski, S. Ekern, Ch. Chapo, and M. Vala. Infrared spectroscopy of matrix-isolated carbon clusters, with emphasis on C_8 and C_9 . *Chemical Physics*, 211(5):359–366, 1996.
- [33] M. Miki, T. Wakabayashi, T. Momose, and T. Shida. Infrared spectroscopic studies of carbon clusters trapped in solid parahydrogen. *J. Phys. Chem.*, 100(30):12135–12137, 1996.
- [34] B.J. Ortman, R.H. Hauge, and J.L. Margrave. Chemical reactions of carbon atoms and molecules from laser-induced vaporization of graphite TaC and WC. *J. Quant. Spectr.*, 40(3):439–447, 1988.
- [35] L. Gausset, G. Herzberg, A. Lagerqvist, and B. Rosen. Analysis of the 4050-A group of the C_3 molecule. *Astrophysical Journal*, 142(1):45–76, 1965.
- [36] K. Kawaguchi, K. Matsumura, H. Kanamori, and E. Hirota. Diode laser spectroscopy of C_3 : The $\nu_2 + \nu_3 - \nu_2$, $\nu_{22} + \nu_3 - \nu_{22}$, and $\nu_{22} + \nu_3$ bands. *J. Chem. Phys.*, 91(4):1953–1957, 1989.
- [37] W.Jr. Weltner and D.Jr. McLeod. Spectroscopy of carbon vapor condensed in rare-gas matrices at 4 and 20K. II. *Journal of Chemical Physics*, 40(5):1305–1316, 1964.
- [38] I. Cermak, M. Förderer, S. Kalhofer, H. Stopka-Ebeler, G. Monninger, and W. Krätschmer. Laser-induced emission spectroscopy of matrix-isolated carbon molecules: Experimental setup and new results on C_3 . *Journal of Chemical Physics*, 108(24):10129–10142, 1998.
- [39] J. R. Heath and R. J. Saykally. The structure of the C_4 cluster radical. *Journal of Chemical Physics*, 94:3271–3273, 1991.
- [40] L.N. Shen and W.M. Graham. Observation of an infrared frequency of the C_4 molecule. *Journal of Chemical Physics*, 91(8):5115–5116, 1989.
- [41] A.M. Smith, J. Agreiter, M. Härtle, C. Engel, and V.E. Bondybey. Rare gas matrix studies of absorption and fluorescence of reactive intermediates formed in discharges through acetylene. *Chemical Physics*, 189:315–334, 1994.

-
- [42] N. Moazzen-Ahmadi, J.J. Thong, and A.R.W. McKellar. Infrared diode laser spectroscopy of the ν_3 fundamental and $\nu_3 + \nu_5 - \nu_5$ sequence bands of the C_4 radical in a hollow cathode discharge. *Journal of Chemical Physics*, 100:4033–4038, 1994.
- [43] P.A. Withey, L.N. Shen, and W.R.M. Graham. Fourier transform far infrared spectroscopy of a C_4 bending mode. *Journal of Chemical Physics*, 95:820–823, 1991.
- [44] J.R. Heath, A. L. Cooksy, M.H.W. Gruebele, C.A. Schmuttenmaer, and R.J. Saykally. Diode-laser absorption spectroscopy of supersonic carbon cluster beams: The spectrum of C_5 . *Science*, 244:564–565, 1989.
- [45] K.H. Hinkle, J.J. Keady, and P.F. Bernath. Detection of C_5 in the circumstellar shell of IRC +10216. *Science*, 244:562–564, 1989.
- [46] K.I. Dismuke, W.R.M. Graham, and W.Jr. Weltner. The C_4 molecule. *Astrophys. J.*, 204:301–310, 1976.
- [47] K.R. Thompson, R.L. DeKock, and W. Jr. Weltner. Spectroscopy of carbon molecules IV. *J. Am. Chem. Soc.*, 93:4688–4695, 1971.
- [48] A.M. Smith, J. Agreiter, M. Härtle, C. Engel, and V.E. Bondybey. Rare gas matrix studies of absorption and fluorescence of reactive intermediates formed in discharges through acetylene. *Chemical Physics*, 189:315–334, 1994.
- [49] R.H. Kranze and W.R.M. Graham. Fourier transform infrared observation of the ν_4 stretching of linear C_5 in Ar at 10K. *J. Chem. Phys.*, 96:2517–2521, 1992.
- [50] H.J. Hwang, A. Van Orden, K. Tanaka, E.W. Kuo, J.R. Heath, and R.J. Saykally. Infrared laser spectroscopy of jet-cooled carbon clusters. Structure of triplet C_6 . *Mol. Phys.*, 79:769–766, 1993.
- [51] J. Kurtz and D.R. Huffman. Combined infrared and ultraviolet-visible spectroscopy of matrix-isolated carbon vapor. *J. Chem. Phys.*, 92:30–35, 1990.

- [52] S. Tam, M. Macler, and M.E. Fajardo. Matrix isolation spectroscopy of laser ablated carbon species in Ne, D₂, and H₂ matrices. *J. Chem. Phys.*, 106:8955–8963, 1997.
- [53] C. Xu, G.R. Burton, T.R. Taylor, and D.M. Neumark. Photoelectron spectroscopy of C₄⁻, C₆⁻, and C₈⁻. *J. Chem. Phys.*, 107:3428–3436, 1997.
- [54] S.L. Wang, C.M. Rittby, and W.R.M. Graham. Detection of cyclic carbon clusters. II. Isotopic study of the $\nu_4(e_u)$ mode of cyclic C₆ in solid Ar. *J. Chem. Phys.*, 107(16):6032–6037, 1997.
- [55] J.D. Presilla-Marquez, J.A. Sheehy, J.D. Mills, P.G. Carrick, and C.W. Larson. Vibrational spectra of cyclic C₆ in solid argon. *Chem.Phys.Lett.*, 274:439–444, 1997.
- [56] J.R. Heath, A. Van Orden, E. Kuo, and R.J. Saykally. The ν_5 band of C₇. *Chem. Phys. Letters*, 182:17–20, 1991.
- [57] R.H. Kranze, C.M.L. Rittby, and W.R.M. Graham. Fourier transform infrared and theoretical isotopic study of the $\nu_4(\sigma_u)$ and $\nu_5(\sigma_u)$ of linear C₇. *J. Chem. Phys.*, 105:5313–5320, 1996.
- [58] D. Forney, M. Grutter, P. Freivogel, and J.P. Maier. New vibrational frequencies of mass selected C₈ and C₉ in neon matrices. In J.P.Maier and M. Quack., editors, *Proceeding SASP.*, pages 106–107, 1996.
- [59] P. Freivogel, M. Grutter, D. Forney, and J.P. Maier. Infrared bands of mass-selected carbon chains C_n (n=8–12) and C_n⁻ (n= 5 - 10, 12) in neon matrices. *Chem. Phys.*, 216:401–406, 1997.
- [60] S.L. Wang, C.M. Rittby, and W.R.M. Graham. Detection of cyclic carbon clusters. II. Isotopic study of the $\nu_{12}(e_u)$ mode of cyclic C₈ in solid Ar. *J. Chem. Phys.*, 107(18):7025–7033, 1997.
- [61] S.L. Wang, C.M. Rittby, and W.R.M. Graham. On the identification of the vibrational spectrum of cyclic C₈ in solid Ar. *J. Chem. Phys.*, 112(3):1457–1461, 2000.

-
- [62] J.D. Presilla-Marquez, J. Harper, J.A. Sheehy, P.G. Carrick, and C.W. Larson. Vibrational spectra of cyclic C_8 in solid argon. *Chem. Phys. Lett.*, 300:719–726, 1999.
- [63] A. Van Orden, R.A. Provencaal, F.N. Keutsch, and R.J. Saykally. Infrared laser spectroscopy of jet-cooled carbon clusters: The ν_5 band of linear C_9 . *J. Chem. Phys.*, 105:6111–6116, 1996.
- [64] J.C. Hayes and R.S. Sheridan. *J. Am. Chem. Soc.*, 112:5879, 1990.
- [65] M. Vala, T.M. Chandrasekhar, J. Szczepanski, and R. Pellow. *High Temp. Sci.*, 27:19, 1988.
- [66] R.H. Kranze, P.A. Withey, C.M.L. Rittby, and W.R.M. Graham. Fourier transform infrared observation of the ν_7 stretching of linear C_9 in Ar at 10K. *J. Chem. Phys.*, 103:6841–6850, 1995.
- [67] M. Grutter, P. Freivogel, D. Forney, and J.P. Maier. Diffusion of mass-selected carbon atoms and molecules in argon and neon matrices. *J. Chem. Phys.*, 107:5356–5360, 1997.
- [68] L. Lapinski and M. Vala. Linear C_{11} cluster: an isotopic infrared study. *Chem. Phys. Lett.*, 300:195–201, 1999.
- [69] X.D. Ding, S.L. Wang, C.M.L. Rittby, and W.R.M. Graham. Fourier transform infrared isotopic study of the C_{12} chain trapped in solid Ar. *J. Chem. Phys.*, 112:5113–5120, 2000.
- [70] M. Grutter, M. Wyss, E. Riaplov, J.P. Maier, S.D. Peyerimhoff, and M. Hanrath. *J. Chem. Phys.*, 111:7397, 1999.
- [71] M. Wyss, M. Grutter, and J.P. Maier. Electronic spectra of long odd-number carbon chains $C_{17} - C_{21}$ and $C_{13}^- - C_{21}^-$. *Chemical Physics letters*, 304:35–38, 1999.
- [72] D. Forney, P. Freivogel, M. Grutter, and J.P. Maier. Electronic absorption spectra of linear carbon chains in neon matrices. IV. C_{2n+1} $n=2 - 7$. *J. Chem. Phys.*, 104(13):4954–4960, 1996.

- [73] T. Wakabayashi. C_n absorptions in Ne. (Private communications).
- [74] J.P. Maier. Electronic spectroscopy of carbon chains and their relevance to astrophysics. In S. Palfzner, C. Kramer, C. Staubmeier, and A. Heithausen, editors, *The Dense Interstellar Medium in Galaxies*, volume 91 of *Springer Proceedings in Physics*, pages 55–60. Springer Verlag Berlin, 2004.
- [75] P. Botschwina. Spectroscopic properties of interstellar molecules: theory and experiment. *Phys. Chem. Chem. Phys.*, 5:3337–2245, 2003.
- [76] J.M.L. Martin, J. El-Yazal, and J.-P. Francois. Structure and relative energetics of C_{2n+1} ($n = 2-7$) carbon clusters using coupled cluster and hybrid density functional methods. *Chem. Phys. Lett.*, 252:9–18, 1996.
- [77] R.A. Broglia, G. Colò, G. Onida, and H.E. Roman. *Solid state physics of finite systems*. Springer–Verlag Berlin Heidelberg edition, 2004. (pp. 123–130).
- [78] M. J. Frisch, G. W. Trucks, H. B. Schlegel, G. E. Scuseria, M. A. Robb, J. R. Cheeseman, V. G. Zakrzewski, J. A. Montgomery, Jr., R. E. Stratmann, J. C. Burant, S. Dapprich, J. M. Millam, A. D. Daniels, K. N. Kudin, M. C. Strain, O. Farkas, J. Tomasi, V. Barone, M. Cossi, R. Cammi, B. Mennucci, C. Pomelli, C. Adamo, S. Clifford, J. Ochterski, G. A. Petersson, P. Y. Ayala, Q. Cui, K. Morokuma, D. K. Malick, A. D. Rabuck, K. Raghavachari, J. B. Foresman, J. Cioslowski, J. V. Ortiz, A. G. Baboul, B. B. Stefanov, G. Liu, A. Liashenko, P. Piskorz, I. Komaromi, R. Gomperts, R. L. Martin, D. J. Fox, T. Keith, M. A. Al-Laham, C. Y. Peng, A. Nanayakkara, M. Challacombe, P. M. W. Gill, B. Johnson, W. Chen, M. W. Wong, J. L. Andres, C. Gonzalez, M. Head-Gordon, E. S. Replogle, and J. A. Pople. *Gaussian 98, Revision A.9*. Gaussian, inc., pittsburgh pa edition, 1998.
- [79] Hyperchem for Windows. Release 6.02.
- [80] A. Szabo and M.S. Ostlund. *Modern quantum chemistry. Introduction to advanced electronic structure theory*. Dover Publications, Inc., 1996.
- [81] *Hyperchem Computational Chemistry. Part 2. Theory and Methods*. Hypercube, Inc. edition, 2002. Publication HC70-00-04-00.

-
- [82] J.J.P. Stewart. *J. Comp. Chem.*, 10:209, 1989.
- [83] J.J.P. Stewart. *J. Comp. Chem.*, 10:221, 1989.
- [84] M.J.S. Dewar and M.L.McKee. *J. Am. Chem. Soc.*, 99:5231, 1977.
- [85] M.J.S. Dewar and W. Thiel. *J. Am. Chem. Soc.*, 99:4899, 1977.
- [86] M.J.S. Dewar and H.S. Rzepa. *J. Am. Chem. Soc.*, 100:58, 1978.
- [87] L.P. Davis, R.M. Guidry, J.R. Williams, M.J.S. Dewar, and H.S. Rzepa. *J. Comp. Chem.*, 2:433, 1981.
- [88] M.J.S. Dewar, E.G. Zoebisch, and E.F. Healy. AM1: a new general purpose quantum mechanical molecular model. *J. Am. Chem. Soc.*, 107:3902, 1985.
- [89] P. Hohenberg and W. Kohn. Inhomogeneous electron gas. *Phys.Rev. B*, 136:864, 1964.
- [90] W. Kohn and L.J. Sham. Self-consistent equations including exchange and correlation effects. *Phys.Rev. A*, 140:1133, 1965.
- [91] A.D. Becke. Density-functional thermochemistry. III. The role of exact exchange. *J. Chem. Phys.*, 98:5648, 1993.
- [92] I. Cermak, G. Monninger, and W. Krätschmer. Absorption spectra of matrix-isolated small carbon molecules. *Advances in Molecular Structure Research.*, 3:117–146, 1997.
- [93] S. Kahlhofer. *Absorptions-, Emissions- und Anregungsspektren von linearen Kohlenstoffmolekülen in Edelgasmatrizen*. PhD thesis, Heidelberg, 2000.
- [94] U. Brackmann. *Lambdachrome Laser Dyes*. Lambda physik gmbh edition, 1994.
- [95] G.R. Smith and W.A. Guillory. Spectroscopy of the thermal oxidation of NO in solid oxygen at cryogenic temperatures. *Journal of Molecular Spectroscopy*, 68:223–235, 1977.

- [96] D. Schmeisser, K. Jacobi, and D. M. Kolb. Copper clusters isolated in oxygen matrices. *Applications of Surface Science*, 11-12:164–171, 1982.
- [97] M. Bahou, L. Schriver-Mazzuoli, C. Camy-Peyret, and A. Schriver. Photolysis of ozone at 693 nm in solid oxygen. Isotopic effects in ozone reformation. *Chemical Physics Letters*, 273:31–36, 1997.
- [98] J.R. Sodeau and E.K.C. Lee. Photooxidation of sulfur dioxide in low-temperature matrices. *Journal of Physical Chemistry*, 84:3358 – 3362, 1980.
- [99] G.C. De Fotis. Magnetism of solid oxygen. *Phys. Rev. B*, 23:4714–4740, 1981.
- [100] R. Eastmond, T. R. Johnson, and D. R. M. Walton. Silylation as a protective method for terminal alkynes in oxidative couplings : A general synthesis of the parent polyynes $H(C=C)_nH$ ($n = 4-10, 12$). *Tetrahedron*, 28:4601–4616, 1972.
- [101] A.V. Benderskii and C.A. Wight. Photochemistry of ozone in solid mixtures with argon. *The Journal of Chemical Physics*, 101:292–298, 1994.
- [102] R.N. Perutz. *Inorganic and organic photochemistry*, pages 239–275. Elsevier Science Publishers, 1989.
- [103] Satoshi Hashimoto and Hajime Akimoto. Absorption spectra of contact-charge-transfer bands and photochemical reactions of simple alkenes in the cryogenic oxygen matrix. *Journal of Physical Chemistry*, 91(6):1347–1354, 1987.
- [104] T. Wakabayashi et al. Laser induced dissociation of linear C_6 and reorientation of trapping sites in solid Neon. In *Nanonetwork materials*, volume CP590, page 513. AIP, 2001.
- [105] G. Monninger. *Optische Spektroskopie von matrix-isolierten Kohlenstoff-Chustern*. PhD thesis, Heidelberg, 1995.
- [106] T. Wakabayashi. DFT calculations of vibrational frequencies of linear C_n molecules. (unpublished data).
- [107] R.S. Mulliken. *J. Chem. Phys.*, 23:1833, 1841, 2338, 2343, 1955.

-
- [108] G.M. Barrow. *Introduction to molecular spectroscopy*. International student edition, 1962.
- [109] R.J. McMahon. Chemical reactions involving quantum tunneling. *Science*, 299:833–834, 2003.
- [110] I. Fleming. *Frontier orbitals and organic chemical reactions*. A Wiley–Interscience Publication edition, 2004.
- [111] G. Herzberg. *Molecular spectra and molecular structure. I. Spectra of diatomic molecules*. D. van nostrand company,inc. princeton edition, 1964.
- [112] G. Herzberg. *Infrared and Raman Spectra of Polyatomic molecules*. D. van nostrand company,inc. princeton edition, 1962.
- [113] G. Maier, H.P. Reisenauer, H. Balli, W. Brandt, and R. Janoschek. C₄O₂ (1,2,3,4-Pentatetraen -1,4-dion), das erste Dioxid des Kohlenstoffs... *Angew. Chem.*, 102:920–925, 1990.
- [114] G. Maier, H.P. Reisenauer, U. Schäfer, and H. Balli. C₅O₂ (1,2,3,4-Pentatetraen -1,5-Dion), ein neuers Oxid des Kohlenstoffs. *Angew. Chem.*, 100:590–592, 1988.
- [115] G. Maier, H.P. Reisenauer, and A. Ulrich. Matrixspectroskopische Untersuchungen zur Existenz von C₇O₂ (1,2,3,4,5,6-Heptahexaen-1,7-Dion). *Tetrahedron Lett.*, 32:4469–4472, 1991.
- [116] M. Dibben, J. Szczepanski, C. Wehlburg, and M. Vala. Complexes of linear carbon clusters with water. *J. Chem. Phys.*, 104:3584–3592, 2000.
- [117] E. Weissberger, W.H. Breckenridge, and H. Taube. Reaction of O(¹D) with CO₂ at low temperatures. *J. Chem. Phys.*, 47:1764–1769, 1967.
- [118] M.E. Jacox, D.E. Milligan, N.G. Moll, and W.E. Thompson. Matrix-isolation infrared spectrum of the free radical CCO+. *J. Chem. Phys.*, 43:3734–3746, 1965.
- [119] R.L. DeKock and W. Jr. Weltner. *J. Am. Chem. Soc.*, 93:7106, 1971.

Bibliography

- [120] R.D. Brown, D.E. Pullin, E.H.N. Rice, and M. Rodler. *J. Am. Chem. Soc.*, 107:7877, 1985.
- [121] P. Botschwina and H.P. Reisenauer. C_3O : ab initio calculations and matrix IR spectra. *Chem. Phys. Lett.*, 183:217–222, 1991.
- [122] T. Shimanouchi. Tables of molecular vibrational frequencies. Consolidated volume II. *Journal of Physical and Chemical Reference Data*, 6:993–1102, 1977.
- [123] S.F. Ahmad, H. Kiefte, and M.J. Clouter. On the solid–solid phase diagrams of Ar–O₂ and Ar–N₂ mixtures. *Journal of Chemical Physics*, 75:5848–5852, 1981.
- [124] R. Ruppel. *Neue Heterokumulene und Carbene*. PhD thesis, Giessen, 1999.
- [125] F. Holland, M. Winnewisser, G. Maier, H.P. Reisenauer, and A. Ulrich. The High–resolution fourier transform infrared spectrum of the band system of OCCCCO. *Journal of Molecular Spectroscopy*, 130:470–474, 1988.

Acknowledgements

I am thankful to

- my scientific supervisor Prof. Wolfgang Krätschmer for providing me an interesting research topic, teaching me physics and chemistry, many discussions which covered not only scientific part of the work, but also general spheres of human knowledge, knowing amazing number of jokes and stories;
- Prof. Ulrich Platt who was very kind to be my second referee;
- my colleague Dr. Aik Loong Ong for discussions, ideas and very helpful tips in the field of spectroscopy;
- Dr. Tomonari Wakabayashi for his really working insights and ideas in carbon research;
- our chemical assistant Frau Ruth Alberts for her help in practical work and nice jokes. I really appreciate it;
- my colleague Roman Reusch for his help, educative discussions and for his tolerance to my character;
- staff of Max-Planck-Institute für Kernphysik for providing needful conditions of the work;
- Max-Planck-Gesellschaft for funding.

Special respects to Frau Zsuzsanna Papp-Krätschmer for creation of comfortable environment of my stay in Heidelberg.